



Search for heavy resonances in final states with four leptons and missing transverse momentum or jets in pp collisions at $\sqrt{s} = 13$ TeV with the ATLAS detector

The ATLAS Collaboration

A search for a new heavy boson produced via gluon-fusion in the four-lepton channel with missing transverse momentum or jets is performed. The search uses proton–proton collision data equivalent to an integrated luminosity of 139 fb^{-1} at a centre-of-mass energy of 13 TeV collected by the ATLAS detector between 2015 and 2018 at the Large Hadron Collider. This study explores the decays of heavy bosons: $R \rightarrow SH$ and $A \rightarrow ZH$, where R is a CP-even boson, A is a CP-odd boson, H is a CP-even boson, and S is considered to decay into invisible particles that are candidates for dark matter. In these processes, $S \rightarrow \text{invisible}$ and $H \rightarrow ZZ$. The Z boson associated with the heavy scalar boson H decays into all decay channels of the Z boson. The mass range under consideration is 390–1300 (320–1300) GeV for the R (A) boson and 220–1000 GeV for the H boson. No significant deviation from the Standard Model backgrounds is observed. The results are interpreted as upper limits at a 95% confidence level on the cross-section times the branching ratio of the heavy resonances.

Contents

1	Introduction	2
2	The ATLAS detector	3
3	Data and simulated event samples	4
4	Object and event selection	6
4.1	Object reconstruction	6
4.2	Event selection	8
5	Analysis strategy	8
6	Signal and background modelling	10
6.1	Signal model	10
6.2	Background model	10
7	Systematic uncertainties	13
7.1	Experimental uncertainties	13
7.2	Theoretical uncertainties	14
7.3	Systematic uncertainties on background shapes	14
8	Statistical procedures	15
9	Results	15
10	Conclusion	22

1 Introduction

In 2012, the ATLAS and CMS collaborations independently discovered a new particle [1, 2] with properties that are consistent with the Higgs boson proposed by the Standard Model (SM) [3–6]. It is still debated whether the Higgs boson is a standalone particle or part of an extended Higgs sector suggested by, e.g., the two-Higgs-doublet model (2HDM) [7, 8]. The 2HDM predicts the existence of five Higgs bosons, including a CP-even particle similar to the SM Higgs boson (h), a heavier CP-even Higgs boson (H), a CP-odd particle (A), and charged Higgs bosons (H^\pm). Another extension of the SM is the 2HDM+S model [9, 10], which introduces a scalar boson (S) in addition to the 2HDM particles. The S boson is assumed to be a dark matter portal and a potential source of missing transverse momentum, achieved through its decay to a pair of dark matter candidates ($\chi\bar{\chi}$) [9].

This paper presents searches for bosonic resonances that decay to four charged leptons (4ℓ , where ℓ is either an electron or a muon), along with missing transverse momentum (E_T^{miss}) or two jets (jj). The study focuses on the mass range of heavy bosons, where the invariant mass of the four leptons ($m_{4\ell}$) is above 200 GeV. This study uses proton–proton collision data at a centre-of-mass energy of 13 TeV and with an integrated luminosity of 139 fb^{-1} collected by the ATLAS detector in 2015–2018 at the Large Hadron Collider (LHC). Two different scenarios are considered for the signal model. First, the 2HDM+S model

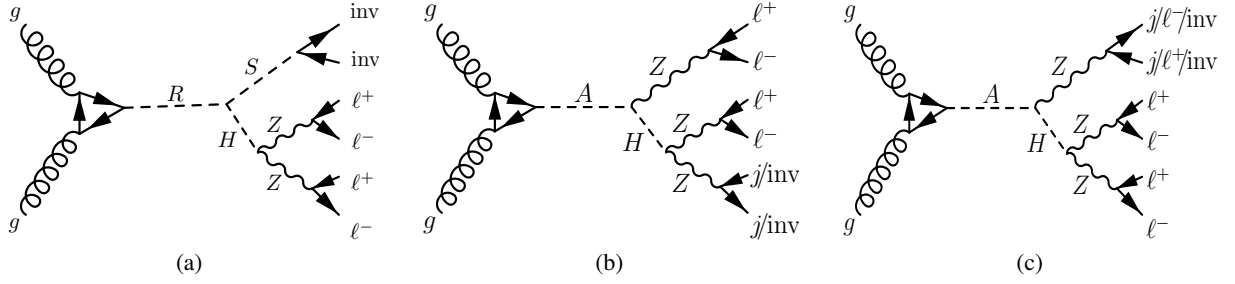


Figure 1: Feynman diagrams representing the production of heavy bosons via gluon-fusion at leading-order for the (a) $R \rightarrow SH \rightarrow 4\ell + E_{\text{T}}^{\text{miss}}$ signal, (b) $A \rightarrow Z(\rightarrow 2\ell)H(\rightarrow 2\ell + jj/\text{invisible})$ signal, and (c) $A \rightarrow Z(\rightarrow jj/\ell^+\ell^-/\text{invisible})H(\rightarrow 4\ell)$ signal, where ℓ could either be an electron or a muon, j represents a jet and inv denotes an invisible particle.

is extended to cover more general situations for various missing energy magnitudes by adding a heavy scalar R , where R decays to H and S bosons with $m_R > m_H + m_S$. The S boson decays into dark matter particles ($S \rightarrow \text{invisible}$), and the H decays to 4ℓ through the decay of two Z bosons ($H \rightarrow ZZ \rightarrow 4\ell$). The phenomenology of the new $R \rightarrow SH$ topology can easily embed into the 2HDM+S model using an approach similar to that of Ref. [9]. The masses of the R and H bosons are varied to control the missing transverse momentum, and the S mass is fixed to 160 GeV, see Section 3. Second, a 2HDM-based baryogenesis scenario is considered, which generates matter and antimatter asymmetry. Searches for models consistent with baryogenesis were conducted at the LHC in several channels, such as $H \rightarrow hh$ [11, 12], $H \rightarrow WW/ZZ$ [13–18] and $A \rightarrow Zh$ [19, 20]. Searches in the $A \rightarrow ZH \rightarrow \ell^+\ell^-b\bar{b}/\ell^+\ell^-\tau^+\tau^-$ [21–24] and $A \rightarrow ZH \rightarrow \ell^+\ell^-\tau\bar{\tau}/\nu\bar{\nu}b\bar{b}$ [25] final states were also carried out at the LHC. In these searches, for a strong first-order phase transition to occur in the early universe, the hypothesis $m_A > m_H$ is preferred. Therefore, the $A \rightarrow ZH \rightarrow 4\ell + X$ channel is added to this study to explore regions with four leptons and jet activities. X could represent two leptons, two jets, or a pair of invisible particles, with the assumption that H decays into two Z bosons. In this signal, A is a CP-odd scalar which decays to a CP-even scalar H and a Z boson. Two decay scenarios are considered for the associated production of Z and H bosons: $A \rightarrow Z(\rightarrow \ell^+\ell^-/jj/\text{invisible})H(\rightarrow 4\ell)$ and $A \rightarrow Z(\rightarrow 2\ell)H(\rightarrow 2\ell + jj/\text{invisible})$, which are combined into one signal referred to as the $A \rightarrow ZH \rightarrow 4\ell + X$ signal. In this analysis, only the gluon-fusion production mode is considered for both the $R \rightarrow SH \rightarrow 4\ell + E_{\text{T}}^{\text{miss}}$ and $A \rightarrow ZH \rightarrow 4\ell + X$ signals, as illustrated by the Feynman diagrams of Figure 1.

This paper is organised as follows. The ATLAS detector is described in Section 2. Section 3 presents the data and Monte Carlo samples, followed by the object reconstruction in Section 4. Section 5 describes the analysis strategy, and the signal and background modelling are discussed in Section 6. Section 7 lists the experimental and theoretical systematic uncertainties. Section 8 explains the statistical model used in the analysis and the results are discussed in Section 9. The conclusion is given in Section 10.

2 The ATLAS detector

The ATLAS detector [26] at the LHC covers nearly the entire solid angle around the collision point.¹ It consists of an inner tracking detector surrounded by a thin superconducting solenoid, electromagnetic and

¹ ATLAS uses a right-handed coordinate system with its origin at the nominal interaction point (IP) in the centre of the detector and the z -axis along the beam pipe. The x -axis points from the IP to the centre of the LHC ring, and the y -axis points upwards.

hadron calorimeters, and a muon spectrometer incorporating three large superconducting air-core toroidal magnets.

The inner-detector system (ID) is immersed in a 2 T axial magnetic field and provides charged-particle tracking in the range $|\eta| < 2.5$. The high-granularity silicon pixel detector covers the vertex region and typically provides four measurements per track, the first hit normally being in the insertable B-layer (IBL) installed before Run 2 [27]. It is followed by the silicon microstrip tracker (SCT), which usually provides eight measurements per track. These silicon detectors are complemented by the transition radiation tracker (TRT), which enables radially extended track reconstruction up to $|\eta| = 2.0$. The TRT also provides electron identification information based on the fraction of hits (typically 30 in total) above a higher energy-deposit threshold corresponding to transition radiation.

The calorimeter system covers the pseudorapidity range $|\eta| < 4.9$. Within the region $|\eta| < 3.2$, electromagnetic calorimetry is provided by barrel and endcap high-granularity lead/liquid-argon (LAr) calorimeters, with an additional thin LAr presampler covering $|\eta| < 1.8$ to correct for energy loss in material upstream of the calorimeters. Hadron calorimetry is provided by the steel/scintillator-tile calorimeter, segmented into three barrel structures within $|\eta| < 1.7$, and two copper/LAr hadron endcap calorimeters. The solid angle coverage is completed with forward copper/LAr and tungsten/LAr calorimeter modules optimised for electromagnetic and hadronic energy measurements respectively.

The muon spectrometer (MS) comprises separate trigger and high-precision tracking chambers measuring the deflection of muons in a magnetic field generated by the superconducting air-core toroidal magnets. The field integral of the toroids ranges between 2.0 and 6.0 T m across most of the detector. Three layers of precision chambers, each consisting of layers of monitored drift tubes, cover the region $|\eta| < 2.7$, complemented by cathode-strip chambers in the forward region, where the background is highest. The muon trigger system covers the range $|\eta| < 2.4$ with resistive-plate chambers in the barrel, and thin-gap chambers in the endcap regions. Interesting events are selected by the first-level trigger system implemented in custom hardware, followed by selections made by algorithms implemented in software in the high-level trigger [28]. The first-level trigger accepts events from the 40 MHz bunch crossings at a rate below 100 kHz, which the high-level trigger further reduces in order to record events to disk at about 1 kHz. An extensive software suite [29] is used in data simulation, in the reconstruction and analysis of real and simulated data, in detector operations, and in the trigger and data acquisition systems of the experiment.

3 Data and simulated event samples

The data used in this analysis were produced through proton–proton (pp) collisions at a centre-of-mass energy of 13 TeV recorded by the ATLAS detector at the LHC from 2015 to 2018. Events are required to satisfy data-quality requirements, and after applying the event cleaning criteria, the total integrated luminosity of the entire data set is 139 fb^{-1} [30]. The data events in the four-lepton final state were recorded using a combination of single-lepton, dilepton, and trilepton triggers [31, 32]. The single-lepton triggers for isolated muons featured p_T thresholds ranging from 20 to 60 GeV and 50 GeV for muons without isolation requirement. In contrast, dilepton triggers had thresholds from 8 to 22 GeV, and trilepton triggers employed thresholds between 4 and 20 GeV. For electrons, the single-lepton triggers encompassed p_T thresholds ranging from 24 to 300 GeV, with dilepton triggers varying from 12 to 24 GeV and trilepton

Polar coordinates (r, ϕ) are used in the transverse plane, ϕ being the azimuthal angle around the z -axis. The pseudorapidity is defined in terms of the polar angle θ as $\eta = -\ln \tan(\theta/2)$. Angular distance is measured in units of $\Delta R \equiv \sqrt{(\Delta\eta)^2 + (\Delta\phi)^2}$.

triggers featuring thresholds between 9 and 24 GeV. Additionally, when a dilepton trigger encountered an event with an electron and a muon, the p_T thresholds for electrons ranged from 7 to 26 GeV. For muons, the thresholds varied from 8 to 24 GeV. These p_T thresholds exhibited variations across the data-taking period from 2015 to 2018 due to rising luminosity [33, 34], but the overall trigger efficiency was about 98%.

Signal and background events were generated according to ATLAS detector configurations and utilised for signal optimisation, background parametrisation, and systematic uncertainty estimation. Each Monte Carlo (MC) generator produced events that underwent ATLAS detector simulation [35] within the GEANT4 framework [36]. The effect of multiple interactions in the same and neighbouring bunch crossings (pile-up) was modelled by overlaying the simulated hard-scattering event with inelastic pp events generated with PYTHIA 8.186 [37] at leading-order (LO) using the NNPDF2.3 LO set of parton distribution functions (PDFs) [38] and the A3 set of tuned parameters (tune) [39].

The $q\bar{q} \rightarrow ZZ$ background process was simulated with SHERPA 2.2.2 [40] using matrix elements at next-to-leading-order (NLO) accuracy in QCD for up to one additional parton and at LO accuracy for up to three additional parton emission. The virtual QCD corrections were provided by the OPENLOOPS library [41–43]. The $gg \rightarrow ZZ$ background process was generated by SHERPA 2.2.2, including off-shell effects and Higgs boson contributions, using LO-accurate matrix elements for up to one additional parton emission. The electroweak $q\bar{q} \rightarrow ZZ$ (EW) events, consisting of four leptons and two jets, were simulated using SHERPA 2.2.2. In addition, the VVV background events, including processes such as ZZZ , ZZW , and WWZ with at least four prompt charged leptons, were simulated using SHERPA 2.2.2. The matrix element calculations for these processes were matched and merged with the SHERPA parton shower based on Catani–Seymour dipole factorisation [44, 45] using the MEPS@NLO prescription [46–48]. The production of Z +jets was simulated with the SHERPA 2.2.1 generator using NLO matrix elements for up to two partons, and LO matrix elements for up to four partons calculated with the Comix [44] and OPENLOOPS libraries. All backgrounds simulated with SHERPA use NNPDF3.0 based on next-to-next-to-leading-order (NNLO) set of PDFs [49], along with the dedicated set of tuned parton shower parameters developed by the SHERPA authors.

Events containing charged leptons coming from the $t\bar{t}V$ background process ($V = Z$ or W^\pm) were modelled using the MADGRAPH5_AMC@NLO 2.3.3 [50] generator at NLO with the NNPDF3.0 NLO PDF. The events were interfaced to PYTHIA 8.210 using the A14 tune [51] and the NNPDF2.3 LO PDF set. The $t\bar{t}$ background was generated using POWHEG-Box v2 [52–54] at NLO with the NNPDF3.0 NLO PDF set. The events were interfaced to PYTHIA 8.230 to model the parton shower, hadronisation, and underlying event, with parameters set according to the A14 tune and using the NNPDF2.3 LO set of PDFs. The POWHEG-Box v2 generator was used to simulate the WZ [55] production process at NLO accuracy in QCD. Events were interfaced to PYTHIA 8.230 for the modelling of the parton shower, hadronisation, and underlying event, with parameters set according to the AZNLO tune [56]. The CT10 PDF set [57] was used for the hard-scattering processes, whereas the CTEQ6L1 PDF set [58] was used for the parton shower. The decays of the bottom and charm hadrons for the top-quark processes were simulated using version 1.2 of the EVTGEN program [59], except for using version 1.6 for $t\bar{t}$ production.

The $R \rightarrow SH \rightarrow 4\ell + E_T^{\text{miss}}$ signal was simulated using PYTHIA 8.244 with the A14 tune and NNPDF2.3 LO PDF set. The $A \rightarrow Z(\rightarrow jj/\ell^+\ell^-/\text{invisible})H(\rightarrow 4\ell)$ and $A \rightarrow Z(\rightarrow 2\ell)H(\rightarrow 2\ell + jj/\text{invisible})$ signals were generated by MADGRAPH5_AMC@NLO 2.7.2 at LO accuracy with the NNPDF2.3 LO PDF set, which is interfaced to PYTHIA 8.244 for parton showering and hadronisation with the A14 tune. The R mass is considered in the range of 390–1300 GeV, with the S mass fixed to 160 GeV, while the A mass is in the range of 320–1300 GeV. The H mass value for all signal processes is in the range of 220–1000 GeV. The assumption of the S mass is motivated by the phenomenology study presented in Ref. [60]. However,

Process	Generator and Parton shower	QCD accuracy	Tune and PDF
$R \rightarrow SH \rightarrow 4\ell + E_T^{\text{miss}}$	Pythia 8.244 [62]	LO	A14 and NNPDF2.3 LO [51, 63]
$A \rightarrow Z(\rightarrow jj/\ell^+\ell^-/\text{invisible})H(\rightarrow 4\ell)$	MADGRAPH5_AMC@NLO 2.7.2 + Pythia 8.244 [50, 62]	LO	A14 and NNPDF2.3 LO [51, 63]
$A \rightarrow Z(\rightarrow 2\ell)H(\rightarrow 2\ell + jj/\text{invisible})$	MADGRAPH5_AMC@NLO 2.7.2 + Pythia 8.244 [50, 62]	LO	A14 and NNPDF2.3 LO [51, 63]
$\tilde{t}\tilde{t}^* (V = W/Z)$	MADGRAPH5_AMC@NLO 2.3.3 + Pythia 8.210 [50, 62]	NLO+LO	A14 and NNPDF3.0 NLO & NNPDF2.3 LO [49, 51, 63]
$q\bar{q} \rightarrow ZZ$	SHERPA 2.2.2 + MEPS@NLO [46–48]	NLO (0- and 1-jet), LO (2- and 3-jet)	SHERPA and NNPDF3.0 NNLO [49]
$gg \rightarrow ZZ$	SHERPA 2.2.2 + MEPS@NLO [46–48]	LO (0- and 1-jet)	SHERPA and NNPDF3.0 NNLO [49]
$q\bar{q} \rightarrow ZZ$ (EW)	SHERPA 2.2.2 + MEPS@NLO [46–48]	LO	SHERPA and NNPDF3.0 NNLO [49]
$ZZ(4\ell 2\nu, 6\ell 0\nu)$	SHERPA 2.2.2 + MEPS@NLO [46–48]	NLO	SHERPA and NNPDF3.0 NNLO [49]
$WZZ(5\ell 1\nu)$	SHERPA 2.2.2 + MEPS@NLO [46–48]	NLO	SHERPA and NNPDF3.0 NNLO [49]
$WWZ(4\ell 2\nu)$	SHERPA 2.2.2 + MEPS@NLO [46–48]	NLO	SHERPA and NNPDF3.0 NNLO [49]
$Z + \text{jets}$	SHERPA 2.2.1 + MEPS@NLO [46–48]	NLO (0- and 2-jet), LO (3- and 4-jet)	SHERPA and NNPDF3.0 NNLO [49]
$t\bar{t}$	POWHEG-Box v2 + Pythia 8.230 [52–54, 62]	NLO+LO	A14 and (NNPDF3.0 NLO & NNPDF2.3 LO) [51, 59, 63]
$WZ \rightarrow 3\ell 1\nu$	POWHEG-Box v2 + Pythia 8.230 [52–54, 62]	NLO	AZNLO and (CT10NLO & CTEQ6L1) [56–58]

Table 1: Summary of the event generators used for the simulated signal and background samples, including the accuracy of the matrix element and parton distribution functions (PDFs). Additionally, the table lists the set of tuned parameters used.

the effect of this choice on the distribution of the missing transverse momentum was studied and it was found that the S mass only affects the distribution if its mass is above 200 GeV. Therefore, fixing the S mass reduces the free parameters and simplifies the analysis. Signals were generated using the narrow width approximation (NWA) [61] for both R and H in the $R \rightarrow SH \rightarrow 4\ell + E_T^{\text{miss}}$ signal, with the width of R and H set to 10 MeV. Similarly, for the $A \rightarrow ZH \rightarrow 4\ell + X$ signal, the narrow width approximation was employed with widths of 1 MeV for both A and H . Two mass points, $(m_A, m_H) = (320, 220)$ GeV and $(m_A, m_H) = (1190, 600)$ GeV, were also generated using the large width approximation (LWA) to evaluate the impact of non-negligible natural widths. Table 1 summarises the generators, shower model, matrix element accuracy, tune, and PDF sets used in signal and background simulation.

4 Object and event selection

4.1 Object reconstruction

The event selection relies on reconstructing and identifying electrons, muons, jets and missing transverse momentum. The electron energy measurement is improved using a dynamic, topological calorimeter-cell clustering-based method. This method is particularly effective in cases where an electron radiates a bremsstrahlung photon. More information about this technique can be found in Ref. [64]. Electron candidates are identified as clusters of energy deposits in the calorimeter associated with ID tracks. The final track-cluster matching uses a Gaussian-sum filter (GSF) [65], accounting for bremsstrahlung energy losses. The electron transverse momentum (p_T) is calculated from the cluster energy and the track direction at the interaction point. The rejection of background noises, which consist of hadrons, non-prompt electrons mainly originating from photon conversions, and heavy flavour hadron decay, depends on the longitudinal and transverse shapes of the electromagnetic showers in the calorimeters, track-cluster matching, and properties of tracks in the ID. All this information, except for hits associated with the track, is used to create a likelihood discriminant. The selection criteria combine the likelihood with the number of track hits and define several working points (WP). Electrons with $p_T > 4.5$ GeV and pseudorapidity range $|\eta| < 2.47$ are selected. The analysis uses a “loose” WP, with an efficiency of at least 90% for electrons with $p_T > 30$ GeV [66].

Muon reconstruction is performed within $|\eta| < 2.7$ [67], covering the entire detector. In the ID coverage range, muon reconstruction primarily applies a global fit of fully reconstructed tracks in the ID and the MS, resulting in combined muons. However, in the central region ($|\eta| < 0.1$), where the MS coverage is limited,

alternative methods are employed for muon identification. Muons in this region can be identified either by matching a fully reconstructed ID track to an MS track segment (segment-tagged muons) or by associating with a calorimetric energy deposit consistent with that of a minimum-ionising particle (calorimeter-tagged muons). In these cases, the muon momentum is determined by the ID track alone. In the forward MS region ($2.5 < |\eta| < 2.7$) outside the ID coverage, standalone muons are accepted if they have hits in all three MS layers. Additionally, if forward ID tracks are available, they are combined with standalone MS tracks to form silicon-associated forward muons. Calorimeter-tagged muons are required to have $p_T > 15$ GeV, while all other muon candidates must have a minimum transverse momentum of 5 GeV. This analysis uses a “loose” muon identification WP that uses all muon types and has an efficiency of 98.5% [67].

Fake leptons from processes such as WZ and Z +jets are suppressed using impact-parameter and track- and calorimeter-based isolation requirements [66, 67]. The transverse impact-parameter significance is the impact parameter calculated with respect to the measured beamline position in the transverse plane divided by its uncertainty, $|d_0|/\sigma_{d_0}$. This significance is required to be less than 3 for muons and less than 5 for electrons. Leptons must be isolated using both track- and calorimeter-based information. The track-based discriminants take into account the scalar p_T sum of all tracks in a cone of width $\Delta R = 0.3$ for muons and 0.2 for electrons (excluding the lepton itself). The ratio of this sum to the lepton p_T is required to be less than 0.15. The pile-up contributions are suppressed by requiring the cone tracks to originate from the primary vertex. To retain efficiency at higher p_T , the size of the track-isolation cone is reduced to $10 \text{ GeV}/p_T$ for p_T above 33 GeV for muons and 50 GeV for electrons. A vertexing algorithm is used to fit the ID tracks of the 4ℓ candidates under the assumption that they emanate from a common vertex. The resulting fit quality, represented by the χ^2/ndof value, provides good discrimination between signal and background. For the 4μ channel, a cut of $\chi^2/\text{ndof} < 9$ is applied, while a cut of $\chi^2/\text{ndof} < 6$ is used for the other channels. This maintains a signal efficiency greater than 99% for all channels.

The reconstruction of jets applies a particle-flow algorithm [68], which combines measurements from the tracker and the calorimeter. The first step is to remove those calorimeter hits that are associated with reconstructed charged particles. Then, the remaining calorimeter energy and tracks matched to the hard interaction are used to create particle-flow objects for the jet reconstruction. The anti- k_t algorithm with a radius parameter of $R = 0.4$ is used to reconstruct particle-flow jets [69]. After the jets are reconstructed, pile-up is subtracted independently of the calibration [70]. Jets are required to have $p_T > 30$ GeV and $|\eta| < 2.5$. A multivariate jet-vertex-tagger algorithm (JVT) is employed to reject low-momentum jets originating from pile-up events. The JVT considers the reconstructed tracks’ properties in the event and applies to jets with $p_T < 60$ GeV and $|\eta| < 2.4$ [71, 72].

Events containing b -hadrons (b -jets) are identified using a multivariate tagging algorithm (b -tagging) [73, 74]. This algorithm assesses the likelihood that a jet originates from b -quark hadronisation by analysing track impact parameters and reconstructed secondary vertices. In simulated $t\bar{t}$ events, the jet identification algorithm exhibits an average efficiency of 77% for identifying jets from b -quarks. Additionally, it achieves a rejection factor of approximately 30 for light-flavour quarks (u -, d -, and s -quarks), while the rejection factor for c -quarks and gluons is smaller, as reported in Ref. [73].

After object reconstruction, an overlap removal procedure is applied to all selected objects to remove ambiguities resulting from objects being reconstructed by several algorithms. The electron with the highest p_T is kept when two electrons have overlapping energy deposits. If a reconstructed electron and muon share the same ID track, the electron is selected if the muon is calorimeter-tagged; otherwise, the muon is selected. Reconstructed jets which overlap with electrons (muons) in a cone of size $\Delta R = 0.2$ (0.1) are removed.

The magnitude of the missing transverse momentum is denoted by E_T^{miss} and is calculated as the magnitude of the negative vectorial sum of the transverse momenta of calibrated leptons and jets. Also, a soft term is included in the calculation, which is constructed from all tracks originating from the primary vertex but not associated with any identified lepton or jet [75]. Selected events must have at least one vertex with two associated tracks with $p_T > 500$ MeV, and the primary vertex is chosen to be the vertex with the largest $\sum p_T^2$.

4.2 Event selection

This analysis classifies events into three channels based on the flavours of the selected four leptons: 4μ , $4e$, and $2\mu 2e$. These channels are assigned based on the triggers activated in the event, which include single-lepton, dilepton, and trilepton triggers. The possible quadruplets in each channel of an event are created from two same flavour and opposite sign lepton pairs (SFOS). The p_T thresholds of the three leading leptons in the quadruplet follow this order: 20 GeV, 15 GeV, and 10 GeV. The leading and the sub-leading lepton pairs in the quadruplet are defined to have an invariant mass closest and second closest to the Z boson mass. The invariant mass of the leading and sub-leading lepton pairs are denoted m_{Z_1} and m_{Z_2} , respectively. In the selected quadruplet, m_{Z_1} must be within $50 \text{ GeV} < m_{Z_1} < 106 \text{ GeV}$, while m_{Z_2} must be within $50 \text{ GeV} < m_{Z_2} < 115 \text{ GeV}$. The selected quadruplets must have their lepton pairs separated from each other by $\Delta R > 0.1$. If any two SFOS leptons are detected with $m_{\ell\ell}$ below 5 GeV for 4μ and $4e$ quadruplets, the quadruplet is excluded to reduce the contamination from J/ψ mesons. In this analysis, the $Z + \Upsilon$ background contribution is negligible. If, at this point, several quadruplets of different channels are selected, only the quadruplet with the highest expected signal rate is retained, in the order: 4μ , $2e2\mu$, $4e$.

The resolution of the four lepton invariant mass system can be improved by recovering the radiative photon production in the Z boson decay (final-state-radiation (FSR)) and by applying constraints on the Z boson mass. In this analysis, the methodology presented in Refs. [76–78] for the $h \rightarrow ZZ$ analysis was used to account for FSR photons in the reconstruction of Z bosons, and for applying constraints on the Z boson mass. The Z -mass constraint is applied to both Z candidates and improves the resolution of $m_{4\ell}$ by around 15%. This analysis employs the combined 4μ , $4e$, and $2\mu 2e$ channels, collectively called 4ℓ , to account for the limited statistics.

5 Analysis strategy

This analysis searches for heavy resonances that decay to four leptons and missing transverse momentum or jets, where the four-lepton invariant mass is above 200 GeV. The main source of background in this kinematic region involves the leptonic decay of two Z bosons. Among the various background processes, quark-antiquark annihilation ($q\bar{q} \rightarrow ZZ$) is the most significant, contributing 84.6% of the expected background, while gluon-initiated production ($gg \rightarrow ZZ$) accounts for approximately 11.7%. Other SM backgrounds, such as $q\bar{q} \rightarrow ZZ$ (EW), $t\bar{t}V$, Z +jets, $t\bar{t}$, WZ , and VVV , account for about 3.7% of the total background events. These numbers are estimated from simulation after the four-lepton quadruplet selection discussed in Section 4.2. In the following, this study models the SM backgrounds using an analytical function, illustrated in Section 6, where the normalisation is taken from the data.

A cut-based optimisation was used to increase the sensitivity of the $R \rightarrow SH \rightarrow 4\ell + E_T^{\text{miss}}$ and $A \rightarrow ZH \rightarrow 4\ell + X$ signals. This involves setting thresholds on various kinematic and topological

Signal region	$R \rightarrow SH \rightarrow 4\ell + E_T^{\text{miss}}$ and $A \rightarrow ZH \rightarrow 4\ell + X$			
SR1	$n_{b\text{-jets}} = 0$	$n_{\text{jets}} = 0$	$p_T^{4\ell} > 20 \text{ GeV}$	E_T^{miss} significance > 2.0
SR2		$n_{\text{jets}} \geq 1$	$p_T^{4\ell} > 10 \text{ GeV}$	E_T^{miss} significance > 3.5
SR3			$p_T^{4\ell} < 10 \text{ GeV}$	$2.5 < E_T^{\text{miss}}$ significance < 3.5
	$A \rightarrow ZH \rightarrow 4\ell + X$			
SR4	$n_{b\text{-jets}} = 0$	$n_{\text{jets}} \geq 2$	$ m_{jj} - m_Z < 20 \text{ GeV}$	
SR5			$ m_{jj} - m_Z > 20 \text{ GeV}$	
SR6		$n_{\text{jets}} = 1$		
SR7		$n_{b\text{-jets}} \geq 1$		

Table 2: Summary of the requirements for the signal regions (SR) defined in the search for the $R \rightarrow SH \rightarrow 4\ell + E_T^{\text{miss}}$ and $A \rightarrow ZH \rightarrow 4\ell + X$ signals for $m_{4\ell} > 200 \text{ GeV}$.

variables, such as the number of jets (n_{jets}) and b -jets ($n_{b\text{-jets}}$), the transverse momentum of the four-lepton system ($p_T^{4\ell}$), and the E_T^{miss} significance ($E_T^{\text{miss}}/\sqrt{\sum E_T}$). The term $\sum E_T$ represents the scalar sum of the transverse energies of all reconstructed objects in the ATLAS detector. These variables exhibit kinematic differences between $R \rightarrow SH \rightarrow 4\ell + E_T^{\text{miss}}$ and $A \rightarrow ZH \rightarrow 4\ell + X$ signals and the background processes. The background composition varies depending on the n_{jets} and $n_{b\text{-jets}}$. For the $p_T^{4\ell}$, most background processes peak around 20 GeV, with a tail stretch toward higher values. In contrast, the signal distribution peaks around 40 GeV. This difference in peak positions reflects the characteristic energy distribution of the signal compared to the background processes. Similarly, the E_T^{miss} significance distribution also demonstrates distinguishable signal and background patterns. Background events peak at a E_T^{miss} significance of around 1, indicating a relatively low significance of missing transverse energy. In contrast, the signal distribution peaks at a higher E_T^{miss} significance of around 3, suggesting a stronger presence of genuine missing transverse energy associated with the signal process. Therefore, events with no b -jets are divided into two categories based on the n_{jets} : those with no jets ($n_{\text{jets}} = 0$) and those with at least one jet ($n_{\text{jets}} \geq 1$). A two-dimensional scan is applied twice to each group using $p_T^{4\ell}$ and E_T^{miss} significance to find the optimal cut between signal and background processes. The first scan determines the optimal threshold values for these variables corresponding to the highest value of the ratio of signal yields to the square root of background yields. After finding the optimal points, the events above these optimal thresholds are removed, and then a second scan is performed on the remaining events. This process results in specific requirements on the variables that define the signal regions (SR). Therefore, events in the SR are required to satisfy the following requirements:

- $n_{b\text{-jets}} = 0$ and $n_{\text{jets}} = 0$ with $p_T^{4\ell} > 20 \text{ GeV}$ and E_T^{miss} significance > 2.0 (SR1)
- $n_{b\text{-jets}} = 0$ and $n_{\text{jets}} \geq 1$ with $p_T^{4\ell} > 10 \text{ GeV}$ and E_T^{miss} significance > 3.5 (SR2)
- $n_{b\text{-jets}} = 0$ and $n_{\text{jets}} \geq 1$ with $p_T^{4\ell} < 10 \text{ GeV}$ and $2.5 < E_T^{\text{miss}}$ significance < 3.5 (SR3)

The SRs mentioned above are used for both the $R \rightarrow SH \rightarrow 4\ell + E_T^{\text{miss}}$ and the $A \rightarrow ZH \rightarrow 4\ell + X$ models.

Jets in the $A \rightarrow ZH \rightarrow 4\ell + X$ signal can arise from initial state radiation and the decay of the Z boson. Therefore, it is crucial to accommodate scenarios with varying jet multiplicities and recover the b -jet events left from the abovementioned categorisation. Additionally, the invariant mass of the two leading jets (m_{jj}) shows a significant difference between the $A \rightarrow ZH \rightarrow 4\ell + X$ signal and backgrounds at $m_{jj} > 300 \text{ GeV}$.

Given these differences, more categorisations were designed for the $A \rightarrow ZH \rightarrow 4\ell + X$ signal. This expanded categorisation comprises four additional SRs to capture distinct jet-related features:

- $n_{b\text{-jets}} = 0, n_{\text{jets}} \geq 2, |m_{jj} - m_Z| < 20 \text{ GeV}$ (SR4)
- $n_{b\text{-jets}} = 0, n_{\text{jets}} \geq 2, |m_{jj} - m_Z| > 20 \text{ GeV}$ (SR5)
- $n_{b\text{-jets}} = 0, n_{\text{jets}} = 1$ (SR6)
- $n_{b\text{-jets}} \geq 1$ (SR7)

These SRs are only considered if the events are not yet classified in SR1-3. SR6 is motivated by the need to capture signal events in which only one jet is detected. A single jet event occurs if the produced jet has very low momentum and falls outside the detector acceptance. SR7 is designed to include events with at least one b -jet, primarily due to the significant branching ratio of the Z boson into b quarks. Table 2 provides a summary of these seven SRs used in the analysis.

6 Signal and background modelling

Simulation is used to model and then parameterise the constructed $m_{4\ell}$ distribution for the SM backgrounds. Meanwhile, the signal shape is taken directly from the simulation, as illustrated below.

6.1 Signal model

Section 3 discussed the generation of signal mass points for $R \rightarrow SH \rightarrow 4\ell + E_{\text{T}}^{\text{miss}}$ and $A \rightarrow ZH \rightarrow 4\ell + X$ signals. Seventy-seven mass points were produced for the $R \rightarrow SH \rightarrow 4\ell + E_{\text{T}}^{\text{miss}}$ signal, while seventy-two were generated for the $A \rightarrow ZH \rightarrow 4\ell + X$ signal. To cover a broader mass range, a linear interpolation method described in Ref. [79] is used to obtain signal shapes between the generated mass planes in either of the (m_R, m_H) or (m_A, m_H) masses. Interpolating the signal involves a two-step process due to its dependence on either (m_R, m_H) or (m_A, m_H) masses. In the first step, the H mass remains constant while interpolating the $(m_R - m_H)$ or $(m_A - m_H)$ mass parameters or interpolating the R or A mass. Subsequently, the interpolated signals obtained in the previous step serve as input for a second interpolation. In this stage, the R or A mass is fixed, while the H mass varies in steps of 10 GeV.

The interpolation was validated by comparing simulated and interpolated signal distributions at a few mass points, as shown in Figure 2 for the $A \rightarrow ZH \rightarrow 4\ell + X$ $R \rightarrow SH \rightarrow 4\ell + E_{\text{T}}^{\text{miss}}$ signals. Some disagreement at the tails of the signals is observed and considered as potential systematic uncertainty. This systematic uncertainty was shown to have a negligible impact on the results and was omitted.

6.2 Background model

The $m_{4\ell}$ shape of the backgrounds is obtained from simulation using a parameterised empirical function to decrease statistical uncertainties originating from the limited number of simulated events. Four background templates are used: $q\bar{q} \rightarrow ZZ$, $gg \rightarrow ZZ$, VVV , and other background processes. The other backgrounds contain processes such as $q\bar{q} \rightarrow ZZ$ (EW), $t\bar{t}V$, $t\bar{t}$, Z +jets and WZ . Each of the background templates is fitted with an analytical function for $m_{4\ell}$ between 200–1200 GeV, as follows:

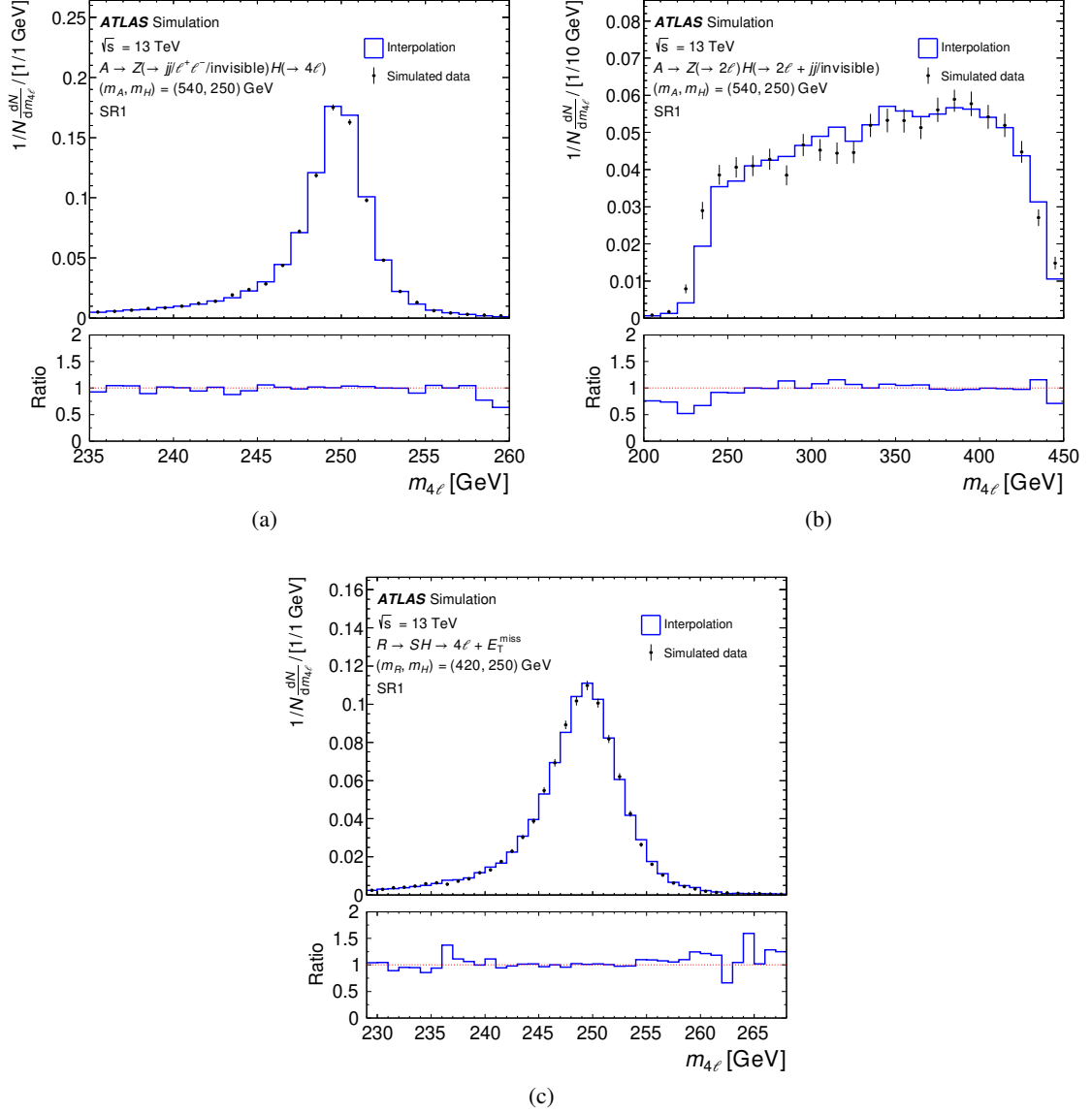


Figure 2: The $m_{4\ell}$ distributions of the interpolated (blue) and simulated (black-filled point) signals for the (a) $A \rightarrow Z(\rightarrow jj/\ell^+\ell^-/\text{invisible})H(\rightarrow 4\ell)$ and (b) $A \rightarrow Z(\rightarrow \ell^+\ell^-)H(\rightarrow 2\ell + jj/\text{invisible})$ signals with the $(m_A, m_H) = (540, 250)$ GeV mass point and the (c) $R \rightarrow SH \rightarrow 4\ell + E_T^{\text{miss}}$ signal with $(m_R, m_H) = (420, 250)$ GeV and $m_S = 160$ GeV. The lower panels show the ratio between the interpolated and simulated histograms. The plots are only shown in SR1 for illustrative purposes.

$$f(m_{4\ell}) = H(m_0 - m_{4\ell})f_1(m_{4\ell})C_1 + H(m_{4\ell} - m_0)f_2(m_{4\ell})C_2, \quad (1)$$

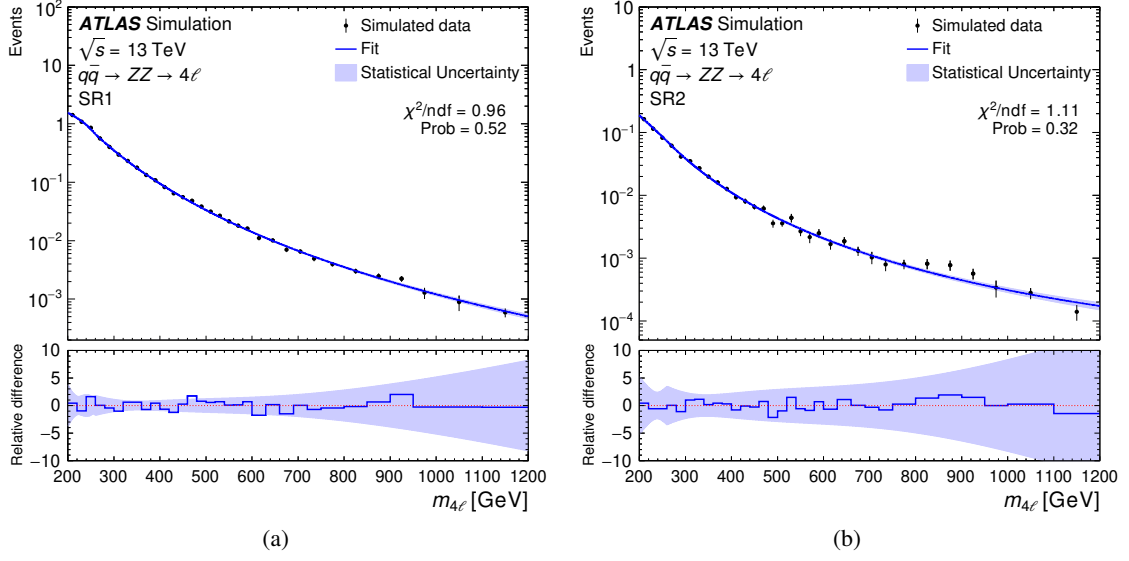


Figure 3: The $m_{4\ell}$ distributions of the analytical function fit (blue) to the simulated $q\bar{q} \rightarrow ZZ$ background (black-filled point) in signal regions (a) SR1 and (b) SR2. The lower panels show the relative difference between the fitted function and simulated histograms. The overlaid light blue band indicates the statistical uncertainty of the fit function.

where:

$$f_1(m_{4\ell}) = \frac{a_1 \cdot m_{4\ell} + a_2 \cdot m_{4\ell}^2}{1 + \exp\left(\frac{m_{4\ell} - a_1}{a_3}\right)}, \quad (2)$$

$$f_2(m_{4\ell}) = \left(1 - \frac{m_{4\ell}}{n_C}\right)^{b_1} \cdot \left(\frac{m_{4\ell}}{n_C}\right)^{\left(b_2 + b_3 \cdot \ln\left(\frac{m_{4\ell}}{n_C}\right)\right)}, \quad (3)$$

$$C_1 = \frac{1}{f_1(m_0)}, \quad C_2 = \frac{1}{f_2(m_0)}.$$

The functional form f_1 models the ZZ threshold around $2 \cdot m_Z$, and f_2 describes the high mass tail. The transition between the f_1 and f_2 functions is performed by the Heaviside step function $H(x)$ around m_0 , where m_0 is fixed to 260 GeV, 240 GeV, 250 GeV and 230 GeV for the $q\bar{q} \rightarrow ZZ$, $gg \rightarrow ZZ$, VVV , and other backgrounds, respectively. The transition point is determined by the smoothness of the functional form. A constant $n_C = 13$ TeV scales $m_{4\ell}$ in the high mass region. C_1 and C_2 ensure the continuity of the function around the point m_0 , where f_1 and f_2 are joined together. The parameters a_i and b_i are determined by fitting the $m_{4\ell}$ distribution in simulation for each specific SR. Overall, all regions achieved a good fit quality with the empirical function, assessed by the chi-squared values, which are approximately equal to unity for all signal regions. As an example, Figure 3 demonstrates the fit of the analytical function given by Equation 1 to the dominant $q\bar{q} \rightarrow ZZ$ background process in SR1 and SR2. The integral error calculated from the fit function is considered a source of systematic uncertainty. It is treated as a nuisance parameter and propagated as a shape systematic uncertainty to the final fit.

7 Systematic uncertainties

This section discusses the sources of systematic uncertainty considered in this analysis, including experimental and theoretical uncertainties for the signal and background processes. Statistical uncertainties arising from the MC event generation are also considered. Additionally, uncertainties introduced by the background parameterisation are considered and propagated to the final fit. The systematic uncertainties are evaluated using the invariant mass of the four lepton system as a discriminant. Each systematic uncertainty component is treated as a nuisance parameter and profiled in the final statistical analysis.

7.1 Experimental uncertainties

Experimental uncertainties, such as object reconstruction and identification, trigger efficiencies, energy scale and resolution, are calculated for signal and background processes. The systematic experimental uncertainties are evaluated by computing the ratio between the integral of the $m_{4\ell}$ distribution with the relevant nuisance parameter weight modified by one standard deviation and the integral of the $m_{4\ell}$ distribution using the nominal weight. Signal samples were divided into three categories depending on the size of the energy gap ($m_A - m_H$ or $m_R - m_H$) to simplify estimating the experimental systematic uncertainties for the signals. The gaps include samples with low (< 500 GeV), medium (> 500 GeV and < 700 GeV) and high (> 1300 GeV) energy gaps. These ranges are for the $R \rightarrow SH \rightarrow 4\ell + E_T^{\text{miss}}$ process, and they are slightly different for the $A \rightarrow ZH \rightarrow 4\ell + X$ process. The systematic uncertainties are evaluated for three signal mass points from each energy gap for both signals. Each result is combined by calculating the mean of the three samples per energy gap. Only the effect on the absolute normalisation was found to be relevant for the signal. For the VVV and other backgrounds, the absolute normalisation and the shape variation were included in the fit. In contrast, only the shape variation for the $q\bar{q} \rightarrow ZZ$ and $gg \rightarrow ZZ$ was included as systematic uncertainty in the fit.

The lepton identification, isolation and reconstruction efficiency, energy/momentum scale, and resolution are derived from data using $J/\psi \rightarrow \ell\ell$ and $Z \rightarrow \ell\ell$ events. The uncertainties in the lepton efficiency are calculated following the method presented in Refs. [66, 80] for muons and electrons. Generally, their effect on the signal yields is less than 1% for the $R \rightarrow SH \rightarrow 4\ell + E_T^{\text{miss}}$ signal, and up to 3.6% for the $A \rightarrow ZH \rightarrow 4\ell + X$ signal. These uncertainties are no more than 1.5% for the VVV background yields and at most 1.7% for the other background processes. The uncertainties in the jet energy scale and resolution come from sources such as uncertainties in the absolute and relative “in situ” calibration and the correction for pile-up [70]. In total, uncertainties due to the jet energy scale and energy resolution are estimated to a maximum of 4.3% for the $R \rightarrow SH \rightarrow 4\ell + E_T^{\text{miss}}$ signal, 4.7% for the $A \rightarrow ZH \rightarrow 4\ell + X$ signal, 7.0% for the VVV background and 10.4% for the other background processes. In addition, flavour tagging uncertainties are calculated by altering the uncertainty of the tagged jet flavour efficiency by $\pm 1\sigma$. The total estimated flavour tagging uncertainties are as high as 4.3% for the $R \rightarrow SH \rightarrow 4\ell + E_T^{\text{miss}}$ and $A \rightarrow ZH \rightarrow 4\ell + X$ signals, 8.9% for the VVV background and 8.5% for the other background processes. The uncertainty in the E_T^{miss} is influenced by uncertainties in the energy scales of both leptons and jets [81]. Furthermore, there are contributions to the E_T^{miss} uncertainty from the momentum scale and resolution of tracks that are not associated with any identified lepton or jet. The overall uncertainty in E_T^{miss} due to scale and resolution for the $R \rightarrow SH \rightarrow 4\ell + E_T^{\text{miss}}$ signal and VVV background is less than 1%. For the $A \rightarrow ZH \rightarrow 4\ell + X$ signal, these uncertainties are up to 4.7% and 6.2% for the scale and resolution, respectively, while for the other background processes, it is at most 6.1% due to the momentum scale and

9.7% due to the resolution. These experimental systematic uncertainties have a negligible impact on the shape, so only normalisation uncertainties are considered.

The uncertainty in the combined 2015–2018 integrated luminosity is 1.7% [82], obtained using the LUCID-2 detector [83] for the primary luminosity measurements. In addition, a systematic uncertainty from re-scaling the simulated pile-up to the data is considered. It is estimated to be up to 2.5% for the $R \rightarrow SH \rightarrow 4\ell + E_T^{\text{miss}}$ signal, less than 1% for the $A \rightarrow ZH \rightarrow 4\ell + X$ signal, and about 3.0% for the VVV and other background processes.

In Section 8, a common normalisation factor is introduced to scale the event yields for both $q\bar{q} \rightarrow ZZ$ and $gg \rightarrow ZZ$ backgrounds while keeping the VVV and other backgrounds fixed to their SM predictions. Subsequently, the relative acceptance difference is calculated between the $q\bar{q} \rightarrow ZZ$ and $gg \rightarrow ZZ$ backgrounds for each source of the experimental systematic uncertainties. These experimental systematic uncertainties are then propagated to the $gg \rightarrow ZZ$ background. Experimental systematic uncertainties, which affect the shape of the $m_{4\ell}$ distribution of the $q\bar{q} \rightarrow ZZ$ and $gg \rightarrow ZZ$ backgrounds, are considered in the analysis as shape systematic uncertainties.

7.2 Theoretical uncertainties

This analysis considers the uncertainties of the PDF, missing high-order QCD correction, initial- and final-state radiation (ISR/FSR), and parton showering (PS) and hadronisation. The theoretical scale uncertainties on the signal samples are assessed by varying the factorisation and renormalisation scales up and down from their nominal values by a factor of two in each SR. The largest effect of the scale uncertainties is taken as the systematic uncertainty. The PDF uncertainty is estimated using the `SysCALC` [84] package in conjunction with `MADGRAPH5_AMC@NLO 2.9.5`. The uncertainty is determined by considering how the envelope of variations among alternative PDFs differs from the internal PDF error sets (NNPDF2.3 PDF). The calculation follows the PDF4LHC recommendations provided in Ref. [85]. Uncertainties related to the ISR/FSR, PS and hadronisation are evaluated by employing variations in tune eigenvectors in `PYTHIA` and comparing `HERWIG 7.1.3` [86] with `PYTHIA 8.230` for the signal samples. The impact of the theoretical uncertainties on the signal acceptance is about 1%. The theoretical systematic uncertainties on the SM backgrounds are included as a shape systematic on the $m_{4\ell}$ distribution and summarised below.

7.3 Systematic uncertainties on background shapes

To account for any possible biases introduced by the analytical function discussed in Section 6.2, uncertainties stemming from the background parameterisation are considered. These uncertainties are calculated by evaluating the error in the fit parameters while also taking into account the errors in the parameters resulting from the fit. The errors are estimated using the correlation values obtained from the fit.

Incorporating PDF and QCD scale uncertainties into the analysis is motivated by their impact on the shape of the $m_{4\ell}$ distributions for the $q\bar{q} \rightarrow ZZ$ and $gg \rightarrow ZZ$ processes. The QCD scale uncertainty is estimated to be up to 10% for the $q\bar{q} \rightarrow ZZ$ and $gg \rightarrow ZZ$ backgrounds. The PDF uncertainty is less than 5% (1%) in the low mass region and about 25% (30%) in the high mass region for the $q\bar{q} \rightarrow ZZ$ ($gg \rightarrow ZZ$) background. A missing higher-order QCD correction uncertainty on the $m_{4\ell}$ shape is considered for the $q\bar{q} \rightarrow ZZ$ background, which is estimated to be less than 10%. The parton shower uncertainty is evaluated by varying parameters in the parton shower tunes, such as the CKKW and QSF settings, and by using different showering options.

8 Statistical procedures

The invariant mass of the four leptons is used as a discriminant to examine the null and alternative hypotheses using the profile likelihood ratio technique [87]. The null hypothesis corresponds to smoothed backgrounds that fall from the low mass range to the higher mass range of the $m_{4\ell}$ distribution. In contrast, the alternative hypothesis incorporates a signal structure around the H mass. The signal and background contributions in the $m_{4\ell}$ distribution are extracted via a binned maximum-likelihood fit of the signal-plus background hypotheses to extract any indication for new physics. The profile likelihood function is defined as the probability of observing n events. It is calculated as the product of the sum of weighted signal and background events, as shown below:

$$\mathcal{L}(m_{4\ell}^n | \sigma(gg \rightarrow A/R), \vec{\theta}) = \prod_{r=\text{SRs}}^{n_r} \prod_{i=\text{bin}}^{n_i} \text{Poisson} \left(n_{r,i} | s_{r,i} + \sum_b b_{r,i}(\vec{\theta}) \right) \times \prod_i G_i(0 | \vec{\theta}, 1), \quad (4)$$

where $\sigma(gg \rightarrow A/R)$ is the parameter of interest for the $A \rightarrow ZH \rightarrow 4\ell + X$ or $R \rightarrow SH \rightarrow 4\ell + E_{\text{T}}^{\text{miss}}$ signal. The expected signal and background yields in each $m_{4\ell}$ distribution bin are represented by s and b , respectively. The expected signal yield s is calculated by:

$$s = \sigma(gg \rightarrow A/R) \times \mathcal{B}(A/R \rightarrow ZH/SH) \times \mathcal{B}(H \rightarrow ZZ) \times AC \times \int L dt, \quad (5)$$

where AC is the acceptance times efficiency, and $\int L dt = 139 \text{ fb}^{-1}$ is the integrated luminosity of the data. A collection of nuisance parameters is introduced to describe how systematic uncertainties influence the predicted number of signal and background events and the shape of the PDFs. These parameters are constrained to their nominal values within the calculated uncertainties using Gaussian constraints by $G(\vec{\theta})$, in which $\vec{\theta}$ is a vector containing the nuisance parameters. In the likelihood fit function, SRs are indicated in the product by the index “ r ”. In each SR, the normalisation for the $q\bar{q} \rightarrow ZZ$ and $gg \rightarrow ZZ$ processes (ZZ background) are calculated by a likelihood fit to the data. The ZZ background normalisation is denoted by the μ_{norm}^{ZZ} parameter. The benefit of taking the ZZ background normalisation from the data is the reduction of the background dependence on the theoretical systematic uncertainties.

9 Results

Table 3 displays the yields in each of the seven SRs described in Section 5. The observed and expected numbers of events in each SR were obtained using a simultaneous binned maximum-likelihood fit, assuming the background-only hypothesis. Signal+background binned maximum-likelihood fits were also performed on the $m_{4\ell}$ distribution to search for potential excesses beyond the expected SM backgrounds. This fit model is based on the statistical framework discussed in Section 8. The m_R (m_A) range 390–1300 (320–1300) GeV and the m_H range 220–1000 GeV were scanned for the $R \rightarrow SH \rightarrow 4\ell + E_{\text{T}}^{\text{miss}}$ ($A \rightarrow ZH \rightarrow 4\ell + X$) search. The fit was performed in steps of 10 GeV, in which 4187 (m_R, m_H) and 4740 (m_A, m_H) mass points in NWA for each SR were tested for the $R \rightarrow SH \rightarrow 4\ell + E_{\text{T}}^{\text{miss}}$ and $A \rightarrow ZH \rightarrow 4\ell + X$ processes, respectively. The resulting test statistics were used to construct p -values and significance estimates, which were then used to evaluate the compatibility of the data with the background-only hypothesis and the presence of new physics in the data.

The four lepton invariant mass distributions for the $R \rightarrow SH \rightarrow 4\ell + E_{\text{T}}^{\text{miss}}$ search with the $(m_R, m_H) = (500, 300)$ GeV mass point in all three SRs are shown in Figure 4. Figures 5 and 6 show the $m_{4\ell}$ distribution

in the seven SRs defined for the $A \rightarrow ZH \rightarrow 4\ell + X$ search with the $(m_A, m_H) = (510, 380)$ GeV mass point. These plots are shown for a background-only fit to data, and signals are overlaid after being scaled to the observed upper limit on the cross-section. In the presented figures, statistical fluctuations are dominant, particularly in the high mass region of the $m_{4\ell}$. The binning was determined by considering the width and the stability of the upper limit on the cross-section of the $R \rightarrow SH \rightarrow 4\ell + E_T^{\text{miss}}$ and $A \rightarrow ZH \rightarrow 4\ell + X$ signals. The upper limit calculations were performed in bins with a fixed width of 5 GeV. However, for better visualisation, the plots are presented with variable binning.

No significant deviation from the SM backgrounds is observed in the data. Local excesses around two standard deviations for a few mass points are shown in Figure 7(a) for the $R \rightarrow SH \rightarrow 4\ell + E_T^{\text{miss}}$ signal and in Figure 7(b) for the $A \rightarrow ZH \rightarrow 4\ell + X$ signal. The most significant excess comes from the $A \rightarrow ZH \rightarrow 4\ell + X$ signal at the $(m_A, m_H) = (510, 380)$ GeV mass point with a local significance of 2.5 standard deviations. The impact of systematic uncertainties on the analysis is investigated based on their impact on the parameter of interest (best-fit cross-section) for the $R \rightarrow SH \rightarrow 4\ell + E_T^{\text{miss}}$ and $A \rightarrow ZH \rightarrow 4\ell + X$ signals. The uncertainties that have the most significant impact vary depending on the choice of the (m_R, m_H) or (m_A, m_H) mass points. Table 4 shows the first five leading sources of uncertainties in the best-fit σ value for three different mass points for each signal. The effect of the uncertainties is estimated using Asimov data produced with the signal cross-section set to the expected limits for the particular (m_R, m_H) or (m_A, m_H) mass points, assuming narrow width R or A and H bosons. In the $R \rightarrow SH \rightarrow 4\ell + E_T^{\text{miss}}$ search, systematic uncertainties related to jet characteristics, such as jet flavour composition, played a significant role and ranked first and second at mass points $(m_R, m_H) = (390, 220)$ GeV and $(m_R, m_H) = (1300, 1000)$ GeV, respectively. It is noteworthy that the uncertainties associated with jet characteristics remained significant and played a pivotal role in the overall uncertainty assessment for both the $R \rightarrow SH \rightarrow 4\ell + E_T^{\text{miss}}$ and $A \rightarrow ZH \rightarrow 4\ell + X$ searches.

As no significant excess was observed in comparison to the background predictions, the results were translated into upper limits on the production cross-section of the $R \rightarrow SH \rightarrow 4\ell + E_T^{\text{miss}}$ and $A \rightarrow ZH \rightarrow 4\ell + X$ signals times the branching fractions. The branching fractions considered are $\mathcal{B}(R \rightarrow SH)$ and $\mathcal{B}(H \rightarrow ZZ)$ for the $R \rightarrow SH \rightarrow 4\ell + E_T^{\text{miss}}$ process. For the $A \rightarrow ZH \rightarrow 4\ell + X$ process, the branching fractions are $\mathcal{B}(A \rightarrow ZH)$ and $\mathcal{B}(H \rightarrow ZZ)$. The CL_s approach in the asymptotic approximation [87, 88]

	SR1	SR2	SR3	SR4	SR5	SR6	SR7
$q\bar{q} \rightarrow ZZ$	132 ± 12	17 ± 6	42 ± 7	40 ± 7	156 ± 13	549 ± 70	86 ± 11
$gg \rightarrow ZZ$	32 ± 6	3.2 ± 3.1	8.3 ± 3.1	6.6 ± 2.8	22.1 ± 3.7	102 ± 70	9.4 ± 4.2
VVV	7.5 ± 0.4	4.77 ± 0.34	1.49 ± 0.19	0.19 ± 0.04	1.08 ± 0.11	1.59 ± 0.13	0.50 ± 0.07
Other backgrounds	5.5 ± 0.9	7.1 ± 1.1	3.6 ± 0.7	2.47 ± 0.30	17.5 ± 0.8	11.3 ± 0.8	37.6 ± 2.3
Total background	177 ± 13	32 ± 6	55 ± 7	49 ± 7	197 ± 14	664 ± 26	134 ± 12
Observed	177	32	55	49	197	664	135
μ_{norm}^{ZZ}	1.15 ± 0.15	1.3 ± 0.6	0.96 ± 0.22	0.90 ± 0.17	0.80 ± 0.08	1.02 ± 0.13	1.4 ± 0.3

Table 3: Observed and expected post-fit event yields for $m_{4\ell} > 200$ GeV with their uncertainties. The expected yields and their uncertainties are obtained from a simultaneous fit to data under the background-only hypothesis on all seven signal regions discussed in Section 5. The μ_{norm}^{ZZ} is the normalisation factor for the $q\bar{q} \rightarrow ZZ$ and $gg \rightarrow ZZ$ backgrounds. The other backgrounds include $q\bar{q} \rightarrow ZZ$ (EW), $t\bar{t}V$, $t\bar{t}$, Z +jets and WZ processes. These backgrounds and the VVV background process were fixed to their SM prediction.

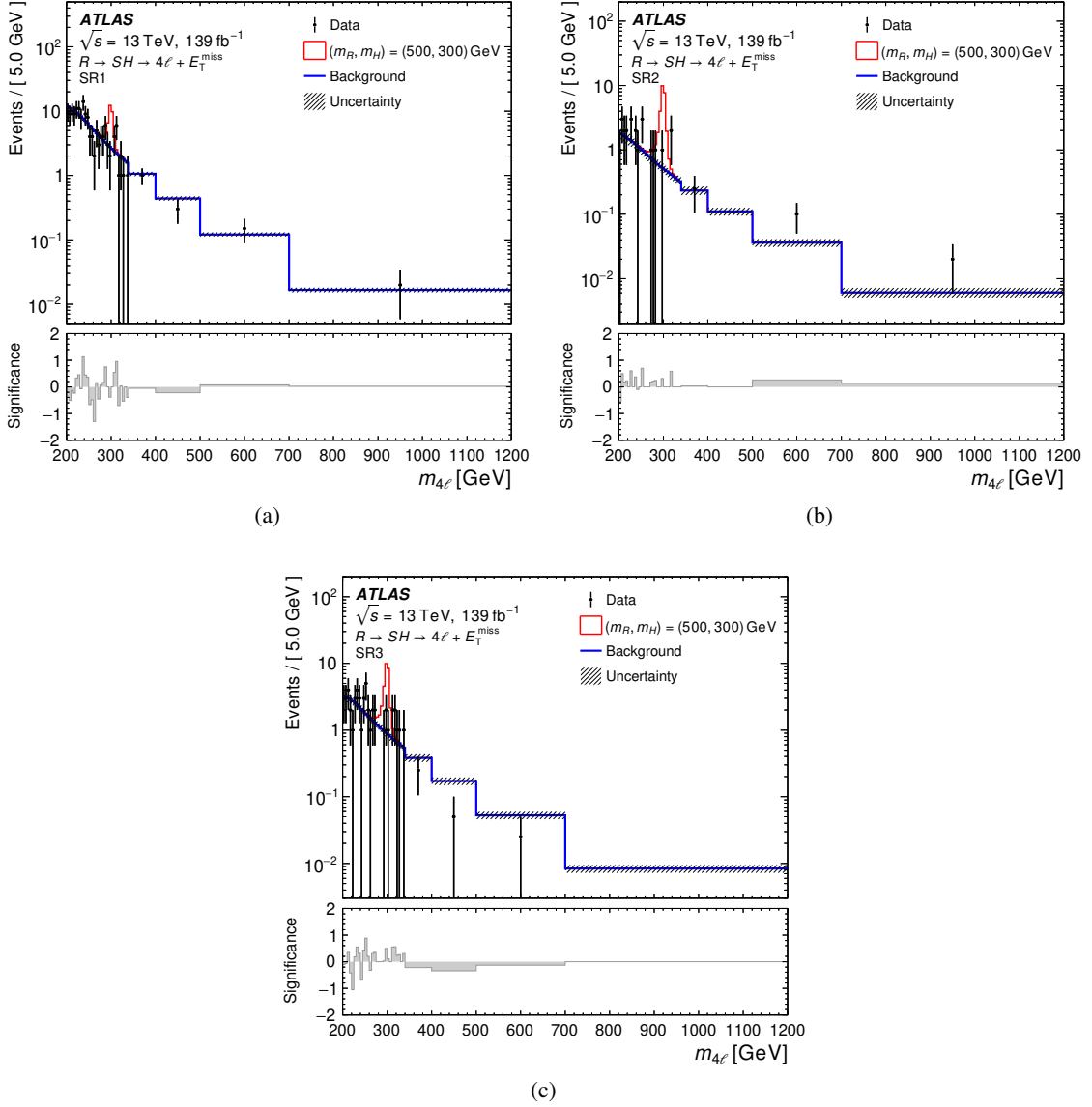


Figure 4: Observed and expected distributions of the invariant mass of the four-lepton system in the $R \rightarrow SH \rightarrow 4\ell + E_T^{\text{miss}}$ search for (a) SR1, (b) SR2 and (c) SR3 under a background-only fit to data. The total background (blue) includes the $q\bar{q} \rightarrow ZZ$, $gg \rightarrow ZZ$, $q\bar{q} \rightarrow ZZ$ (EW), VVV , $t\bar{t}V$, $t\bar{t}$, Z +jets and WZ processes. The overlaid distribution of the $(m_R, m_H) = (500, 300)$ GeV signal (red) is normalised to the observed upper limit on the cross-section (25.0 fb) discussed in Section 9. The hatched lines show the systematic uncertainty of the background prediction, while the error bar on the data denote the statistical uncertainty. The lower panel displays the significance of each bin, which is determined by the residual of the data corresponding to the fitted background taking the statistical uncertainty of the data into account. The fit is performed in bins of 5 GeV width, while the plots are re-binned using variable binning for presentation purposes.

was used to calculate upper limits at 95% confidence level (CL) across the explored phase space. The upper limit, either on $\sigma(gg \rightarrow R) \times \mathcal{B}(R \rightarrow SH) \times \mathcal{B}(H \rightarrow ZZ)$ or on $\sigma(gg \rightarrow A) \times \mathcal{B}(A \rightarrow ZH) \times \mathcal{B}(H \rightarrow ZZ)$, for a specific mass hypothesis, is obtained by fixing the H mass parameter to a constant value and optimising

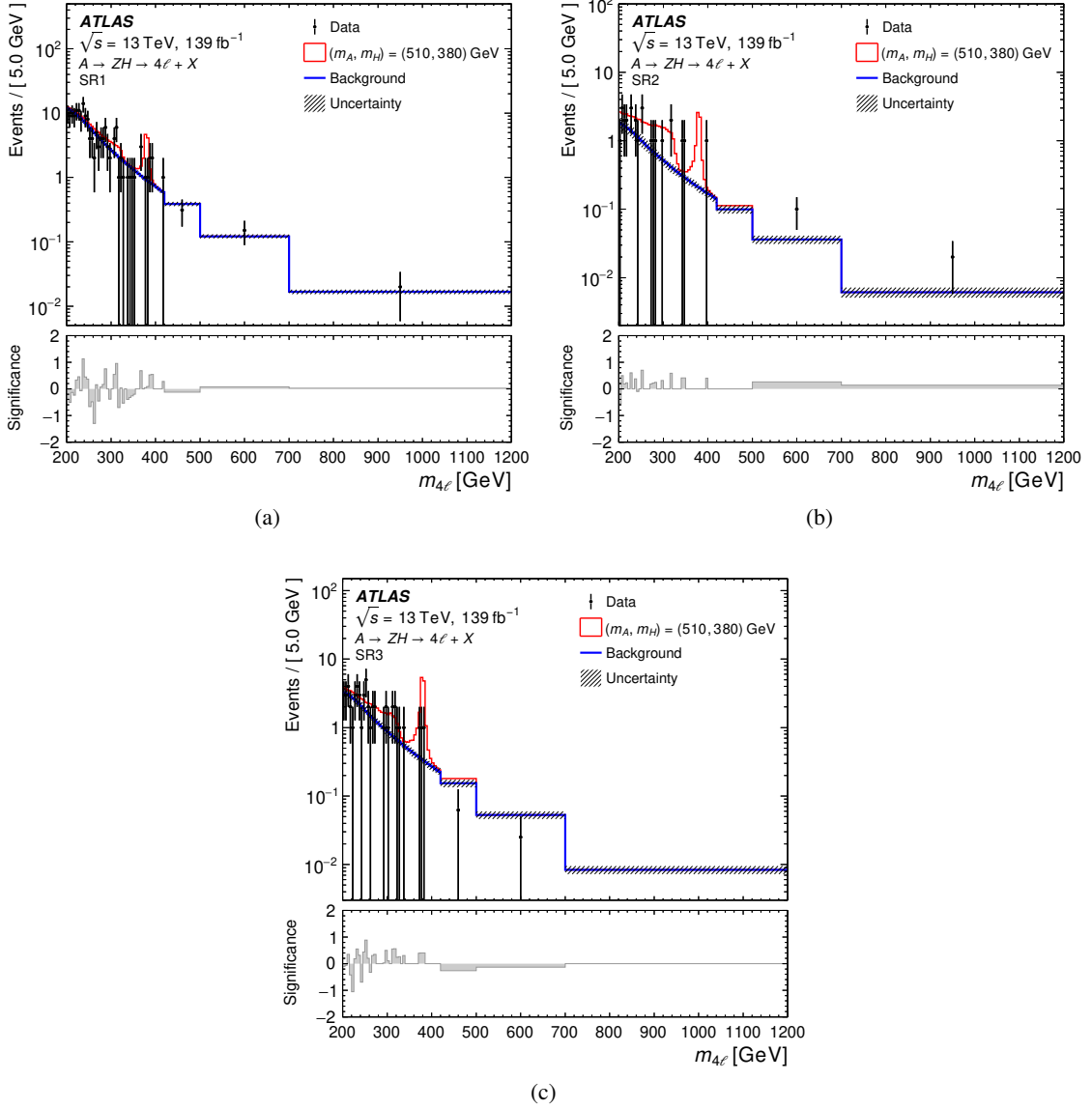


Figure 5: Observed and expected distributions of the invariant mass of the four-lepton system in the $A \rightarrow ZH \rightarrow 4\ell + X$ search for (a) SR1, (b) SR2 and (c) SR3 under a background-only fit to data. The total background (blue) includes the $q\bar{q} \rightarrow ZZ$, $gg \rightarrow ZZ$, $q\bar{q} \rightarrow ZZ$ (EW), VVV , $t\bar{t}V$, $t\bar{t}$, Z +jets and WZ processes. The overlaid distribution of the $(m_A, m_H) = (510, 380)$ GeV signal (red) is normalised to the observed upper limit on the cross-section (29.9 fb) discussed in Section 9. The hatched lines show the systematic uncertainty of the background prediction, while the error bar on the data denote the statistical uncertainty. The lower panel displays the significance of each bin, which is determined by the residual of the data corresponding to the fitted background taking the statistical uncertainty of the data into account. The fit is performed in bins of 5 GeV width, while the plots are re-binned using variable binning for presentation purposes.

the probability function for nuisance parameters. The observed and expected upper limits of NWA R and H bosons for the $R \rightarrow SH \rightarrow 4\ell + E_T^{\text{miss}}$ search are shown in Figures 8(a) and 8(b) in the (m_H, m_R) plane where the z -axis displays the upper limits on $\sigma(gg \rightarrow R) \times \mathcal{B}(R \rightarrow SH) \times \mathcal{B}(H \rightarrow ZZ)$ in fb. The observed

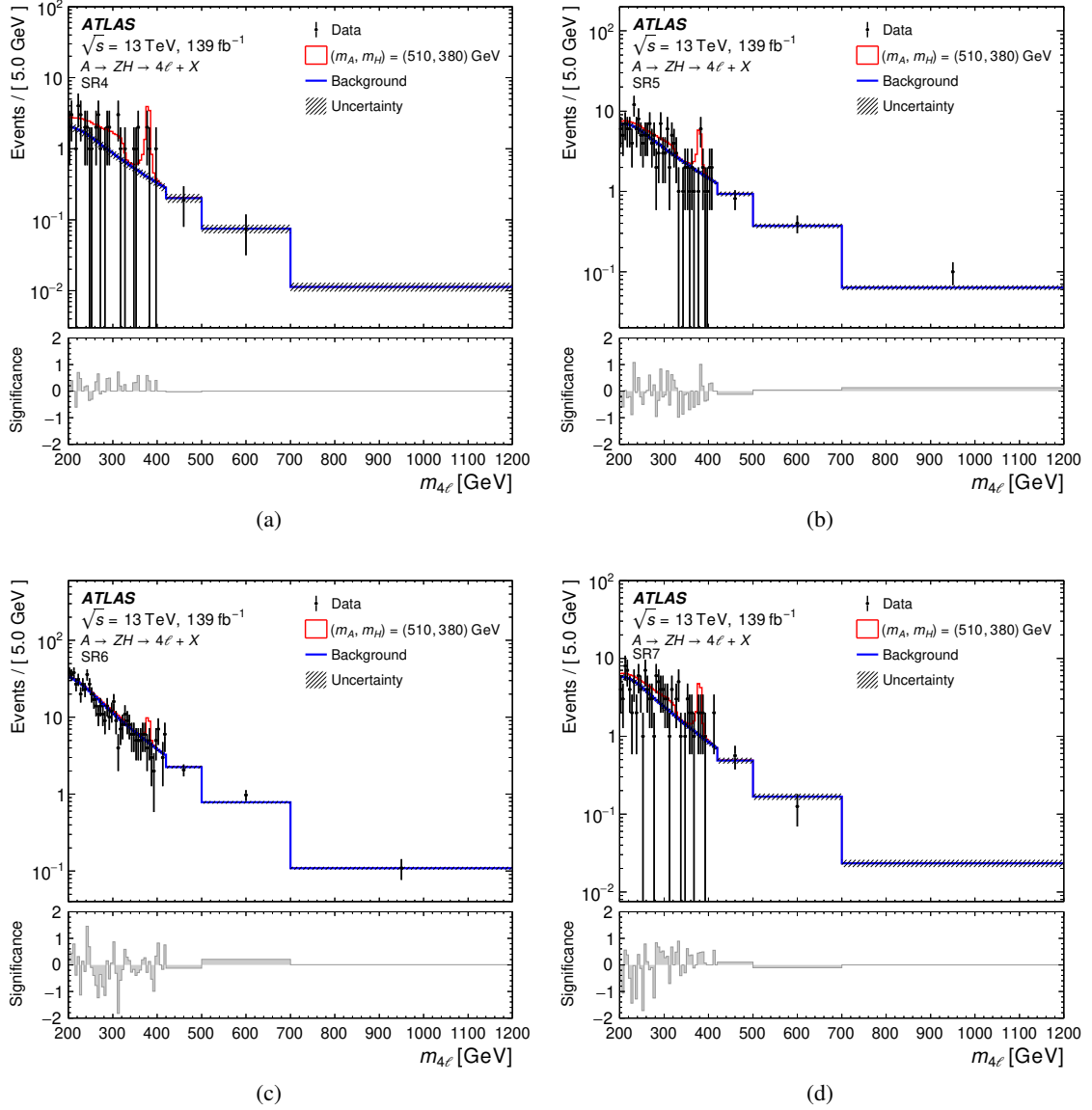


Figure 6: Observed and expected distributions of the invariant mass of the four-lepton system in the $A \rightarrow ZH \rightarrow 4\ell + X$ search for (a) SR4, (b) SR5, (c) SR6 and (d) SR7 under a background-only fit to data. The total background (blue) includes the $q\bar{q} \rightarrow ZZ$, $gg \rightarrow ZZ$, $q\bar{q} \rightarrow ZZ$ (EW), VVV , $t\bar{t}V$, $t\bar{t}$, Z +jets and WZ processes. The overlaid distribution of the $(m_A, m_H) = (510, 380)$ GeV signal (red) is normalised to the observed upper limit on the cross-section (29.9 fb) discussed in Section 9. The hatched lines show the systematic uncertainty of the background prediction, while the error bar on the data denote the statistical uncertainty. The lower panel displays the significance of each bin, which is determined by the residual of the data corresponding to the fitted background taking the statistical uncertainty of the data into account. The fit is performed in bins of 5 GeV width, while the plots are re-binned using variable binning for presentation purposes.

upper limits for the $R \rightarrow SH \rightarrow 4\ell + E_T^{\text{miss}}$ search range from 6.8 fb for $(m_R, m_H) = (1300, 980)$ GeV to 119.2 fb for $(m_R, m_H) = (410, 240)$ GeV. In contrast, the expected upper limits vary from 7.7 fb to 70.3 fb for the same mass points. Similarly, Figures 8(c) and 8(d) show the observed and expected upper limits

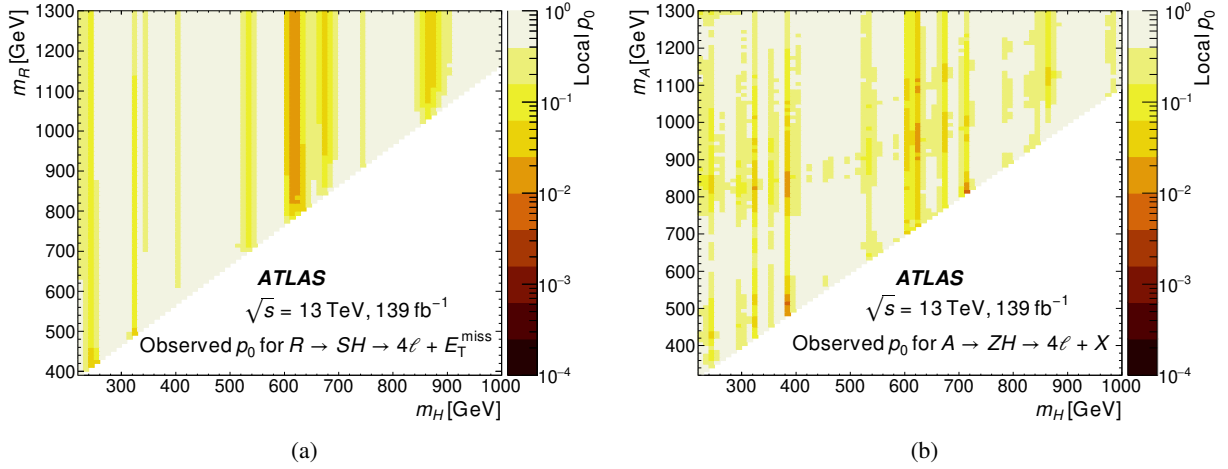


Figure 7: Local p_0 -values in the (m_H, m_R) plane for (a) the $R \rightarrow SH \rightarrow 4\ell + E_T^{\text{miss}}$ search with $m_S = 160$ GeV, and in the (m_H, m_A) plane for (b) the $A \rightarrow ZH \rightarrow 4\ell + X$ search.

$R \rightarrow SH \rightarrow 4\ell + E_T^{\text{miss}}$			$A \rightarrow ZH \rightarrow 4\ell + X$		
(m_R, m_H) [GeV]	Uncertainty source	$\Delta\sigma/\sigma$ [%]	(m_A, m_H) [GeV]	Uncertainty source	$\Delta\sigma/\sigma$ [%]
(390, 220)	Jet flavour composition	6.2	(320, 220)	Other backgrounds parameterisation SR7	5.0
	Jet flavour response	4.8		$q\bar{q} \rightarrow ZZ$ parameterisation SR7	3.9
	Jet energy scale	4.2		Jet flavour composition	3.9
	Pile-up reweighting	4.0		Luminosity	3.7
	CKKW parton showering ($gg \rightarrow ZZ$) SR2	3.8		$gg \rightarrow ZZ$ parameterisation SR6	3.6
(500, 300)	CKKW parton showering ($gg \rightarrow ZZ$) SR2	3.1	(510, 380)	Luminosity	2.4
	QSF parton showering ($gg \rightarrow ZZ$) SR2	3.0		Jet flavour composition	2.4
	$q\bar{q} \rightarrow ZZ$ parameterisation SR2	2.0		Jet energy scale	1.7
	Pile-up reweighting	1.9		Jet energy resolution	1.5
	VVV parameterisation SR2	1.9		Signal PDF	1.4
(1300, 1000)	$q\bar{q} \rightarrow ZZ$ parameterisation SR2	9.3	(1300, 1000)	CKKW parton showering ($gg \rightarrow ZZ$) SR2	3.3
	Jet flavour composition	7.3		QSF parton showering ($gg \rightarrow ZZ$) SR2	3.3
	Jet flavour response	3.5		Other backgrounds parameterisation SR2	2.6
	Pile-up reweighting	2.9		$q\bar{q} \rightarrow ZZ$ parameterisation SR5	2.1
	CKKW parton showering ($gg \rightarrow ZZ$) SR2	2.9		VVV parameterisation SR2	2.1

Table 4: The impact of the most important sources of uncertainty on the best-fit value of the signal cross-section for three mass points for each $R \rightarrow SH \rightarrow 4\ell + E_T^{\text{miss}}$ and $A \rightarrow ZH \rightarrow 4\ell + X$ signals after the fit. Sum in quadrature of the upward and downward effects ($\Delta\sigma$) is divided by the best fit value of the signal cross-section (σ) for each signal. Shape uncertainties are uncorrelated and hence affect each region separately.

for the $A \rightarrow ZH \rightarrow 4\ell + X$ search in the (m_H, m_A) plane, in which the z -axis represents the upper limits on $\sigma(gg \rightarrow A) \times \mathcal{B}(A \rightarrow ZH) \times \mathcal{B}(H \rightarrow ZZ)$. For the $A \rightarrow ZH \rightarrow 4\ell + X$ search, the observed upper limits range from 2.1 fb for $(m_A, m_H) = (1300, 760)$ GeV to 32.3 fb for $(m_A, m_H) = (430, 240)$ GeV, whereas the corresponding expected upper limits range from 2.9 fb to 18.8 fb. Pseudo-experiments were used to calculate upper limits for various mass points, but the results did not significantly deviate from the asymptotic upper limits.

The analysis focuses on studying heavy resonances with NWA A or R and H bosons produced via gluon-fusion for the $A \rightarrow ZH \rightarrow 4\ell + X$ and $R \rightarrow SH \rightarrow 4\ell + E_T^{\text{miss}}$ processes. However, the effect of the LWA in a similar scenario was also checked. For this purpose, two low and high mass points,

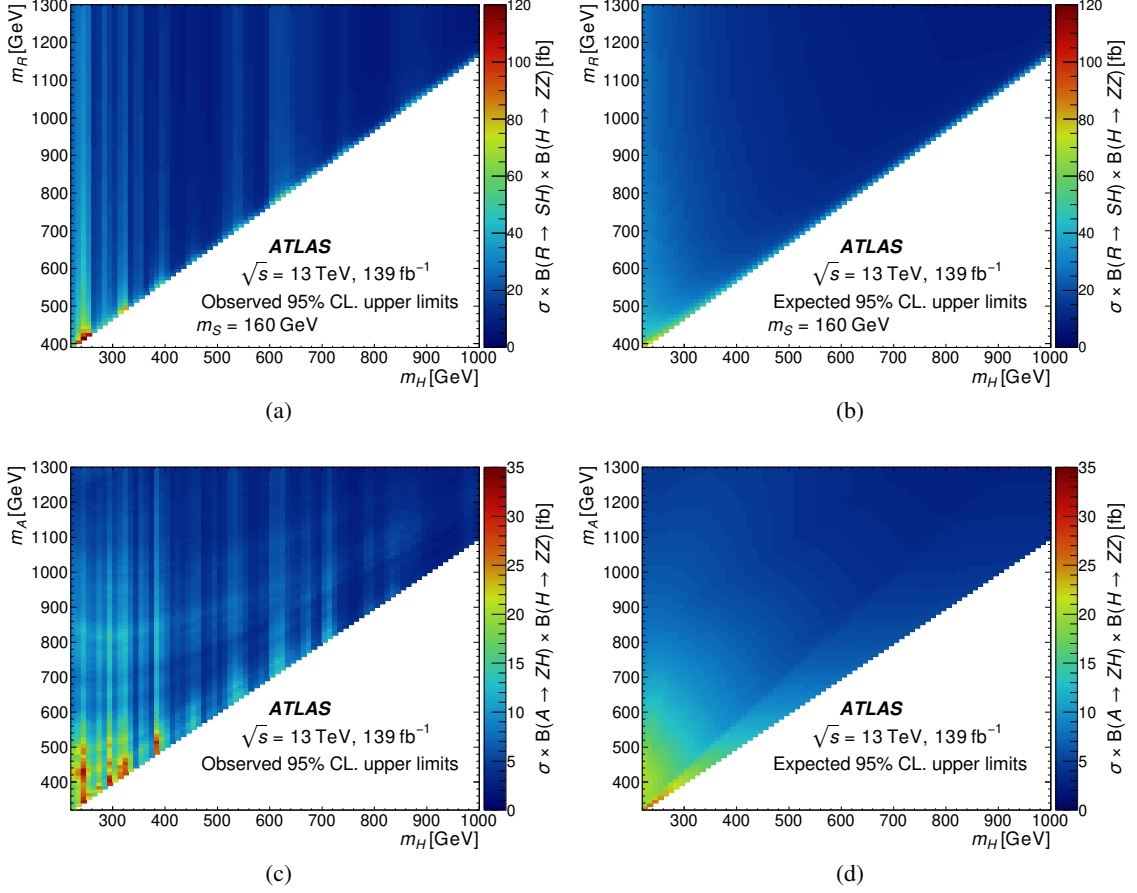


Figure 8: The observed (left) and expected (right) upper limits at 95% confidence level on (a)–(b) $\sigma(gg \rightarrow R) \times \mathcal{B}(R \rightarrow SH) \times \mathcal{B}(H \rightarrow ZZ)$ across the (m_H, m_R) plane with $m_S = 160$ GeV for the $R \rightarrow SH \rightarrow 4\ell + E_T^{\text{miss}}$ search, and on (c)–(d) $\sigma(gg \rightarrow A) \times \mathcal{B}(A \rightarrow ZH) \times \mathcal{B}(H \rightarrow ZZ)$ across the (m_H, m_A) plane for the $A \rightarrow ZH \rightarrow 4\ell + X$ search.

$(m_A, m_H) = (320, 220)$ GeV and $(m_A, m_H) = (1190, 600)$ GeV, for the $A \rightarrow ZH \rightarrow 4\ell + X$ signal were generated using similar configurations as for the NWA signal. Upper limits were computed for signal assumptions in which the A and H bosons have a significant natural width relative to the true mass. They were found to increase as the natural width of the A and H bosons increases. For example, in the case of an $A \rightarrow ZH \rightarrow 4\ell + X$ signal that produces A and H bosons with natural widths of 15% and 5%, respectively, of their true mass, the upper limit worsened by a factor of 1.4 for the low mass point and 1.7 for the high mass point compared to the NWA upper limit. In the $(\Gamma_A/m_A, \Gamma_H/m_H) = (30\%, 10\%)$ case, the upper limit is worsened by a factor of 1.7 for the low mass point and by a factor of 1.9 for the high mass point when compared to the NWA scenario. Table 5 summarises width assumptions, mass points and upper limits for LWA and NWA signals.

Width assumptions	Mass points [GeV]	Upper limits in the $\sigma(gg \rightarrow A)$ [fb]		Ratio w.r.t Narrow width
		Observed	Expected	
Narrow width	$(m_A, m_H) = (320, 220)$	19.6	25.1	1.0
	$(m_A, m_H) = (1190, 600)$	4.8	3.5	1.0
$(\Gamma_A/m_A, \Gamma_H/m_H) = (15\%, 5\%)$	$(m_A, m_H) = (320, 220)$	31.5	36.2	1.4
	$(m_A, m_H) = (1190, 600)$	8.3	6.0	1.7
$(\Gamma_A/m_A, \Gamma_H/m_H) = (30\%, 10\%)$	$(m_A, m_H) = (320, 220)$	38.9	42.5	1.7
	$(m_A, m_H) = (1190, 600)$	8.9	6.6	1.9

Table 5: Observed and expected upper limits at 95% confidence level (CL) on the $\sigma(gg \rightarrow A) \times \mathcal{B}(A \rightarrow ZH) \times \mathcal{B}(H \rightarrow ZZ)$ for different large width approximation signals for comparison with the narrow width approximation. The fraction in the rightmost column corresponds to the ratio between the expected upper limits with large- or narrow width signals. The Γ_A and Γ_H denote the widths of the A and H bosons, respectively.

10 Conclusion

A search for new heavy resonances is performed in a final state with four leptons and missing transverse energy or jets. The search uses proton-proton collision data at a centre-of-mass energy of 13 TeV collected by the ATLAS detector from 2015 to 2018 at the Large Hadron Collider corresponding to a total integrated luminosity of 139 fb^{-1} . The search focuses on two signal processes: $R \rightarrow SH \rightarrow 4\ell + E_{\text{T}}^{\text{miss}}$ and $A \rightarrow ZH \rightarrow 4\ell + X$. For the $R \rightarrow SH \rightarrow 4\ell + E_{\text{T}}^{\text{miss}}$ search, the R boson decays to S and H bosons, where $S \rightarrow \text{invisible}$ and $H \rightarrow ZZ \rightarrow 4\ell$. In the $A \rightarrow ZH \rightarrow 4\ell + X$ search, the A boson decays to Z and H bosons, with two possible decay modes considered for the associated production of Z and H bosons: $A \rightarrow Z(\rightarrow jj/\ell^+\ell^-/\text{invisible})H(\rightarrow 4\ell)$ and $A \rightarrow Z(\rightarrow 2\ell)H(\rightarrow 2\ell + jj/\text{invisible})$. For both the $A \rightarrow ZH \rightarrow 4\ell + X$ and $R \rightarrow SH \rightarrow 4\ell + E_{\text{T}}^{\text{miss}}$ processes, the heavy boson H mass is between 220 GeV and 1000 GeV. The mass range considered for the hypothetical resonance is in the range of 320–1300 GeV for the A boson and 390–1300 GeV for the R boson, while the S boson mass is fixed at 160 GeV, without any significant impact on the results.

No significant deviation above the SM backgrounds is observed. The results are translated into upper limits on $\sigma(gg \rightarrow R) \times \mathcal{B}(R \rightarrow SH) \times \mathcal{B}(H \rightarrow ZZ)$ and $\sigma(gg \rightarrow A) \times \mathcal{B}(A \rightarrow ZH) \times \mathcal{B}(H \rightarrow ZZ)$ at 95% confidence level. For the $R \rightarrow SH \rightarrow 4\ell + E_{\text{T}}^{\text{miss}}$ search, the observed (expected) upper limits range from 6.8–119.2 (7.6–75.8) fb for $(m_R, m_H) = (390, 220)$ GeV to $(m_R, m_H) = (1300, 1000)$ GeV. For the $A \rightarrow ZH \rightarrow 4\ell + X$ search, the observed (expected) upper limits range from 2.1–32.3 (2.7–25.8) fb for $(m_A, m_H) = (320, 220)$ GeV to $(m_A, m_H) = (1300, 1000)$ GeV. This complements previous $A \rightarrow ZH$ searches in various channels (as discussed in Section 1) and contributes to a more comprehensive understanding of the behaviour of A and H bosons. Furthermore, the $R \rightarrow SH \rightarrow 4\ell + E_{\text{T}}^{\text{miss}}$ search extends the gluon-fusion production of the $H \rightarrow ZZ \rightarrow 4\ell$ inclusive analysis, incorporating the possibility of missing transverse energy in the four-lepton final states and extending the phase-space of the search.

Acknowledgements

We thank CERN for the very successful operation of the LHC and its injectors, as well as the support staff at CERN and at our institutions worldwide without whom ATLAS could not be operated efficiently.

The crucial computing support from all WLCG partners is acknowledged gratefully, in particular from CERN, the ATLAS Tier-1 facilities at TRIUMF/SFU (Canada), NDGF (Denmark, Norway, Sweden), CC-IN2P3 (France), KIT/GridKA (Germany), INFN-CNAF (Italy), NL-T1 (Netherlands), PIC (Spain), RAL (UK) and BNL (USA), the Tier-2 facilities worldwide and large non-WLCG resource providers. Major contributors of computing resources are listed in Ref. [89].

We gratefully acknowledge the support of ANPCyT, Argentina; YerPhI, Armenia; ARC, Australia; BMWFW and FWF, Austria; ANAS, Azerbaijan; CNPq and FAPESP, Brazil; NSERC, NRC and CFI, Canada; CERN; ANID, Chile; CAS, MOST and NSFC, China; Minciencias, Colombia; MEYS CR, Czech Republic; DNRF and DNSRC, Denmark; IN2P3-CNRS and CEA-DRF/IRFU, France; SRNSFG, Georgia; BMBF, HGF and MPG, Germany; GSRI, Greece; RGC and Hong Kong SAR, China; ISF and Benoziyo Center, Israel; INFN, Italy; MEXT and JSPS, Japan; CNRST, Morocco; NWO, Netherlands; RCN, Norway; MEiN, Poland; FCT, Portugal; MNE/IFA, Romania; MESTD, Serbia; MSSR, Slovakia; ARIS and MVZI, Slovenia; DSI/NRF, South Africa; MICINN, Spain; SRC and Wallenberg Foundation, Sweden; SERI, SNSF and Cantons of Bern and Geneva, Switzerland; NSTC, Taipei; TENMAK, Türkiye; STFC/UKRI, United Kingdom; DOE and NSF, United States of America.

Individual groups and members have received support from BCKDF, CANARIE, CRC and DRAC, Canada; CERN-CZ, PRIMUS 21/SCI/017 and UNCE SCI/013, Czech Republic; COST, ERC, ERDF, Horizon 2020, ICSC-NextGenerationEU and Marie Skłodowska-Curie Actions, European Union; Investissements d’Avenir Labex, Investissements d’Avenir Idex and ANR, France; DFG and AvH Foundation, Germany; Herakleitos, Thales and Aristeia programmes co-financed by EU-ESF and the Greek NSRF, Greece; BSF-NSF and MINERVA, Israel; Norwegian Financial Mechanism 2014-2021, Norway; NCN and NAWA, Poland; La Caixa Banking Foundation, CERCA Programme Generalitat de Catalunya and PROMETEO and GenT Programmes Generalitat Valenciana, Spain; Göran Gustafssons Stiftelse, Sweden; The Royal Society and Leverhulme Trust, United Kingdom.

In addition, individual members wish to acknowledge support from CERN: European Organization for Nuclear Research (CERN PJA5); Chile: Agencia Nacional de Investigación y Desarrollo (FONDECYT 1190886, FONDECYT 1210400, FONDECYT 1230812, FONDECYT 1230987); China: National Natural Science Foundation of China (NSFC - 12175119, NSFC 12275265, NSFC-12075060); Czech Republic: PRIMUS Research Programme (PRIMUS/21/SCI/017); EU: H2020 European Research Council (ERC - 101002463); European Union: European Research Council (ERC - 948254, ERC 101089007), Horizon 2020 Framework Programme (MUCCA - CHIST-ERA-19-XAI-00), European Union, Future Artificial Intelligence Research (FAIR-NextGenerationEU PE00000013), Italian Center for High Performance Computing, Big Data and Quantum Computing (ICSC, NextGenerationEU); France: Agence Nationale de la Recherche (ANR-20-CE31-0013, ANR-21-CE31-0013, ANR-21-CE31-0022, ANR-22-EDIR-0002), Investissements d’Avenir Labex (ANR-11-LABX-0012); Germany: Baden-Württemberg Stiftung (BW Stiftung-Postdoc Eliteprogramme), Deutsche Forschungsgemeinschaft (DFG - 469666862, DFG - CR 312/5-1); Italy: Istituto Nazionale di Fisica Nucleare (ICSC, NextGenerationEU), Ministero dell’Università e della Ricerca (PRIN - 20223N7F8K - PNRR M4.C2.1.1); Japan: Japan Society for the Promotion of Science (JSPS KAKENHI JP21H05085, JSPS KAKENHI JP22H01227, JSPS KAKENHI JP22H04944, JSPS KAKENHI JP22KK0227); Netherlands: Netherlands Organisation for

Scientific Research (NWO Veni 2020 - VI.Veni.202.179); Norway: Research Council of Norway (RCN-314472); Poland: Polish National Agency for Academic Exchange (PPN/PPO/2020/1/00002/U/00001), Polish National Science Centre (NCN 2021/42/E/ST2/00350, NCN OPUS nr 2022/47/B/ST2/03059, NCN UMO-2019/34/E/ST2/00393, UMO-2020/37/B/ST2/01043, UMO-2021/40/C/ST2/00187, UMO-2022/47/O/ST2/00148); Slovenia: Slovenian Research Agency (ARIS grant J1-3010); Spain: BBVA Foundation (LEO22-1-603), Generalitat Valenciana (Artemisa, FEDER, IDIFEDER/2018/048), La Caixa Banking Foundation (LCF/BQ/PI20/11760025), Ministry of Science and Innovation (MCIN & NextGenEU PCI2022-135018-2, MICIN & FEDER PID2021-125273NB, RYC2019-028510-I, RYC2020-030254-I, RYC2021-031273-I, RYC2022-038164-I), PROMETEO and GenT Programmes Generalitat Valenciana (CIDEAGENT/2019/023, CIDEAGENT/2019/027); Sweden: Swedish Research Council (VR 2018-00482, VR 2022-03845, VR 2022-04683, VR grant 2021-03651), Knut and Alice Wallenberg Foundation (KAW 2017.0100, KAW 2018.0157, KAW 2018.0458, KAW 2019.0447); Switzerland: Swiss National Science Foundation (SNSF - PCEFP2_194658); United Kingdom: Leverhulme Trust (Leverhulme Trust RPG-2020-004); United States of America: U.S. Department of Energy (ECA DE-AC02-76SF00515), Neubauer Family Foundation.

References

- [1] ATLAS Collaboration, *Observation of a new particle in the search for the Standard Model Higgs boson with the ATLAS detector at the LHC*, *Phys. Lett. B* **716** (2012) 1, arXiv: [1207.7214 \[hep-ex\]](#).
- [2] CMS Collaboration, *Observation of a new boson at a mass of 125 GeV with the CMS experiment at the LHC*, *Phys. Lett. B* **716** (2012) 30, arXiv: [1207.7235 \[hep-ex\]](#).
- [3] ATLAS Collaboration, *Measurements of the Higgs boson production and decay rates and coupling strengths using pp collision data at $\sqrt{s} = 7$ and 8 TeV in the ATLAS experiment*, *Eur. Phys. J. C* **76** (2016) 6, arXiv: [1507.04548 \[hep-ex\]](#).
- [4] ATLAS Collaboration, *Study of the spin and parity of the Higgs boson in diboson decays with the ATLAS detector*, *Eur. Phys. J. C* **75** (2015) 476, arXiv: [1506.05669 \[hep-ex\]](#),
Erratum: *Eur. Phys. J. C* **76** (2016) 152.
- [5] CMS Collaboration, *Precise determination of the mass of the Higgs boson and tests of compatibility of its couplings with the standard model predictions using proton collisions at 7 and 8 TeV*, *Eur. Phys. J. C* **75** (2015) 212, arXiv: [1412.8662 \[hep-ex\]](#).
- [6] CMS Collaboration, *Constraints on the spin-parity and anomalous HVV couplings of the Higgs boson in proton collisions at 7 and 8 TeV*, *Phys. Rev. D* **92** (2015) 012004, arXiv: [1411.3441 \[hep-ex\]](#).
- [7] G. C. Branco et al., *Theory and phenomenology of two-Higgs-doublet models*, *Phys. Rept.* **516** (2012) 1, arXiv: [1106.0034](#).
- [8] T. D. Lee, *A Theory of Spontaneous T Violation*, *Phys. Rev. D* **8** (1973) 1226, ed. by G. Feinberg.
- [9] S. von Buddenbrock et al., *Phenomenological signatures of additional scalar bosons at the LHC*, *Eur. Phys. J. C* **76** (2016) 580, arXiv: [1606.01674](#).
- [10] M. Mühlleitner, M. O. P. Sampaio, R. Santos and J. Wittbrodt, *The N2HDM under Theoretical and Experimental Scrutiny*, *JHEP* **03** (2017) 094, arXiv: [1612.01309](#).
- [11] ATLAS Collaboration, *Combination of searches for Higgs boson pairs in pp collisions at $\sqrt{s} = 13$ TeV with the ATLAS detector*, *Phys. Lett. B* **800** (2020) 135103, arXiv: [1906.02025](#).
- [12] CMS Collaboration, *Combination of searches for Higgs boson pair production in proton-proton collisions at $\sqrt{s} = 13$ TeV*, *Phys. Rev. Lett.* **122** (2019) 121803, arXiv: [1811.09689](#).
- [13] ATLAS Collaboration, *Searches for heavy ZZ and ZW resonances in the $\ell\ell qq$ and $\nu\nu qq$ final states in pp collisions at $\sqrt{s} = 13$ TeV with the ATLAS detector*, *JHEP* **03** (2018) 009, arXiv: [1708.09638](#).
- [14] ATLAS Collaboration, *Search for WW/WZ resonance production in $\ell\nu qq$ final states in pp collisions at $\sqrt{s} = 13$ TeV with the ATLAS detector*, *JHEP* **03** (2018) 042, arXiv: [1710.07235](#).
- [15] ATLAS Collaboration, *Search for heavy diboson resonances in semileptonic final states in pp collisions at $\sqrt{s} = 13$ TeV with the ATLAS detector*, *Eur. Phys. J. C* **80** (2020) 1165, arXiv: [2004.14636](#).

- [16] ATLAS Collaboration, *Search for diboson resonances in hadronic final states in 139 fb^{-1} of pp collisions at $\sqrt{s} = 13 \text{ TeV}$ with the ATLAS detector*, [JHEP **09** \(2019\) 091](#), arXiv: [1906.08589](#), Erratum: [JHEP **06** \(2020\) 042](#).
- [17] CMS Collaboration, *Search for a heavy Higgs boson decaying to a pair of W bosons in proton-proton collisions at $\sqrt{s} = 13 \text{ TeV}$* , [JHEP **03** \(2020\) 034](#), arXiv: [1912.01594](#).
- [18] CMS Collaboration, *Search for a new scalar resonance decaying to a pair of Z bosons in proton-proton collisions at $\sqrt{s} = 13 \text{ TeV}$* , [JHEP **06** \(2018\) 127](#), arXiv: [1804.01939](#), Erratum: [JHEP **03** \(2019\) 128](#).
- [19] ATLAS Collaboration, *Search for heavy resonances decaying into a W or Z boson and a Higgs boson in final states with leptons and b -jets in 36 fb^{-1} of $\sqrt{s} = 13 \text{ TeV}$ pp collisions with the ATLAS detector*, [JHEP **03** \(2018\) 174](#), arXiv: [1712.06518](#), Erratum: [JHEP **11** \(2018\) 051](#).
- [20] CMS Collaboration, *Search for a heavy pseudoscalar Higgs boson decaying into a 125 GeV Higgs boson and a Z boson in final states with two tau and two light leptons at $\sqrt{s} = 13 \text{ TeV}$* , [JHEP **03** \(2020\) 065](#), arXiv: [1910.11634](#).
- [21] CMS Collaboration, *Search for neutral resonances decaying into a Z boson and a pair of b jets or τ leptons*, [Phys. Lett. B **759** \(2016\) 369](#), arXiv: [1603.02991](#).
- [22] CMS Collaboration, *Search for new neutral Higgs bosons through the $H \rightarrow ZA \rightarrow \ell^+ \ell^- b \bar{b}$ process in pp collisions at $\sqrt{s} = 13 \text{ TeV}$* , [JHEP **03** \(2020\) 055](#), arXiv: [1911.03781 \[hep-ex\]](#).
- [23] ATLAS Collaboration, *Search for a heavy Higgs boson decaying into a Z boson and another heavy Higgs boson in the $\ell \ell b \bar{b}$ final state in pp collisions at $\sqrt{s} = 13 \text{ TeV}$ with the ATLAS detector*, [Phys. Lett. B **783** \(2018\) 392](#), arXiv: [1804.01126](#).
- [24] ATLAS Collaboration, *Search for a heavy Higgs boson decaying into a Z boson and another heavy Higgs boson in the $\ell \ell b \bar{b}$ and $\ell \ell W W$ final states in pp collisions at $\sqrt{s} = 13 \text{ TeV}$ with the ATLAS detector*, [Eur. Phys. J. C **81** \(2021\) 396](#), arXiv: [2011.05639](#).
- [25] ATLAS Collaboration, *Search for a CP -odd Higgs boson decaying into a heavy CP -even Higgs boson and a Z boson in the $\ell^+ \ell^- t \bar{t}$ and $\nu \bar{\nu} b \bar{b}$ final states using 140 fb^{-1} of data collected with the ATLAS detector*, [JHEP **02** \(2023\) 197](#), arXiv: [2311.04033 \[hep-ex\]](#).
- [26] ATLAS Collaboration, *The ATLAS Experiment at the CERN Large Hadron Collider*, [JINST **3** \(2008\) S08003](#).
- [27] B. Abbott et al., *Production and integration of the ATLAS Insertable B-Layer*, [JINST **13** \(2018\) T05008](#), arXiv: [1803.00844 \[physics.ins-det\]](#).
- [28] ATLAS Collaboration, *Performance of the ATLAS trigger system in 2015*, [Eur. Phys. J. C **77** \(2017\) 317](#), arXiv: [1611.09661 \[hep-ex\]](#).
- [29] ATLAS Collaboration, *The ATLAS Collaboration Software and Firmware*, ATL-SOFT-PUB-2021-001, 2021, URL: <https://cds.cern.ch/record/2767187>.
- [30] ATLAS Collaboration, *ATLAS data quality operations and performance for 2015–2018 data-taking*, [JINST **15** \(2020\) P04003](#), arXiv: [1911.04632 \[physics.ins-det\]](#).

- [31] ATLAS Collaboration, *Performance of electron and photon triggers in ATLAS during LHC Run 2*, *Eur. Phys. J. C* **80** (2020) 47, arXiv: 1909.00761 [hep-ex].
- [32] ATLAS Collaboration, *Performance of the ATLAS muon triggers in Run 2*, *JINST* **15** (2020) P09015, arXiv: 2004.13447 [physics.ins-det].
- [33] ATLAS Collaboration, *2015 start-up trigger menu and initial performance assessment of the ATLAS trigger using Run-2 data*, ATL-DAQ-PUB-2016-001, 2016, URL: <https://cds.cern.ch/record/2136007>.
- [34] ATLAS Collaboration, *Trigger Menu in 2016*, ATL-DAQ-PUB-2017-001, 2017, URL: <https://cds.cern.ch/record/2242069>.
- [35] ATLAS Collaboration, *The ATLAS Simulation Infrastructure*, *Eur. Phys. J. C* **70** (2010) 823, arXiv: 1005.4568 [physics.ins-det].
- [36] S. Agostinelli et al., *GEANT4—a simulation toolkit*, *Nucl. Instrum. Meth. A* **506** (2003) 250.
- [37] T. Sjöstrand, S. Mrenna and P. Skands, *A brief introduction to PYTHIA 8.1*, *Comput. Phys. Commun.* **178** (2008) 852, arXiv: 0710.3820 [hep-ph].
- [38] NNPDF Collaboration, R. D. Ball et al., *Parton distributions with LHC data*, *Nucl. Phys. B* **867** (2013) 244, arXiv: 1207.1303 [hep-ph].
- [39] ATLAS Collaboration, *The Pythia 8 A3 tune description of ATLAS minimum bias and inelastic measurements incorporating the Donnachie–Landshoff diffractive model*, ATL-PHYS-PUB-2016-017, 2016, URL: <https://cds.cern.ch/record/2206965>.
- [40] E. Bothmann et al., *Event generation with Sherpa 2.2*, *SciPost Phys.* **7** (2019) 034, arXiv: 1905.09127 [hep-ph].
- [41] F. Buccioni et al., *OpenLoops 2*, *Eur. Phys. J. C* **79** (2019) 866, arXiv: 1907.13071 [hep-ph].
- [42] F. Cascioli, P. Maierhöfer and S. Pozzorini, *Scattering Amplitudes with Open Loops*, *Phys. Rev. Lett.* **108** (2012) 111601, arXiv: 1111.5206 [hep-ph].
- [43] A. Denner, S. Dittmaier and L. Hofer, *COLLIER: A fortran-based complex one-loop library in extended regularizations*, *Comput. Phys. Commun.* **212** (2017) 220, arXiv: 1604.06792 [hep-ph].
- [44] T. Gleisberg and S. Höche, *Comix, a new matrix element generator*, *JHEP* **12** (2008) 039, arXiv: 0808.3674 [hep-ph].
- [45] S. Schumann and F. Krauss, *A parton shower algorithm based on Catani–Seymour dipole factorisation*, *JHEP* **03** (2008) 038, arXiv: 0709.1027 [hep-ph].
- [46] S. Höche, F. Krauss, M. Schönherr and F. Siegert, *A critical appraisal of NLO+PS matching methods*, *JHEP* **09** (2012) 049, arXiv: 1111.1220 [hep-ph].
- [47] S. Höche, F. Krauss, M. Schönherr and F. Siegert, *QCD matrix elements + parton showers. The NLO case*, *JHEP* **04** (2013) 027, arXiv: 1207.5030 [hep-ph].
- [48] S. Höche, F. Krauss, S. Schumann and F. Siegert, *QCD matrix elements and truncated showers*, *JHEP* **05** (2009) 053, arXiv: 0903.1219 [hep-ph].

- [49] NNPDF Collaboration, R. D. Ball et al., *Parton distributions for the LHC run II*, *JHEP* **04** (2015) 040, arXiv: [1410.8849](#) [[hep-ph](#)].
- [50] J. Alwall, M. Herquet, F. Maltoni, O. Mattelaer and T. Stelzer, *MadGraph 5: going beyond*, *JHEP* **06** (2011) 128, arXiv: [1106.0522](#) [[hep-ph](#)].
- [51] ATLAS Collaboration, *ATLAS Pythia 8 tunes to 7 TeV data*, ATL-PHYS-PUB-2014-021, 2014, URL: <https://cds.cern.ch/record/1966419>.
- [52] S. Alioli, P. Nason, C. Oleari and E. Re, *A general framework for implementing NLO calculations in shower Monte Carlo programs: the POWHEG BOX*, *JHEP* **06** (2010) 043, arXiv: [1002.2581](#) [[hep-ph](#)].
- [53] P. Nason, *A new method for combining NLO QCD with shower Monte Carlo algorithms*, *JHEP* **11** (2004) 040, arXiv: [hep-ph/0409146](#).
- [54] S. Frixione, P. Nason and C. Oleari, *Matching NLO QCD computations with parton shower simulations: the POWHEG method*, *JHEP* **11** (2007) 070, arXiv: [0709.2092](#) [[hep-ph](#)].
- [55] P. Nason and G. Zanderighi, *W^+W^- , WZ and ZZ production in the POWHEG-BOX-V2*, *Eur. Phys. J. C* **74** (2014) 2702, arXiv: [1311.1365](#) [[hep-ph](#)].
- [56] ATLAS Collaboration, *Measurement of the Z/γ^* boson transverse momentum distribution in pp collisions at $\sqrt{s} = 7$ TeV with the ATLAS detector*, *JHEP* **09** (2014) 145, arXiv: [1406.3660](#) [[hep-ex](#)].
- [57] H.-L. Lai et al., *New parton distributions for collider physics*, *Phys. Rev. D* **82** (2010) 074024, arXiv: [1007.2241](#) [[hep-ph](#)].
- [58] J. Pumplin et al., *New Generation of Parton Distributions with Uncertainties from Global QCD Analysis*, *JHEP* **07** (2002) 012, arXiv: [hep-ph/0201195](#).
- [59] D. J. Lange, *The EvtGen particle decay simulation package*, *Nucl. Instrum. Meth. A* **462** (2001) 152.
- [60] S. von Buddenbrock et al., *Multi-lepton signatures of additional scalar bosons beyond the Standard Model at the LHC*, *J. Phys. G* **45** (2018) 115003, arXiv: [1711.07874](#).
- [61] D. Berdine, N. Kauer and D. Rainwater, *Breakdown of the Narrow Width Approximation for New Physics*, *Phys. Rev. Lett.* **99** (2007) 111601, arXiv: [0703058](#).
- [62] T. Sjöstrand et al., *An introduction to PYTHIA 8.2*, *Comput. Phys. Commun.* **191** (2015) 159, arXiv: [1410.3012](#) [[hep-ph](#)].
- [63] R. D. Ball et al., *Impact of Heavy Quark Masses on Parton Distributions and LHC Phenomenology*, *Nucl. Phys. B* **849** (2011) 296, arXiv: [1101.1300](#).
- [64] ATLAS Collaboration, *Electron and photon performance measurements with the ATLAS detector using the 2015–2017 LHC proton–proton collision data*, *JINST* **14** (2019) P12006, arXiv: [1908.00005](#) [[hep-ex](#)].
- [65] ATLAS Collaboration, *Improved electron reconstruction in ATLAS using the Gaussian Sum Filter-based model for bremsstrahlung*, ATLAS-CONF-2012-047, 2012, URL: <https://cds.cern.ch/record/1449796>.

- [66] ATLAS Collaboration, *Electron reconstruction and identification in the ATLAS experiment using the 2015 and 2016 LHC proton–proton collision data at $\sqrt{s} = 13$ TeV*, *Eur. Phys. J. C* **79** (2019) 639, arXiv: [1902.04655 \[physics.ins-det\]](#).
- [67] ATLAS Collaboration, *Muon reconstruction and identification efficiency in ATLAS using the full Run 2 pp collision data set at $\sqrt{s} = 13$ TeV*, *Eur. Phys. J. C* **81** (2021) 578, arXiv: [2012.00578 \[hep-ex\]](#).
- [68] ATLAS Collaboration, *Jet reconstruction and performance using particle flow with the ATLAS Detector*, *Eur. Phys. J. C* **77** (2017) 466, arXiv: [1703.10485 \[hep-ex\]](#).
- [69] M. Cacciari, G. P. Salam and G. Soyez, *The anti- k_t jet clustering algorithm*, *JHEP* **04** (2008) 063, arXiv: [0802.1189 \[hep-ph\]](#).
- [70] ATLAS Collaboration, *Jet energy scale and resolution measured in proton–proton collisions at $\sqrt{s} = 13$ TeV with the ATLAS detector*, *Eur. Phys. J. C* **81** (2021) 689, arXiv: [2007.02645 \[hep-ex\]](#).
- [71] ATLAS Collaboration, *Performance of pile-up mitigation techniques for jets in pp collisions at $\sqrt{s} = 8$ TeV using the ATLAS detector*, *Eur. Phys. J. C* **76** (2016) 581, arXiv: [1510.03823 \[hep-ex\]](#).
- [72] ATLAS Collaboration, *Tagging and suppression of pileup jets with the ATLAS detector*, ATLAS-CONF-2014-018, 2014, URL: <https://cds.cern.ch/record/1700870>.
- [73] ATLAS Collaboration, *ATLAS b -jet identification performance and efficiency measurement with $t\bar{t}$ events in pp collisions at $\sqrt{s} = 13$ TeV*, *Eur. Phys. J. C* **79** (2019) 970, arXiv: [1907.05120 \[hep-ex\]](#).
- [74] ATLAS Collaboration, *Optimisation and performance studies of the ATLAS b -tagging algorithms for the 2017-18 LHC run*, ATL-PHYS-PUB-2017-013, 2017, URL: <https://cds.cern.ch/record/2273281>.
- [75] ATLAS Collaboration, *E_T^{miss} performance in the ATLAS detector using 2015–2016 LHC pp collisions*, ATLAS-CONF-2018-023, 2018, URL: <https://cds.cern.ch/record/2625233>.
- [76] ATLAS Collaboration, *Search for an additional, heavy Higgs boson in the $H \rightarrow ZZ$ decay channel at $\sqrt{s} = 8$ TeV in pp collision data with the ATLAS detector*, *Eur. Phys. J. C* **76** (2016) 45, arXiv: [1507.05930 \[hep-ex\]](#).
- [77] ATLAS Collaboration, *Search for heavy ZZ resonances in the $\ell^+\ell^-\ell^+\ell^-$ and $\ell^+\ell^-\nu\bar{\nu}$ final states using proton–proton collisions at $\sqrt{s} = 13$ TeV with the ATLAS detector*, *Eur. Phys. J. C* **78** (2018) 293, arXiv: [1712.06386 \[hep-ex\]](#).
- [78] ATLAS Collaboration, *Search for heavy resonances decaying into a pair of Z bosons in the $\ell^+\ell^-\ell^+\ell^-$ and $\ell^+\ell^-\nu\bar{\nu}$ final states using 139fb^{-1} of proton–proton collisions at $\sqrt{s} = 13$ TeV with the ATLAS detector*, *Eur. Phys. J. C* **81** (2021) 332, arXiv: [2009.14791 \[hep-ex\]](#).
- [79] A. L. Read, *Linear interpolation of histograms*, *Nucl. Instrum. Meth. A* **425** (1999) 357.
- [80] ATLAS Collaboration, *Muon reconstruction performance of the ATLAS detector in proton–proton collision data at $\sqrt{s} = 13$ TeV*, *Eur. Phys. J. C* **76** (2016) 292, arXiv: [1603.05598 \[hep-ex\]](#).

- [81] ATLAS Collaboration, *Performance of the missing transverse momentum triggers for the ATLAS detector during Run-2 data taking*, *JHEP* **08** (2020) 080, arXiv: [2005.09554](#).
- [82] ATLAS Collaboration, *Luminosity determination in pp collisions at $\sqrt{s} = 13$ TeV using the ATLAS detector at the LHC*, ATLAS-CONF-2019-021, 2019, URL: <https://cds.cern.ch/record/2677054>.
- [83] G. Avoni et al., *The new LUCID-2 detector for luminosity measurement and monitoring in ATLAS*, *JINST* **13** (2018) P07017.
- [84] A. Kalogeropoulos and J. Alwall, *The SysCalc code: A tool to derive theoretical systematic uncertainties*, 2018, arXiv: [1801.08401](#).
- [85] J. Butterworth et al., *PDF4LHC recommendations for LHC Run II*, *J. Phys. G* **43** (2016) 023001, arXiv: [1510.03865](#) [[hep-ph](#)].
- [86] J. Bellm et al., *Herwig 7.0/Herwig++ 3.0 release note*, *Eur. Phys. J. C* **76** (2016) 196, arXiv: [1512.01178](#) [[hep-ph](#)].
- [87] G. Cowan, K. Cranmer, E. Gross and O. Vitells, *Asymptotic formulae for likelihood-based tests of new physics*, *Eur. Phys. J. C* **71** (2011) 1554, arXiv: [1007.1727](#) [[physics.data-an](#)], Erratum: *Eur. Phys. J. C* **73** (2013) 2501.
- [88] A. L. Read, *Presentation of search results: the CL_S technique*, *J. Phys. G* **28** (2002) 2693.
- [89] ATLAS Collaboration, *ATLAS Computing Acknowledgements*, ATL-SOFT-PUB-2023-001, 2023, URL: <https://cds.cern.ch/record/2869272>.

The ATLAS Collaboration

G. Aad ¹⁰², E. Aakvaag ¹⁶, B. Abbott ¹²⁰, K. Abeling ⁵⁵, N.J. Abicht ⁴⁹, S.H. Abidi ²⁹, A. Aboulhorma ^{35e}, H. Abramowicz ¹⁵¹, H. Abreu ¹⁵⁰, Y. Abulaiti ¹¹⁷, B.S. Acharya ^{69a,69b,m}, C. Adam Bourdarios ⁴, L. Adamczyk ^{86a}, S.V. Addepalli ²⁶, M.J. Addison ¹⁰¹, J. Adelman ¹¹⁵, A. Adiguzel ^{21c}, T. Adye ¹³⁴, A.A. Affolder ¹³⁶, Y. Afik ³⁹, M.N. Agaras ¹³, J. Agarwala ^{73a,73b}, A. Aggarwal ¹⁰⁰, C. Agheorghiesei ^{27c}, A. Ahmad ³⁶, F. Ahmadov ^{38,aa}, W.S. Ahmed ¹⁰⁴, S. Ahuja ⁹⁵, X. Ai ^{62e}, G. Aielli ^{76a,76b}, A. Aikot ¹⁶³, M. Ait Tamlihat ^{35e}, B. Aitbenchikh ^{35a}, I. Aizenberg ¹⁶⁹, M. Akbiyik ¹⁰⁰, T.P.A. Åkesson ⁹⁸, A.V. Akimov ³⁷, D. Akiyama ¹⁶⁸, N.N. Akolkar ²⁴, S. Aktas ^{21a}, K. Al Houry ⁴¹, G.L. Alberghi ^{23b}, J. Albert ¹⁶⁵, P. Albicocco ⁵³, G.L. Albouy ⁶⁰, S. Alderweireldt ⁵², Z.L. Alegria ¹²¹, M. Aleksa ³⁶, I.N. Aleksandrov ³⁸, C. Alexa ^{27b}, T. Alexopoulos ¹⁰, F. Alfonsi ^{23b}, M. Algren ⁵⁶, M. Alhroob ¹⁴¹, B. Ali ¹³², H.M.J. Ali ⁹¹, S. Ali ¹⁴⁸, S.W. Alibocus ⁹², M. Aliev ^{33c}, G. Alimonti ^{71a}, W. Alkakh ⁵⁵, C. Allaire ⁶⁶, B.M.M. Allbrooke ¹⁴⁶, J.F. Allen ⁵², C.A. Allendes Flores ^{137f}, P.P. Allport ²⁰, A. Aloisio ^{72a,72b}, F. Alonso ⁹⁰, C. Alpigiani ¹³⁸, M. Alvarez Estevez ⁹⁹, A. Alvarez Fernandez ¹⁰⁰, M. Alves Cardoso ⁵⁶, M.G. Alviggi ^{72a,72b}, M. Aly ¹⁰¹, Y. Amaral Coutinho ^{83b}, A. Ambler ¹⁰⁴, C. Amelung ³⁶, M. Amerl ¹⁰¹, C.G. Ames ¹⁰⁹, D. Amidei ¹⁰⁶, S.P. Amor Dos Santos ^{130a}, K.R. Amos ¹⁶³, V. Ananiev ¹²⁵, C. Anastopoulos ¹³⁹, T. Andeen ¹¹, J.K. Anders ³⁶, S.Y. Andreat ^{47a,47b}, A. Andreatza ^{71a,71b}, S. Angelidakis ⁹, A. Angerami ^{41,ad}, A.V. Anisenkov ³⁷, A. Annovi ^{74a}, C. Antel ⁵⁶, M.T. Anthony ¹³⁹, E. Antipov ¹⁴⁵, M. Antonelli ⁵³, F. Anulli ^{75a}, M. Aoki ⁸⁴, T. Aoki ¹⁵³, J.A. Aparisi Pozo ¹⁶³, M.A. Aparo ¹⁴⁶, L. Aperio Bella ⁴⁸, C. Appelt ¹⁸, A. Apyan ²⁶, S.J. Arbiol Val ⁸⁷, C. Arcangeletti ⁵³, A.T.H. Arce ⁵¹, E. Arena ⁹², J-F. Arguin ¹⁰⁸, S. Argyropoulos ⁵⁴, J.-H. Arling ⁴⁸, O. Arnaez ⁴, H. Arnold ¹¹⁴, G. Artoni ^{75a,75b}, H. Asada ¹¹¹, K. Asai ¹¹⁸, S. Asai ¹⁵³, N.A. Asbah ³⁶, K. Assamagan ²⁹, R. Astalos ^{28a}, S. Atashi ¹⁵⁹, R.J. Atkin ^{33a}, M. Atkinson ¹⁶², H. Atmani ^{35f}, P.A. Atlasiddha ¹²⁸, K. Augsten ¹³², S. Auricchio ^{72a,72b}, A.D. Auriol ²⁰, V.A. Austrup ¹⁰¹, G. Avolio ³⁶, K. Axiotis ⁵⁶, G. Azuelos ^{108,ah}, D. Babal ^{28b}, H. Bachacou ¹³⁵, K. Bachas ^{152,q}, A. Bachi ³⁴, F. Backman ^{47a,47b}, A. Badea ³⁹, T.M. Baer ¹⁰⁶, P. Bagnaia ^{75a,75b}, M. Bahmani ¹⁸, D. Bahner ⁵⁴, K. Bai ¹²³, A.J. Bailey ¹⁶³, V.R. Bailey ¹⁶², J.T. Baines ¹³⁴, L. Baines ⁹⁴, O.K. Baker ¹⁷², E. Bakos ¹⁵, D. Bakshi Gupta ⁸, V. Balakrishnan ¹²⁰, R. Balasubramanian ¹¹⁴, E.M. Baldin ³⁷, P. Balek ^{86a}, E. Ballabene ^{23b,23a}, F. Balli ¹³⁵, L.M. Baltes ^{63a}, W.K. Balunas ³², J. Balz ¹⁰⁰, E. Banas ⁸⁷, M. Bandieramonte ¹²⁹, A. Bandyopadhyay ²⁴, S. Bansal ²⁴, L. Barak ¹⁵¹, M. Barakat ⁴⁸, E.L. Barberio ¹⁰⁵, D. Barberis ^{57b,57a}, M. Barbero ¹⁰², M.Z. Barel ¹¹⁴, K.N. Barends ^{33a}, T. Barillari ¹¹⁰, M-S. Barisits ³⁶, T. Barklow ¹⁴³, P. Baron ¹²², D.A. Baron Moreno ¹⁰¹, A. Baroncelli ^{62a}, G. Barone ²⁹, A.J. Barr ¹²⁶, J.D. Barr ⁹⁶, F. Barreiro ⁹⁹, J. Barreiro Guimarães da Costa ^{14a}, U. Barron ¹⁵¹, M.G. Barros Teixeira ^{130a}, S. Barsov ³⁷, F. Bartels ^{63a}, R. Bartoldus ¹⁴³, A.E. Barton ⁹¹, P. Bartos ^{28a}, A. Basan ¹⁰⁰, M. Baselga ⁴⁹, A. Bassalat ^{66,b}, M.J. Basso ^{156a}, C.R. Basson ¹⁰¹, R.L. Bates ⁵⁹, S. Batlamous ^{35e}, B. Batool ¹⁴¹, M. Battaglia ¹³⁶, D. Battulga ¹⁸, M. Baucé ^{75a,75b}, M. Bauer ³⁶, P. Bauer ²⁴, L.T. Bazzano Hurrell ³⁰, J.B. Beacham ⁵¹, T. Beau ¹²⁷, J.Y. Beauchamp ⁹⁰, P.H. Beauchemin ¹⁵⁸, P. Bechtel ²⁴, H.P. Beck ^{19,p}, K. Becker ¹⁶⁷, A.J. Beddall ⁸², V.A. Bednyakov ³⁸, C.P. Bee ¹⁴⁵, L.J. Beemster ¹⁵, T.A. Beermann ³⁶, M. Begalli ^{83d}, M. Begel ²⁹, A. Behera ¹⁴⁵, J.K. Behr ⁴⁸, J.F. Beirer ³⁶, F. Beisiegel ²⁴, M. Belfkir ^{116b}, G. Bella ¹⁵¹, L. Bellagamba ^{23b}, A. Bellerive ³⁴, P. Bellos ²⁰, K. Beloborodov ³⁷, D. Benchechroun ^{35a}, F. Bendebba ^{35a}, Y. Benhammou ¹⁵¹, K.C. Benkendorfer ⁶¹, L. Beresford ⁴⁸, M. Beretta ⁵³, E. Bergeas Kuutmann ¹⁶¹, N. Berger ⁴,

B. Bergmann [ID132](#), J. Beringer [ID17a](#), G. Bernardi [ID5](#), C. Bernius [ID143](#), F.U. Bernlochner [ID24](#),
 F. Bernon [ID36,102](#), A. Berrocal Guardia [ID13](#), T. Berry [ID95](#), P. Berta [ID133](#), A. Berthold [ID50](#), S. Bethke [ID110](#),
 A. Betti [ID75a,75b](#), A.J. Bevan [ID94](#), N.K. Bhalla [ID54](#), M. Bhamjee [ID33c](#), S. Bhatta [ID145](#),
 D.S. Bhattacharya [ID166](#), P. Bhattarai [ID143](#), K.D. Bhide [ID54](#), V.S. Bhopatkar [ID121](#), R.M. Bianchi [ID129](#),
 G. Bianco [ID23b,23a](#), O. Biebel [ID109](#), R. Bielski [ID123](#), M. Biglietti [ID77a](#), C.S. Billingsley [ID44](#), M. Bindi [ID55](#),
 A. Bingul [ID21b](#), C. Bini [ID75a,75b](#), A. Biondini [ID92](#), C.J. Birch-sykes [ID101](#), G.A. Bird [ID32](#), M. Birman [ID169](#),
 M. Biros [ID133](#), S. Biryukov [ID146](#), T. Bisanz [ID49](#), E. Bisceglie [ID43b,43a](#), J.P. Biswal [ID134](#), D. Biswas [ID141](#),
 K. Bjørke [ID125](#), I. Bloch [ID48](#), A. Blue [ID59](#), U. Blumenschein [ID94](#), J. Blumenthal [ID100](#),
 V.S. Bobrovnikov [ID37](#), M. Boehler [ID54](#), B. Boehm [ID166](#), D. Bogavac [ID36](#), A.G. Bogdanchikov [ID37](#),
 C. Bohm [ID47a](#), V. Boisvert [ID95](#), P. Bokan [ID36](#), T. Bold [ID86a](#), M. Bomben [ID5](#), M. Bona [ID94](#),
 M. Boonekamp [ID135](#), C.D. Booth [ID95](#), A.G. Borbély [ID59](#), I.S. Bordulev [ID37](#), H.M. Borecka-Bielska [ID108](#),
 G. Borissov [ID91](#), D. Bortoletto [ID126](#), D. Boscherini [ID23b](#), M. Bosman [ID13](#), J.D. Bossio Sola [ID36](#),
 K. Bouaouda [ID35a](#), N. Bouchhar [ID163](#), J. Boudreau [ID129](#), E.V. Bouhova-Thacker [ID91](#), D. Boumediene [ID40](#),
 R. Bouquet [ID57b,57a](#), A. Boveia [ID119](#), J. Boyd [ID36](#), D. Boye [ID29](#), I.R. Boyko [ID38](#), J. Bracinik [ID20](#),
 N. Brahim [ID4](#), G. Brandt [ID171](#), O. Brandt [ID32](#), F. Braren [ID48](#), B. Brau [ID103](#), J.E. Brau [ID123](#),
 R. Brenner [ID169](#), L. Brenner [ID114](#), R. Brenner [ID161](#), S. Bressler [ID169](#), D. Britton [ID59](#), D. Britzger [ID110](#),
 I. Brock [ID24](#), G. Brooijmans [ID41](#), E. Brost [ID29](#), L.M. Brown [ID165](#), L.E. Bruce [ID61](#), T.L. Bruckler [ID126](#),
 P.A. Bruckman de Renstrom [ID87](#), B. Brüers [ID48](#), A. Bruni [ID23b](#), G. Bruni [ID23b](#), M. Bruschi [ID23b](#),
 N. Brusino [ID75a,75b](#), T. Buanes [ID16](#), Q. Buat [ID138](#), D. Buchin [ID110](#), A.G. Buckley [ID59](#), O. Bulekov [ID37](#),
 B.A. Bullard [ID143](#), S. Burdin [ID92](#), C.D. Burgard [ID49](#), A.M. Burger [ID36](#), B. Burghgrave [ID8](#),
 O. Burlayenko [ID54](#), J.T.P. Burr [ID32](#), C.D. Burton [ID11](#), J.C. Burzynski [ID142](#), E.L. Busch [ID41](#),
 V. Büscher [ID100](#), P.J. Bussey [ID59](#), J.M. Butler [ID25](#), C.M. Buttar [ID59](#), J.M. Butterworth [ID96](#),
 W. Buttinger [ID134](#), C.J. Buxo Vazquez [ID107](#), A.R. Buzykaev [ID37](#), S. Cabrera Urbán [ID163](#),
 L. Cadamuro [ID66](#), D. Caforio [ID58](#), H. Cai [ID129](#), Y. Cai [ID14a,14e](#), Y. Cai [ID14c](#), V.M.M. Cairo [ID36](#),
 O. Cakir [ID3a](#), N. Calace [ID36](#), P. Calafura [ID17a](#), G. Calderini [ID127](#), P. Calfayan [ID68](#), G. Callea [ID59](#),
 L.P. Caloba [ID83b](#), D. Calvet [ID40](#), S. Calvet [ID40](#), M. Calvetti [ID74a,74b](#), R. Camacho Toro [ID127](#),
 S. Camarda [ID36](#), D. Camarero Munoz [ID26](#), P. Camarri [ID76a,76b](#), M.T. Camerlingo [ID72a,72b](#),
 D. Cameron [ID36](#), C. Camincher [ID165](#), M. Campanelli [ID96](#), A. Camplani [ID42](#), V. Canale [ID72a,72b](#),
 A.C. Canbay [ID3a](#), J. Cantero [ID163](#), Y. Cao [ID162](#), F. Capocasa [ID26](#), M. Capua [ID43b,43a](#), A. Carbone [ID71a,71b](#),
 R. Cardarelli [ID76a](#), J.C.J. Cardenas [ID8](#), F. Cardillo [ID163](#), G. Carducci [ID43b,43a](#), T. Carli [ID36](#),
 G. Carlino [ID72a](#), J.I. Carlotto [ID13](#), B.T. Carlson [ID129,r](#), E.M. Carlson [ID165,156a](#), L. Carminati [ID71a,71b](#),
 A. Carnelli [ID135](#), M. Carnesale [ID75a,75b](#), S. Caron [ID113](#), E. Carquin [ID137f](#), S. Carrá [ID71a](#),
 G. Carratta [ID23b,23a](#), A.M. Carroll [ID123](#), T.M. Carter [ID52](#), M.P. Casado [ID13,i](#), M. Caspar [ID48](#),
 F.L. Castillo [ID4](#), L. Castillo Garcia [ID13](#), V. Castillo Gimenez [ID163](#), N.F. Castro [ID130a,130e](#),
 A. Catinaccio [ID36](#), J.R. Catmore [ID125](#), T. Cavaliere [ID4](#), V. Cavaliere [ID29](#), N. Cavalli [ID23b,23a](#),
 Y.C. Cekmecelioglu [ID48](#), E. Celebi [ID21a](#), F. Celli [ID126](#), M.S. Centonze [ID70a,70b](#), V. Cepaitis [ID56](#),
 K. Cerny [ID122](#), A.S. Cerqueira [ID83a](#), A. Cerri [ID146](#), L. Cerrito [ID76a,76b](#), F. Cerutti [ID17a](#), B. Cervato [ID141](#),
 A. Cervelli [ID23b](#), G. Cesarini [ID53](#), S.A. Cetin [ID82](#), D. Chakraborty [ID115](#), J. Chan [ID17a](#), W.Y. Chan [ID153](#),
 J.D. Chapman [ID32](#), E. Chapon [ID135](#), B. Chargeishvili [ID149b](#), D.G. Charlton [ID20](#), M. Chatterjee [ID19](#),
 C. Chauhan [ID133](#), Y. Che [ID14c](#), S. Chekanov [ID6](#), S.V. Chekulaev [ID156a](#), G.A. Chelkov [ID38,a](#),
 A. Chen [ID106](#), B. Chen [ID151](#), B. Chen [ID165](#), H. Chen [ID14c](#), H. Chen [ID29](#), J. Chen [ID62c](#), J. Chen [ID142](#),
 M. Chen [ID126](#), S. Chen [ID153](#), S.J. Chen [ID14c](#), X. Chen [ID62c,135](#), X. Chen [ID14b,ag](#), Y. Chen [ID62a](#),
 C.L. Cheng [ID170](#), H.C. Cheng [ID64a](#), S. Cheong [ID143](#), A. Cheplakov [ID38](#), E. Cheremushkina [ID48](#),
 E. Cherepanova [ID114](#), R. Cherkaoui El Moursli [ID35e](#), E. Cheu [ID7](#), K. Cheung [ID65](#), L. Chevalier [ID135](#),
 V. Chiarella [ID53](#), G. Chiarelli [ID74a](#), N. Chiedde [ID102](#), G. Chiodini [ID70a](#), A.S. Chisholm [ID20](#),
 A. Chitan [ID27b](#), M. Chitishvili [ID163](#), M.V. Chizhov [ID38,s](#), K. Choi [ID11](#), Y. Chou [ID138](#), E.Y.S. Chow [ID113](#),
 K.L. Chu [ID169](#), M.C. Chu [ID64a](#), X. Chu [ID14a,14e](#), J. Chudoba [ID131](#), J.J. Chwastowski [ID87](#), D. Cieri [ID110](#),

K.M. Ciesla ^{86a}, V. Cindro ⁹³, A. Ciocio ^{17a}, F. Cirotto ^{72a,72b}, Z.H. Citron ^{169,k}, M. Citterio ^{71a},
 D.A. Ciubotaru ^{27b}, A. Clark ⁵⁶, P.J. Clark ⁵², C. Clarry ¹⁵⁵, J.M. Clavijo Columbie ⁴⁸,
 S.E. Clawson ⁴⁸, C. Clement ^{47a,47b}, J. Clercx ⁴⁸, Y. Coadou ¹⁰², M. Cobal ^{69a,69c},
 A. Coccaro ^{57b}, R.F. Coelho Barrue ^{130a}, R. Coelho Lopes De Sa ¹⁰³, S. Coelli ^{71a}, B. Cole ⁴¹,
 J. Collot ⁶⁰, P. Conde Muiño ^{130a,130g}, M.P. Connell ^{33c}, S.H. Connell ^{33c}, E.I. Conroy ¹²⁶,
 F. Conventi ^{72a,ai}, H.G. Cooke ²⁰, A.M. Cooper-Sarkar ¹²⁶, A. Cordeiro Oudot Choi ¹²⁷,
 L.D. Corpe ⁴⁰, M. Corradi ^{75a,75b}, F. Corriveau ^{104,y}, A. Cortes-Gonzalez ¹⁸, M.J. Costa ¹⁶³,
 F. Costanza ⁴, D. Costanzo ¹³⁹, B.M. Cote ¹¹⁹, G. Cowan ⁹⁵, K. Cranmer ¹⁷⁰,
 D. Cremonini ^{23b,23a}, S. Crépe-Renaudin ⁶⁰, F. Crescioli ¹²⁷, M. Cristinziani ¹⁴¹,
 M. Cristoforetti ^{78a,78b}, V. Croft ¹¹⁴, J.E. Crosby ¹²¹, G. Crosetti ^{43b,43a}, A. Cueto ⁹⁹,
 T. Cuhadar Donszelmann ¹⁵⁹, H. Cui ^{14a,14e}, Z. Cui ⁷, W.R. Cunningham ⁵⁹, F. Curcio ^{43b,43a},
 P. Czodrowski ³⁶, M.M. Czurylo ^{63b}, M.J. Da Cunha Sargedas De Sousa ^{57b,57a},
 J.V. Da Fonseca Pinto ^{83b}, C. Da Via ¹⁰¹, W. Dabrowski ^{86a}, T. Dado ⁴⁹, S. Dahbi ¹⁴⁸,
 T. Dai ¹⁰⁶, D. Dal Santo ¹⁹, C. Dallapiccola ¹⁰³, M. Dam ⁴², G. D'amen ²⁹, V. D'Amico ¹⁰⁹,
 J. Damp ¹⁰⁰, J.R. Dandoy ³⁴, M. Danninger ¹⁴², V. Dao ³⁶, G. Darbo ^{57b}, S. Darmora ⁶,
 S.J. Das ^{29,aj}, S. D'Auria ^{71a,71b}, A. D'Avanzo ^{130a}, C. David ^{33a}, T. Davidek ¹³³,
 B. Davis-Purcell ³⁴, I. Dawson ⁹⁴, H.A. Day-hall ¹³², K. De ⁸, R. De Asmundis ^{72a},
 N. De Biase ⁴⁸, S. De Castro ^{23b,23a}, N. De Groot ¹¹³, P. de Jong ¹¹⁴, H. De la Torre ¹¹⁵,
 A. De Maria ^{14c}, A. De Salvo ^{75a}, U. De Sanctis ^{76a,76b}, F. De Santis ^{70a,70b}, A. De Santo ¹⁴⁶,
 J.B. De Vivie De Regie ⁶⁰, D.V. Dedovich ³⁸, J. Degens ¹¹⁴, A.M. Deiana ⁴⁴, F. Del Corso ^{23b,23a},
 J. Del Peso ⁹⁹, F. Del Rio ^{63a}, L. Delagrangé ¹²⁷, F. Deliot ¹³⁵, C.M. Delitzsch ⁴⁹,
 M. Della Pietra ^{72a,72b}, D. Della Volpe ⁵⁶, A. Dell'Acqua ³⁶, L. Dell'Asta ^{71a,71b}, M. Delmastro ⁴,
 P.A. Delsart ⁶⁰, S. Demers ¹⁷², M. Demichev ³⁸, S.P. Denisov ³⁷, L. D'Eramo ⁴⁰,
 D. Derendarz ⁸⁷, F. Derue ¹²⁷, P. Dervan ⁹², K. Desch ²⁴, C. Deutsch ²⁴, F.A. Di Bello ^{57b,57a},
 A. Di Ciaccio ^{76a,76b}, L. Di Ciaccio ⁴, A. Di Domenico ^{75a,75b}, C. Di Donato ^{72a,72b},
 A. Di Girolamo ³⁶, G. Di Gregorio ³⁶, A. Di Luca ^{78a,78b}, B. Di Micco ^{77a,77b}, R. Di Nardo ^{77a,77b},
 M. Diamantopoulou ³⁴, F.A. Dias ¹¹⁴, T. Dias Do Vale ¹⁴², M.A. Diaz ^{137a,137b},
 F.G. Diaz Capriles ²⁴, M. Didenko ¹⁶³, E.B. Diehl ¹⁰⁶, S. Díez Cornell ⁴⁸, C. Diez Pardos ¹⁴¹,
 C. Dimitriadi ^{161,24}, A. Dimitrievska ^{17a}, J. Dingfelder ²⁴, I-M. Dinu ^{27b}, S.J. Dittmeier ^{63b},
 F. Dittus ³⁶, F. Djama ¹⁰², T. Djobava ^{149b}, C. Doglioni ^{101,98}, A. Dohnalova ^{28a}, J. Dolejsi ¹³³,
 Z. Dolezal ¹³³, K.M. Dona ³⁹, M. Donadelli ^{83c}, B. Dong ¹⁰⁷, J. Donini ⁴⁰, A. D'Onofrio ^{72a,72b},
 M. D'Onofrio ⁹², J. Dopke ¹³⁴, A. Doria ^{72a}, N. Dos Santos Fernandes ^{130a}, P. Dougan ¹⁰¹,
 M.T. Dova ⁹⁰, A.T. Doyle ⁵⁹, M.A. Draguet ¹²⁶, E. Dreyer ¹⁶⁹, I. Drivas-koulouris ¹⁰,
 M. Drnevich ¹¹⁷, M. Drozdova ⁵⁶, D. Du ^{62a}, T.A. du Pree ¹¹⁴, F. Dubinin ³⁷, M. Dubovsky ^{28a},
 E. Duchovni ¹⁶⁹, G. Duckeck ¹⁰⁹, O.A. Ducu ^{27b}, D. Duda ⁵², A. Dudarev ³⁶, E.R. Duden ²⁶,
 M. D'uffizi ¹⁰¹, L. Duflot ⁶⁶, M. Dührssen ³⁶, A.E. Dumitriu ^{27b}, M. Dunford ^{63a}, S. Dungs ⁴⁹,
 K. Dunne ^{47a,47b}, A. Duperrin ¹⁰², H. Duran Yildiz ^{3a}, M. Düren ⁵⁸, A. Durglishvili ^{149b},
 B.L. Dwyer ¹¹⁵, G.I. Dyckes ^{17a}, M. Dyndal ^{86a}, B.S. Dziedzic ⁸⁷, Z.O. Earnshaw ¹⁴⁶,
 G.H. Eberwein ¹²⁶, B. Eckerova ^{28a}, S. Eggebrecht ⁵⁵, E. Egidio Purcino De Souza ¹²⁷,
 L.F. Ehrke ⁵⁶, G. Eigen ¹⁶, K. Einsweiler ^{17a}, T. Ekelof ¹⁶¹, P.A. Ekman ⁹⁸, S. El Farkh ^{35b},
 Y. El Ghazali ^{35b}, H. El Jarrari ³⁶, A. El Moussaouy ¹⁰⁸, V. Ellajosyula ¹⁶¹, M. Ellert ¹⁶¹,
 F. Ellinghaus ¹⁷¹, N. Ellis ³⁶, J. Elmsheuser ²⁹, M. Elsing ³⁶, D. Emeliyanov ¹³⁴, Y. Enari ¹⁵³,
 I. Ene ^{17a}, S. Epari ¹³, P.A. Erland ⁸⁷, M. Errenst ¹⁷¹, M. Escalier ⁶⁶, C. Escobar ¹⁶³,
 E. Etzion ¹⁵¹, G. Evans ^{130a}, H. Evans ⁶⁸, L.S. Evans ⁹⁵, A. Ezhilov ³⁷, S. Ezzarqtouni ^{35a},
 F. Fabbri ^{23b,23a}, L. Fabbri ^{23b,23a}, G. Facini ⁹⁶, V. Fadeyev ¹³⁶, R.M. Fakhrutdinov ³⁷,
 D. Fakoudis ¹⁰⁰, S. Falciano ^{75a}, L.F. Falda Ulhoa Coelho ³⁶, P.J. Falke ²⁴, J. Faltova ¹³³,
 C. Fan ¹⁶², Y. Fan ^{14a}, Y. Fang ^{14a,14e}, M. Fanti ^{71a,71b}, M. Faraj ^{69a,69b}, Z. Farazpay ⁹⁷,

A. Farbin ⁸, A. Farilla ^{77a}, T. Farooque ¹⁰⁷, S.M. Farrington ⁵², F. Fassi ^{35e}, D. Fassouliotis ⁹,
 M. Faucci Giannelli ^{76a,76b}, W.J. Fawcett ³², L. Fayard ⁶⁶, P. Federic ¹³³, P. Federicova ¹³¹,
 O.L. Fedin ^{37,a}, M. Feickert ¹⁷⁰, L. Feligioni ¹⁰², D.E. Fellers ¹²³, C. Feng ^{62b}, M. Feng ^{14b},
 Z. Feng ¹¹⁴, M.J. Fenton ¹⁵⁹, L. Ferencz ⁴⁸, R.A.M. Ferguson ⁹¹, S.I. Fernandez Luengo ^{137f},
 P. Fernandez Martinez ¹³, M.J.V. Fernoux ¹⁰², J. Ferrando ⁹¹, A. Ferrari ¹⁶¹, P. Ferrari ^{114,113},
 R. Ferrari ^{73a}, D. Ferrere ⁵⁶, C. Ferretti ¹⁰⁶, F. Fiedler ¹⁰⁰, P. Fiedler ¹³², A. Filipčič ⁹³,
 E.K. Filmer ¹, F. Filthaut ¹¹³, M.C.N. Fiolhais ^{130a,130c,c}, L. Fiorini ¹⁶³, W.C. Fisher ¹⁰⁷,
 T. Fitschen ¹⁰¹, P.M. Fitzhugh ¹³⁵, I. Fleck ¹⁴¹, P. Fleischmann ¹⁰⁶, T. Flick ¹⁷¹, M. Flores ^{33d,ae},
 L.R. Flores Castillo ^{64a}, L. Flores Sanz De Acedo ³⁶, F.M. Follega ^{78a,78b}, N. Fomin ¹⁶,
 J.H. Foo ¹⁵⁵, A. Formica ¹³⁵, A.C. Forti ¹⁰¹, E. Fortin ³⁶, A.W. Fortman ^{17a}, M.G. Foti ^{17a},
 L. Fountas ^{9j}, D. Fournier ⁶⁶, H. Fox ⁹¹, P. Francavilla ^{74a,74b}, S. Francescato ⁶¹,
 S. Franchellucci ⁵⁶, M. Franchini ^{23b,23a}, S. Franchino ^{63a}, D. Francis ³⁶, L. Franco ¹¹³,
 V. Franco Lima ³⁶, L. Franconi ⁴⁸, M. Franklin ⁶¹, G. Frattari ²⁶, W.S. Freund ^{83b}, Y.Y. Frid ¹⁵¹,
 J. Friend ⁵⁹, N. Fritzsche ⁵⁰, A. Froch ⁵⁴, D. Froidevaux ³⁶, J.A. Frost ¹²⁶, Y. Fu ^{62a},
 S. Fuenzalida Garrido ^{137f}, M. Fujimoto ¹⁰², K.Y. Fung ^{64a}, E. Furtado De Simas Filho ^{83b},
 M. Furukawa ¹⁵³, J. Fuster ¹⁶³, A. Gabrielli ^{23b,23a}, A. Gabrielli ¹⁵⁵, P. Gadow ³⁶,
 G. Gagliardi ^{57b,57a}, L.G. Gagnon ^{17a}, S. Galantzan ¹⁵¹, E.J. Gallas ¹²⁶, B.J. Gallop ¹³⁴,
 K.K. Gan ¹¹⁹, S. Ganguly ¹⁵³, Y. Gao ⁵², F.M. Garay Walls ^{137a,137b}, B. Garcia ²⁹, C. García ¹⁶³,
 A. Garcia Alonso ¹¹⁴, A.G. Garcia Caffaro ¹⁷², J.E. García Navarro ¹⁶³, M. Garcia-Sciveres ^{17a},
 G.L. Gardner ¹²⁸, R.W. Gardner ³⁹, N. Garelli ¹⁵⁸, D. Garg ⁸⁰, R.B. Garg ^{143,n}, J.M. Gargan ⁵²,
 C.A. Garner ¹⁵⁵, C.M. Garvey ^{33a}, P. Gaspar ^{83b}, V.K. Gassmann ¹⁵⁸, G. Gaudio ^{73a}, V. Gautam ¹³,
 P. Gauzzi ^{75a,75b}, I.L. Gavrilenko ³⁷, A. Gavrilyuk ³⁷, C. Gay ¹⁶⁴, G. Gaycken ⁴⁸, E.N. Gazis ¹⁰,
 A.A. Geanta ^{27b}, C.M. Gee ¹³⁶, A. Gekow ¹¹⁹, C. Gemme ^{57b}, M.H. Genest ⁶⁰, A.D. Gentry ¹¹²,
 S. George ⁹⁵, W.F. George ²⁰, T. Gerialis ⁴⁶, P. Gessinger-Befurt ³⁶, M.E. Geyik ¹⁷¹,
 M. Ghani ¹⁶⁷, M. Ghneimat ¹⁴¹, K. Ghorbanian ⁹⁴, A. Ghosal ¹⁴¹, A. Ghosh ¹⁵⁹, A. Ghosh ⁷,
 B. Giacobbe ^{23b}, S. Giagu ^{75a,75b}, T. Giani ¹¹⁴, P. Giannetti ^{74a}, A. Giannini ^{62a}, S.M. Gibson ⁹⁵,
 M. Gignac ¹³⁶, D.T. Gil ^{86b}, A.K. Gilbert ^{86a}, B.J. Gilbert ⁴¹, D. Gillberg ³⁴, G. Gilles ¹¹⁴,
 L. Ginabat ¹²⁷, D.M. Gingrich ^{2,ah}, M.P. Giordani ^{69a,69c}, P.F. Giraud ¹³⁵, G. Giugliarelli ^{69a,69c},
 D. Giugni ^{71a}, F. Giuli ³⁶, I. Gkialas ^{9j}, L.K. Gladilin ³⁷, C. Glasman ⁹⁹, G.R. Gledhill ¹²³,
 G. Glemža ⁴⁸, M. Glisic ¹²³, I. Gnesi ^{43b,f}, Y. Go ²⁹, M. Goblirsch-Kolb ³⁶, B. Gocke ⁴⁹,
 D. Godin ¹⁰⁸, B. Gokturk ^{21a}, S. Goldfarb ¹⁰⁵, T. Golling ⁵⁶, M.G.D. Gololo ^{33g}, D. Golubkov ³⁷,
 J.P. Gombas ¹⁰⁷, A. Gomes ^{130a,130b}, G. Gomes Da Silva ¹⁴¹, A.J. Gomez Delegido ¹⁶³,
 R. Gonçalves ^{130a,130c}, L. Gonella ²⁰, A. Gongadze ^{149c}, F. Gonnella ²⁰, J.L. Gonski ¹⁴³,
 R.Y. González Andana ⁵², S. González de la Hoz ¹⁶³, R. Gonzalez Lopez ⁹²,
 C. Gonzalez Renteria ^{17a}, M.V. Gonzalez Rodrigues ⁴⁸, R. Gonzalez Suarez ¹⁶¹,
 S. Gonzalez-Sevilla ⁵⁶, G.R. Gonzalvo Rodriguez ¹⁶³, L. Goossens ³⁶, B. Gorini ³⁶,
 E. Gorini ^{70a,70b}, A. Gorišek ⁹³, T.C. Gosart ¹²⁸, A.T. Goshaw ⁵¹, M.I. Gostkin ³⁸,
 S. Goswami ¹²¹, C.A. Gottardo ³⁶, S.A. Gotz ¹⁰⁹, M. Goughri ^{35b}, V. Goumarre ⁴⁸,
 A.G. Goussiou ¹³⁸, N. Govender ^{33c}, I. Grabowska-Bold ^{86a}, K. Graham ³⁴, E. Gramstad ¹²⁵,
 S. Grancagnolo ^{70a,70b}, C.M. Grant ^{1,135}, P.M. Gravila ^{27f}, F.G. Gravili ^{70a,70b}, H.M. Gray ^{17a},
 M. Greco ^{70a,70b}, C. Grefe ²⁴, I.M. Gregor ⁴⁸, P. Grenier ¹⁴³, S.G. Grewe ¹¹⁰, A.A. Grillo ¹³⁶,
 K. Grimm ³¹, S. Grinstein ^{13,u}, J.-F. Grivaz ⁶⁶, E. Gross ¹⁶⁹, J. Grosse-Knetter ⁵⁵,
 J.C. Grundy ¹²⁶, L. Guan ¹⁰⁶, C. Gubbels ¹⁶⁴, J.G.R. Guerrero Rojas ¹⁶³, G. Guerrieri ^{69a,69c},
 F. Guescini ¹¹⁰, R. Gugel ¹⁰⁰, J.A.M. Guhit ¹⁰⁶, A. Guida ¹⁸, E. Guilloton ¹⁶⁷, S. Guindon ³⁶,
 F. Guo ^{14a,14e}, J. Guo ^{62c}, L. Guo ⁴⁸, Y. Guo ¹⁰⁶, R. Gupta ⁴⁸, R. Gupta ¹²⁹, S. Gurbuz ²⁴,
 S.S. Gurdasani ⁵⁴, G. Gustavino ³⁶, M. Guth ⁵⁶, P. Gutierrez ¹²⁰, L.F. Gutierrez Zagazeta ¹²⁸,
 M. Gutsche ⁵⁰, C. Gutschow ⁹⁶, C. Gwenlan ¹²⁶, C.B. Gwilliam ⁹², E.S. Haaland ¹²⁵,

A. Haas ¹¹⁷, M. Habedank ⁴⁸, C. Haber ^{17a}, H.K. Hadavand ⁸, A. Hadeef ⁵⁰, S. Hadzic ¹¹⁰,
 A.I. Hagan ⁹¹, J.J. Hahn ¹⁴¹, E.H. Haines ⁹⁶, M. Haleem ¹⁶⁶, J. Haley ¹²¹, J.J. Hall ¹³⁹,
 G.D. Hallewell ¹⁰², L. Halser ¹⁹, K. Hamano ¹⁶⁵, M. Hamer ²⁴, G.N. Hamity ⁵²,
 E.J. Hampshire ⁹⁵, J. Han ^{62b}, K. Han ^{62a}, L. Han ^{14c}, L. Han ^{62a}, S. Han ^{17a}, Y.F. Han ¹⁵⁵,
 K. Hanagaki ⁸⁴, M. Hance ¹³⁶, D.A. Hangal ⁴¹, H. Hanif ¹⁴², M.D. Hank ¹²⁸, J.B. Hansen ⁴²,
 P.H. Hansen ⁴², K. Hara ¹⁵⁷, D. Harada ⁵⁶, T. Harenberg ¹⁷¹, S. Harkusha ³⁷, M.L. Harris ¹⁰³,
 Y.T. Harris ¹²⁶, J. Harrison ¹³, N.M. Harrison ¹¹⁹, P.F. Harrison ¹⁶⁷, N.M. Hartman ¹¹⁰,
 N.M. Hartmann ¹⁰⁹, Y. Hasegawa ¹⁴⁰, R. Hauser ¹⁰⁷, C.M. Hawkes ²⁰, R.J. Hawkings ³⁶,
 Y. Hayashi ¹⁵³, S. Hayashida ¹¹¹, D. Hayden ¹⁰⁷, C. Hayes ¹⁰⁶, R.L. Hayes ¹¹⁴, C.P. Hays ¹²⁶,
 J.M. Hays ⁹⁴, H.S. Hayward ⁹², F. He ^{62a}, M. He ^{14a,14e}, Y. He ¹⁵⁴, Y. He ⁴⁸, Y. He ⁹⁶,
 N.B. Heatley ⁹⁴, V. Hedberg ⁹⁸, A.L. Heggelund ¹²⁵, N.D. Hehir ^{94,*}, C. Heidegger ⁵⁴,
 K.K. Heidegger ⁵⁴, W.D. Heidorn ⁸¹, J. Heilman ³⁴, S. Heim ⁴⁸, T. Heim ^{17a}, J.G. Heinlein ¹²⁸,
 J.J. Heinrich ¹²³, L. Heinrich ^{110,af}, J. Hejbal ¹³¹, A. Held ¹⁷⁰, S. Hellesund ¹⁶,
 C.M. Helling ¹⁶⁴, S. Hellman ^{47a,47b}, R.C.W. Henderson ⁹¹, L. Henkelmann ³²,
 A.M. Henriques Correia ³⁶, H. Herde ⁹⁸, Y. Hernández Jiménez ¹⁴⁵, L.M. Herrmann ²⁴,
 T. Herrmann ⁵⁰, G. Herten ⁵⁴, R. Hertenberger ¹⁰⁹, L. Hervas ³⁶, M.E. Hespig ¹⁰⁰,
 N.P. Hessey ^{156a}, E. Hill ¹⁵⁵, S.J. Hillier ²⁰, J.R. Hinds ¹⁰⁷, F. Hinterkeuser ²⁴, M. Hirose ¹²⁴,
 S. Hirose ¹⁵⁷, D. Hirschbuehl ¹⁷¹, T.G. Hitchings ¹⁰¹, B. Hiti ⁹³, J. Hobbs ¹⁴⁵, R. Hobincu ^{27e},
 N. Hod ¹⁶⁹, M.C. Hodgkinson ¹³⁹, B.H. Hodgkinson ¹²⁶, A. Hoecker ³⁶, D.D. Hofer ¹⁰⁶,
 J. Hofer ⁴⁸, T. Holm ²⁴, M. Holzbock ¹¹⁰, L.B.A.H. Hommels ³², B.P. Honan ¹⁰¹, J. Hong ^{62c},
 T.M. Hong ¹²⁹, B.H. Hooberman ¹⁶², W.H. Hopkins ⁶, Y. Horii ¹¹¹, S. Hou ¹⁴⁸, A.S. Howard ⁹³,
 J. Howarth ⁵⁹, J. Hoya ⁶, M. Hrabovsky ¹²², A. Hrynevich ⁴⁸, T. Hryn'ova ⁴, P.J. Hsu ⁶⁵,
 S.-C. Hsu ¹³⁸, Q. Hu ^{62a}, S. Huang ^{64b}, X. Huang ^{14c}, X. Huang ^{14a,14e}, Y. Huang ¹³⁹,
 Y. Huang ^{14a}, Z. Huang ¹⁰¹, Z. Hubacek ¹³², M. Huebner ²⁴, F. Huegging ²⁴, T.B. Huffman ¹²⁶,
 C.A. Hugli ⁴⁸, M. Huhtinen ³⁶, S.K. Huiberts ¹⁶, R. Hulsken ¹⁰⁴, N. Huseynov ¹², J. Huston ¹⁰⁷,
 J. Huth ⁶¹, R. Hyneman ¹⁴³, G. Iacobucci ⁵⁶, G. Iakovidis ²⁹, I. Ibragimov ¹⁴¹,
 L. Iconomidou-Fayard ⁶⁶, J.P. Iddon ³⁶, P. Iengo ^{72a,72b}, R. Iguchi ¹⁵³, T. Iizawa ¹²⁶,
 Y. Ikegami ⁸⁴, N. Ilic ¹⁵⁵, H. Imam ^{35a}, M. Ince Lezki ⁵⁶, T. Ingebretsen Carlson ^{47a,47b},
 G. Introzzi ^{73a,73b}, M. Iodice ^{77a}, V. Ippolito ^{75a,75b}, R.K. Irwin ⁹², M. Ishino ¹⁵³, W. Islam ¹⁷⁰,
 C. Issever ^{18,48}, S. Istin ^{21a,al}, H. Ito ¹⁶⁸, R. Iuppa ^{78a,78b}, A. Ivina ¹⁶⁹, J.M. Izen ⁴⁵, V. Izzo ^{72a},
 P. Jacka ^{131,132}, P. Jackson ¹, B.P. Jaeger ¹⁴², C.S. Jagfeld ¹⁰⁹, G. Jain ^{156a}, P. Jain ⁵⁴,
 K. Jakobs ⁵⁴, T. Jakoubek ¹⁶⁹, J. Jamieson ⁵⁹, K.W. Janas ^{86a}, M. Javurkova ¹⁰³, L. Jeanty ¹²³,
 J. Jejelava ^{149a,ab}, P. Jenni ^{54,g}, C.E. Jessiman ³⁴, C. Jia ^{62b}, J. Jia ¹⁴⁵, X. Jia ⁶¹, X. Jia ^{14a,14e},
 Z. Jia ^{14c}, S. Jiggins ⁴⁸, J. Jimenez Pena ¹³, S. Jin ^{14c}, A. Jinaru ^{27b}, O. Jinnouchi ¹⁵⁴,
 P. Johansson ¹³⁹, K.A. Johns ⁷, J.W. Johnson ¹³⁶, D.M. Jones ³², E. Jones ⁴⁸, P. Jones ³²,
 R.W.L. Jones ⁹¹, T.J. Jones ⁹², H.L. Joos ^{55,36}, R. Joshi ¹¹⁹, J. Jovicevic ¹⁵, X. Ju ^{17a},
 J.J. Junggeburth ¹⁰³, T. Junkermann ^{63a}, A. Juste Rozas ^{13,u}, M.K. Juzek ⁸⁷, S. Kabana ^{137e},
 A. Kaczmarzka ⁸⁷, M. Kado ¹¹⁰, H. Kagan ¹¹⁹, M. Kagan ¹⁴³, A. Kahn ⁴¹, A. Kahn ¹²⁸,
 C. Kahra ¹⁰⁰, T. Kaji ¹⁵³, E. Kajomovitz ¹⁵⁰, N. Kakati ¹⁶⁹, I. Kalaitzidou ⁵⁴, C.W. Kalderon ²⁹,
 N.J. Kang ¹³⁶, D. Kar ^{33g}, K. Karava ¹²⁶, M.J. Kareem ^{156b}, E. Karentzos ⁵⁴, I. Karkanias ¹⁵²,
 O. Karkout ¹¹⁴, S.N. Karpov ³⁸, Z.M. Karpova ³⁸, V. Kartvelishvili ⁹¹, A.N. Karyukhin ³⁷,
 E. Kasimi ¹⁵², J. Katzy ⁴⁸, S. Kaur ³⁴, K. Kawade ¹⁴⁰, M.P. Kawale ¹²⁰, C. Kawamoto ⁸⁸,
 T. Kawamoto ^{62a}, E.F. Kay ³⁶, F.I. Kaya ¹⁵⁸, S. Kazakos ¹⁰⁷, V.F. Kazanin ³⁷, Y. Ke ¹⁴⁵,
 J.M. Keaveney ^{33a}, R. Keeler ¹⁶⁵, G.V. Kehris ⁶¹, J.S. Keller ³⁴, A.S. Kelly ⁹⁶, J.J. Kempster ¹⁴⁶,
 P.D. Kennedy ¹⁰⁰, O. Kepka ¹³¹, B.P. Kerridge ¹³⁴, S. Kersten ¹⁷¹, B.P. Kerševan ⁹³,
 S. Keshri ⁶⁶, L. Keszezhova ^{28a}, S. Ketabchi Haghghat ¹⁵⁵, R.A. Khan ¹²⁹, A. Khanov ¹²¹,
 A.G. Kharlamov ³⁷, T. Kharlamova ³⁷, E.E. Khoda ¹³⁸, M. Kholodenko ³⁷, T.J. Khoo ¹⁸,

G. Khorauli [id](#)¹⁶⁶, J. Khubua [id](#)^{149b,*}, Y.A.R. Khwaira [id](#)⁶⁶, B. Kibirige^{33g}, A. Kilgallon [id](#)¹²³, D.W. Kim [id](#)^{47a,47b}, Y.K. Kim [id](#)³⁹, N. Kimura [id](#)⁹⁶, M.K. Kingston [id](#)⁵⁵, A. Kirchhoff [id](#)⁵⁵, C. Kirfel [id](#)²⁴, F. Kirfel [id](#)²⁴, J. Kirk [id](#)¹³⁴, A.E. Kiryunin [id](#)¹¹⁰, C. Kitsaki [id](#)¹⁰, O. Kivernyk [id](#)²⁴, M. Klassen [id](#)^{63a}, C. Klein [id](#)³⁴, L. Klein [id](#)¹⁶⁶, M.H. Klein [id](#)⁴⁴, S.B. Klein [id](#)⁵⁶, U. Klein [id](#)⁹², P. Klimek [id](#)³⁶, A. Klimentov [id](#)²⁹, T. Klioutchnikova [id](#)³⁶, P. Kluit [id](#)¹¹⁴, S. Kluth [id](#)¹¹⁰, E. Kneringer [id](#)⁷⁹, T.M. Knight [id](#)¹⁵⁵, A. Knue [id](#)⁴⁹, R. Kobayashi [id](#)⁸⁸, D. Kobylanski [id](#)¹⁶⁹, S.F. Koch [id](#)¹²⁶, M. Kocian [id](#)¹⁴³, P. Kodyš [id](#)¹³³, D.M. Koeck [id](#)¹²³, P.T. Koenig [id](#)²⁴, T. Koffas [id](#)³⁴, O. Kolay [id](#)⁵⁰, I. Koletsou [id](#)⁴, T. Komarek [id](#)¹²², K. Köneke [id](#)⁵⁴, A.X.Y. Kong [id](#)¹, T. Kono [id](#)¹¹⁸, N. Konstantinidis [id](#)⁹⁶, P. Kontaxakis [id](#)⁵⁶, B. Konya [id](#)⁹⁸, R. Kopeliansky [id](#)⁶⁸, S. Koperny [id](#)^{86a}, K. Korcyl [id](#)⁸⁷, K. Kordas [id](#)^{152,e}, A. Korn [id](#)⁹⁶, S. Korn [id](#)⁵⁵, I. Korolkov [id](#)¹³, N. Korotkova [id](#)³⁷, B. Kortman [id](#)¹¹⁴, O. Kortner [id](#)¹¹⁰, S. Kortner [id](#)¹¹⁰, W.H. Kostecka [id](#)¹¹⁵, V.V. Kostyukhin [id](#)¹⁴¹, A. Kotsokechagia [id](#)¹³⁵, A. Kotwal [id](#)⁵¹, A. Koulouris [id](#)³⁶, A. Kourkoumeli-Charalampidi [id](#)^{73a,73b}, C. Kourkoumelis [id](#)⁹, E. Kourlitis [id](#)^{110,af}, O. Kovanda [id](#)¹²³, R. Kowalewski [id](#)¹⁶⁵, W. Kozanecki [id](#)¹³⁵, A.S. Kozhin [id](#)³⁷, V.A. Kramarenko [id](#)³⁷, G. Kramberger [id](#)⁹³, P. Kramer [id](#)¹⁰⁰, M.W. Krasny [id](#)¹²⁷, A. Krasnahorkay [id](#)³⁶, J.W. Kraus [id](#)¹⁷¹, J.A. Kremer [id](#)⁴⁸, T. Kresse [id](#)⁵⁰, J. Kretschmar [id](#)⁹², K. Kreul [id](#)¹⁸, P. Krieger [id](#)¹⁵⁵, S. Krishnamurthy [id](#)¹⁰³, M. Krivos [id](#)¹³³, K. Krizka [id](#)²⁰, K. Kroeninger [id](#)⁴⁹, H. Kroha [id](#)¹¹⁰, J. Kroll [id](#)¹³¹, J. Kroll [id](#)¹²⁸, K.S. Krowpman [id](#)¹⁰⁷, U. Kruchonak [id](#)³⁸, H. Krüger [id](#)²⁴, N. Krumnack⁸¹, M.C. Kruse [id](#)⁵¹, O. Kuchinskaia [id](#)³⁷, S. Kuday [id](#)^{3a}, S. Kuehn [id](#)³⁶, R. Kuesters [id](#)⁵⁴, T. Kuhl [id](#)⁴⁸, V. Kukhtin [id](#)³⁸, Y. Kulchitsky [id](#)^{37,a}, S. Kuleshov [id](#)^{137d,137b}, M. Kumar [id](#)^{33g}, N. Kumari [id](#)⁴⁸, P. Kumari [id](#)^{156b}, A. Kupco [id](#)¹³¹, T. Kupfer⁴⁹, A. Kupich [id](#)³⁷, O. Kuprash [id](#)⁵⁴, H. Kurashige [id](#)⁸⁵, L.L. Kurchaninov [id](#)^{156a}, O. Kurdysh [id](#)⁶⁶, Y.A. Kurochkin [id](#)³⁷, A. Kurova [id](#)³⁷, M. Kuze [id](#)¹⁵⁴, A.K. Kvam [id](#)¹⁰³, J. Kvita [id](#)¹²², T. Kwan [id](#)¹⁰⁴, N.G. Kyriacou [id](#)¹⁰⁶, L.A.O. Laatu [id](#)¹⁰², C. Lacasta [id](#)¹⁶³, F. Lacava [id](#)^{75a,75b}, H. Lacker [id](#)¹⁸, D. Lacour [id](#)¹²⁷, N.N. Lad [id](#)⁹⁶, E. Ladygin [id](#)³⁸, B. Laforge [id](#)¹²⁷, T. Lagouri [id](#)^{27b}, F.Z. Lahbabi [id](#)^{35a}, S. Lai [id](#)⁵⁵, I.K. Lakomic [id](#)^{86a}, N. Lalloue [id](#)⁶⁰, J.E. Lambert [id](#)¹⁶⁵, S. Lammers [id](#)⁶⁸, W. Lampl [id](#)⁷, C. Lampoudis [id](#)^{152,e}, G. Lamprinoudis¹⁰⁰, A.N. Lancaster [id](#)¹¹⁵, E. Lançon [id](#)²⁹, U. Landgraf [id](#)⁵⁴, M.P.J. Landon [id](#)⁹⁴, V.S. Lang [id](#)⁵⁴, O.K.B. Langrekken [id](#)¹²⁵, A.J. Lankford [id](#)¹⁵⁹, F. Lanni [id](#)³⁶, K. Lantzs [id](#)²⁴, A. Lanza [id](#)^{73a}, A. Lapertosa [id](#)^{57b,57a}, J.F. Laporte [id](#)¹³⁵, T. Lari [id](#)^{71a}, F. Lasagni Manghi [id](#)^{23b}, M. Lassnig [id](#)³⁶, V. Latonova [id](#)¹³¹, A. Laudrain [id](#)¹⁰⁰, A. Laurier [id](#)¹⁵⁰, S.D. Lawlor [id](#)¹³⁹, Z. Lawrence [id](#)¹⁰¹, R. Lazaridou¹⁶⁷, M. Lazzaroni [id](#)^{71a,71b}, B. Le¹⁰¹, E.M. Le Boulicaut [id](#)⁵¹, B. Leban [id](#)⁹³, A. Lebedev [id](#)⁸¹, M. LeBlanc [id](#)¹⁰¹, F. Ledroit-Guillon [id](#)⁶⁰, A.C.A. Lee⁹⁶, S.C. Lee [id](#)¹⁴⁸, S. Lee [id](#)^{47a,47b}, T.F. Lee [id](#)⁹², L.L. Leeuw [id](#)^{33c}, H.P. Lefebvre [id](#)⁹⁵, M. Lefebvre [id](#)¹⁶⁵, C. Leggett [id](#)^{17a}, G. Lehmann Miotto [id](#)³⁶, M. Leigh [id](#)⁵⁶, W.A. Leight [id](#)¹⁰³, W. Leinonen [id](#)¹¹³, A. Leisos [id](#)^{152,t}, M.A.L. Leite [id](#)^{83c}, C.E. Leitgeb [id](#)¹⁸, R. Leitner [id](#)¹³³, K.J.C. Leney [id](#)⁴⁴, T. Lenz [id](#)²⁴, S. Leone [id](#)^{74a}, C. Leonidopoulos [id](#)⁵², A. Leopold [id](#)¹⁴⁴, C. Leroy [id](#)¹⁰⁸, R. Les [id](#)¹⁰⁷, C.G. Lester [id](#)³², M. Levchenko [id](#)³⁷, J. Levêque [id](#)⁴, L.J. Levinson [id](#)¹⁶⁹, G. Levrini [id](#)^{23b,23a}, M.P. Lewicki [id](#)⁸⁷, D.J. Lewis [id](#)⁴, A. Li [id](#)⁵, B. Li [id](#)^{62b}, C. Li [id](#)^{62a}, C-Q. Li [id](#)¹¹⁰, H. Li [id](#)^{62a}, H. Li [id](#)^{62b}, H. Li [id](#)^{14c}, H. Li [id](#)^{14b}, H. Li [id](#)^{62b}, J. Li [id](#)^{62c}, K. Li [id](#)¹³⁸, L. Li [id](#)^{62c}, M. Li [id](#)^{14a,14e}, Q.Y. Li [id](#)^{62a}, S. Li [id](#)^{14a,14e}, S. Li [id](#)^{62d,62c,d}, T. Li [id](#)⁵, X. Li [id](#)¹⁰⁴, Z. Li [id](#)¹²⁶, Z. Li [id](#)¹⁰⁴, Z. Li [id](#)^{14a,14e}, S. Liang [id](#)^{14a,14e}, Z. Liang [id](#)^{14a}, M. Liberatore [id](#)¹³⁵, B. Liberti [id](#)^{76a}, K. Lie [id](#)^{64c}, J. Lieber Marin [id](#)^{83b}, H. Lien [id](#)⁶⁸, K. Lin [id](#)¹⁰⁷, R.E. Lindley [id](#)⁷, J.H. Lindon [id](#)², E. Lipeles [id](#)¹²⁸, A. Lipniacka [id](#)¹⁶, A. Lister [id](#)¹⁶⁴, J.D. Little [id](#)⁴, B. Liu [id](#)^{14a}, B.X. Liu [id](#)¹⁴², D. Liu [id](#)^{62d,62c}, J.B. Liu [id](#)^{62a}, J.K.K. Liu [id](#)³², K. Liu [id](#)^{62d,62c}, M. Liu [id](#)^{62a}, M.Y. Liu [id](#)^{62a}, P. Liu [id](#)^{14a}, Q. Liu [id](#)^{62d,138,62c}, X. Liu [id](#)^{62a}, X. Liu [id](#)^{62b}, Y. Liu [id](#)^{14d,14e}, Y.L. Liu [id](#)^{62b}, Y.W. Liu [id](#)^{62a}, J. Llorente Merino [id](#)¹⁴², S.L. Lloyd [id](#)⁹⁴, E.M. Lobodzinska [id](#)⁴⁸, P. Loch [id](#)⁷, T. Lohse [id](#)¹⁸, K. Lohwasser [id](#)¹³⁹, E. Loiacono [id](#)⁴⁸, M. Lokajicek [id](#)^{131,*}, J.D. Lomas [id](#)²⁰, J.D. Long [id](#)¹⁶², I. Longarini [id](#)¹⁵⁹, L. Longo [id](#)^{70a,70b}, R. Longo [id](#)¹⁶², I. Lopez Paz [id](#)⁶⁷, A. Lopez Solis [id](#)⁴⁸, N. Lorenzo Martinez [id](#)⁴, A.M. Lory [id](#)¹⁰⁹, G. Lösckce Centeno [id](#)¹⁴⁶, O. Loseva [id](#)³⁷, X. Lou [id](#)^{47a,47b}, X. Lou [id](#)^{14a,14e}, A. Lounis [id](#)⁶⁶,








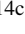

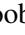







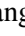






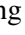
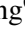
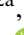


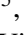


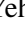




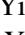
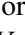
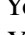

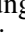

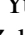
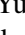
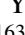
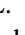

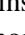
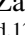







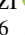




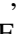


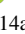
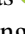
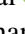
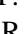
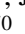
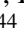


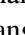
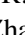
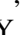
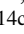



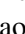
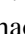

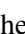
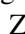

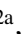


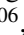

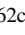


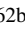
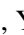









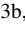




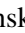





P.A. Love ⁹¹, G. Lu ^{14a,14e}, M. Lu ⁸⁰, S. Lu ¹²⁸, Y.J. Lu ⁶⁵, H.J. Lubatti ¹³⁸, C. Luci ^{75a,75b}, F.L. Lucio Alves ^{14c}, F. Luehring ⁶⁸, I. Luise ¹⁴⁵, O. Lukianchuk ⁶⁶, O. Lundberg ¹⁴⁴, B. Lund-Jensen ^{144,*}, N.A. Luongo ⁶, M.S. Lutz ³⁶, A.B. Lux ²⁵, D. Lynn ²⁹, R. Lysak ¹³¹, E. Lytken ⁹⁸, V. Lyubushkin ³⁸, T. Lyubushkina ³⁸, M.M. Lyukova ¹⁴⁵, H. Ma ²⁹, K. Ma ^{62a}, L.L. Ma ^{62b}, W. Ma ^{62a}, Y. Ma ¹²¹, D.M. Mac Donell ¹⁶⁵, G. Maccarrone ⁵³, J.C. MacDonald ¹⁰⁰, P.C. Machado De Abreu Farias ^{83b}, R. Madar ⁴⁰, W.F. Mader ⁵⁰, T. Madula ⁹⁶, J. Maeda ⁸⁵, T. Maeno ²⁹, H. Maguire ¹³⁹, V. Maiboroda ¹³⁵, A. Maio ^{130a,130b,130d}, K. Maj ^{86a}, O. Majersky ⁴⁸, S. Majewski ¹²³, N. Makovec ⁶⁶, V. Maksimovic ¹⁵, B. Malaescu ¹²⁷, Pa. Malecki ⁸⁷, V.P. Maleev ³⁷, F. Malek ^{60,o}, M. Mali ⁹³, D. Malito ⁹⁵, U. Mallik ^{80,*}, S. Maltezos ¹⁰, S. Malyukov ³⁸, J. Mamuzic ¹³, G. Mancini ⁵³, M.N. Mancini ²⁶, G. Manco ^{73a,73b}, J.P. Mandalia ⁹⁴, I. Mandić ⁹³, L. Manhaes de Andrade Filho ^{83a}, I.M. Maniatis ¹⁶⁹, J. Manjarres Ramos ^{102,ac}, D.C. Mankad ¹⁶⁹, A. Mann ¹⁰⁹, S. Manzoni ³⁶, L. Mao ^{62c}, X. Mapekula ^{33c}, A. Marantis ^{152,t}, G. Marchiori ⁵, M. Marcisovsky ¹³¹, C. Marcon ^{71a}, M. Marinescu ²⁰, S. Marium ⁴⁸, M. Marjanovic ¹²⁰, E.J. Marshall ⁹¹, Z. Marshall ^{17a}, S. Marti-Garcia ¹⁶³, T.A. Martin ¹⁶⁷, V.J. Martin ⁵², B. Martin dit Latour ¹⁶, L. Martinelli ^{75a,75b}, M. Martinez ^{13,u}, P. Martinez Agullo ¹⁶³, V.I. Martinez Outschoorn ¹⁰³, P. Martinez Suarez ¹³, S. Martin-Haugh ¹³⁴, V.S. Martoiu ^{27b}, A.C. Martyniuk ⁹⁶, A. Marzin ³⁶, D. Mascione ^{78a,78b}, L. Masetti ¹⁰⁰, T. Mashimo ¹⁵³, J. Masik ¹⁰¹, A.L. Maslennikov ³⁷, P. Massarotti ^{72a,72b}, P. Mastrandrea ^{74a,74b}, A. Mastroberardino ^{43b,43a}, T. Masubuchi ¹⁵³, T. Mathisen ¹⁶¹, J. Matousek ¹³³, N. Matsuzawa ¹⁵³, J. Maurer ^{27b}, B. Maček ⁹³, D.A. Maximov ³⁷, R. Mazini ¹⁴⁸, I. Maznas ¹¹⁵, M. Mazza ¹⁰⁷, S.M. Mazza ¹³⁶, E. Mazzeo ^{71a,71b}, C. Mc Ginn ²⁹, J.P. Mc Gowan ¹⁰⁴, S.P. Mc Kee ¹⁰⁶, C.C. McCracken ¹⁶⁴, E.F. McDonald ¹⁰⁵, A.E. McDougall ¹¹⁴, J.A. Mcfayden ¹⁴⁶, R.P. McGovern ¹²⁸, G. Mchedlidze ^{149b}, R.P. Mckenzie ^{33g}, T.C. Mclachlan ⁴⁸, D.J. McLaughlin ⁹⁶, S.J. McMahon ¹³⁴, C.M. Mcpartland ⁹², R.A. McPherson ^{165,y}, S. Mehlhase ¹⁰⁹, A. Mehta ⁹², D. Melini ¹⁶³, B.R. Mellado Garcia ^{33g}, A.H. Melo ⁵⁵, F. Meloni ⁴⁸, A.M. Mendes Jacques Da Costa ¹⁰¹, H.Y. Meng ¹⁵⁵, L. Meng ⁹¹, S. Menke ¹¹⁰, M. Mentink ³⁶, E. Meoni ^{43b,43a}, G. Mercado ¹¹⁵, C. Merlassino ^{69a,69c}, L. Merola ^{72a,72b}, C. Meroni ^{71a,71b}, J. Metcalfe ⁶, A.S. Mete ⁶, C. Meyer ⁶⁸, J-P. Meyer ¹³⁵, R.P. Middleton ¹³⁴, L. Mijović ⁵², G. Mikenberg ¹⁶⁹, M. Mikestikova ¹³¹, M. Mikuž ⁹³, H. Mildner ¹⁰⁰, A. Milic ³⁶, D.W. Miller ³⁹, E.H. Miller ¹⁴³, L.S. Miller ³⁴, A. Milov ¹⁶⁹, D.A. Milstead ^{47a,47b}, T. Min ^{14c}, A.A. Minaenko ³⁷, I.A. Minashvili ^{149b}, L. Mince ⁵⁹, A.I. Mincer ¹¹⁷, B. Mindur ^{86a}, M. Mineev ³⁸, Y. Mino ⁸⁸, L.M. Mir ¹³, M. Miralles Lopez ⁵⁹, M. Mironova ^{17a}, A. Mishima ¹⁵³, M.C. Missio ¹¹³, A. Mitra ¹⁶⁷, V.A. Mitsou ¹⁶³, Y. Mitsumori ¹¹¹, O. Miu ¹⁵⁵, P.S. Miyagawa ⁹⁴, T. Mkrtychyan ^{63a}, M. Mlinarevic ⁹⁶, T. Mlinarevic ⁹⁶, M. Mlynarikova ³⁶, S. Mobius ¹⁹, P. Mogg ¹⁰⁹, M.H. Mohamed Farook ¹¹², A.F. Mohammed ^{14a,14e}, S. Mohapatra ⁴¹, G. Mokgatitswane ^{33g}, L. Moleri ¹⁶⁹, B. Mondal ¹⁴¹, S. Mondal ¹³², K. Mönig ⁴⁸, E. Monnier ¹⁰², L. Monsonis Romero ¹⁶³, J. Montejo Berlingen ¹³, M. Montella ¹¹⁹, F. Montekali ^{77a,77b}, F. Monticelli ⁹⁰, S. Monzani ^{69a,69c}, N. Morange ⁶⁶, A.L. Moreira De Carvalho ^{130a}, M. Moreno Llácer ¹⁶³, C. Moreno Martinez ⁵⁶, P. Morettini ^{57b}, S. Morgenstern ³⁶, M. Morii ⁶¹, M. Morinaga ¹⁵³, F. Morodei ^{75a,75b}, L. Morvaj ³⁶, P. Moschovakos ³⁶, B. Moser ³⁶, M. Mosidze ^{149b}, T. Moskalets ⁵⁴, P. Moskvitina ¹¹³, J. Moss ^{31,1}, A. Moussa ^{35d}, E.J.W. Moyses ¹⁰³, O. Mtintsilana ^{33g}, S. Muanza ¹⁰², J. Mueller ¹²⁹, D. Muenstermann ⁹¹, R. Müller ¹⁹, G.A. Mullier ¹⁶¹, A.J. Mullin ³², J.J. Mullin ¹²⁸, D.P. Mungo ¹⁵⁵, D. Munoz Perez ¹⁶³, F.J. Munoz Sanchez ¹⁰¹, M. Murin ¹⁰¹, W.J. Murray ^{167,134}, M. Muškinja ⁹³, C. Mwewa ²⁹, A.G. Myagkov ^{37,a}, A.J. Myers ⁸, G. Myers ¹⁰⁶, M. Myska ¹³², B.P. Nachman ^{17a}, O. Nackenhorst ⁴⁹, K. Nagai ¹²⁶, K. Nagano ⁸⁴, J.L. Nagle ^{29,aj}, E. Nagy ¹⁰²,

A.M. Nairz ³⁶, Y. Nakahama ⁸⁴, K. Nakamura ⁸⁴, K. Nakkalil ⁵, H. Nanjo ¹²⁴, R. Narayan ⁴⁴,
 E.A. Narayanan ¹¹², I. Naryshkin ³⁷, M. Naseri ³⁴, S. Nasri ^{116b}, C. Nass ²⁴, G. Navarro ^{22a},
 J. Navarro-Gonzalez ¹⁶³, R. Nayak ¹⁵¹, A. Nayaz ¹⁸, P.Y. Nechaeva ³⁷, F. Nechansky ⁴⁸,
 L. Nedic ¹²⁶, T.J. Neep ²⁰, A. Negri ^{73a,73b}, M. Negrini ^{23b}, C. Nellist ¹¹⁴, C. Nelson ¹⁰⁴,
 K. Nelson ¹⁰⁶, S. Nemecek ¹³¹, M. Nessi ^{36,h}, M.S. Neubauer ¹⁶², F. Neuhaus ¹⁰⁰,
 J. Neundorf ⁴⁸, R. Newhouse ¹⁶⁴, P.R. Newman ²⁰, C.W. Ng ¹²⁹, Y.W.Y. Ng ⁴⁸, B. Ngair ^{116a},
 H.D.N. Nguyen ¹⁰⁸, R.B. Nickerson ¹²⁶, R. Nicolaidou ¹³⁵, J. Nielsen ¹³⁶, M. Niemeyer ⁵⁵,
 J. Niermann ⁵⁵, N. Nikiforou ³⁶, V. Nikolaenko ^{37,a}, I. Nikolic-Audit ¹²⁷, K. Nikolopoulos ²⁰,
 P. Nilsson ²⁹, I. Ninca ⁴⁸, H.R. Nindhito ⁵⁶, G. Ninio ¹⁵¹, A. Nisati ^{75a}, N. Nishu ²,
 R. Nisius ¹¹⁰, J-E. Nitschke ⁵⁰, E.K. Nkadimeng ^{33g}, T. Nobe ¹⁵³, D.L. Noel ³²,
 T. Nommensen ¹⁴⁷, M.B. Norfolk ¹³⁹, R.R.B. Norisam ⁹⁶, B.J. Norman ³⁴, M. Noury ^{35a},
 J. Novak ⁹³, T. Novak ⁴⁸, L. Novotny ¹³², R. Novotny ¹¹², L. Nozka ¹²², K. Ntekas ¹⁵⁹,
 N.M.J. Nunes De Moura Junior ^{83b}, J. Ocariz ¹²⁷, A. Ochi ⁸⁵, I. Ochoa ^{130a}, S. Oerdek ^{48,v},
 J.T. Offermann ³⁹, A. Ogrodnik ¹³³, A. Oh ¹⁰¹, C.C. Ohm ¹⁴⁴, H. Oide ⁸⁴, R. Oishi ¹⁵³,
 M.L. Ojeda ⁴⁸, Y. Okumura ¹⁵³, L.F. Oleiro Seabra ^{130a}, S.A. Olivares Pino ^{137d},
 D. Oliveira Damazio ²⁹, D. Oliveira Goncalves ^{83a}, J.L. Oliver ¹⁵⁹, Ö.O. Öncel ⁵⁴,
 A.P. O'Neill ¹⁹, A. Onofre ^{130a,130e}, P.U.E. Onyisi ¹¹, M.J. Oreglia ³⁹, G.E. Orellana ⁹⁰,
 D. Orestano ^{77a,77b}, N. Orlando ¹³, R.S. Orr ¹⁵⁵, V. O'Shea ⁵⁹, L.M. Osojnak ¹²⁸,
 R. Ospanov ^{62a}, G. Otero y Garzon ³⁰, H. Otono ⁸⁹, P.S. Ott ^{63a}, G.J. Ottino ^{17a}, M. Ouchrif ^{35d},
 F. Ould-Saada ¹²⁵, M. Owen ⁵⁹, R.E. Owen ¹³⁴, K.Y. Oyulmaz ^{21a}, V.E. Ozcan ^{21a},
 F. Ozturk ⁸⁷, N. Ozturk ⁸, S. Ozturk ⁸², H.A. Pacey ¹²⁶, A. Pacheco Pages ¹³,
 C. Padilla Aranda ¹³, G. Padovano ^{75a,75b}, S. Pagan Griso ^{17a}, G. Palacino ⁶⁸, A. Palazzo ^{70a,70b},
 J. Pampel ²⁴, J. Pan ¹⁷², T. Pan ^{64a}, D.K. Panchal ¹¹, C.E. Pandini ¹¹⁴, J.G. Panduro Vazquez ⁹⁵,
 H.D. Pandya ¹, H. Pang ^{14b}, P. Pani ⁴⁸, G. Panizzo ^{69a,69c}, L. Panwar ¹²⁷, L. Paolozzi ⁵⁶,
 S. Parajuli ¹⁶², A. Paramonov ⁶, C. Paraskevopoulos ⁵³, D. Paredes Hernandez ^{64b},
 A. Pareti ^{73a,73b}, K.R. Park ⁴¹, T.H. Park ¹⁵⁵, M.A. Parker ³², F. Parodi ^{57b,57a}, E.W. Parrish ¹¹⁵,
 V.A. Parrish ⁵², J.A. Parsons ⁴¹, U. Parzefall ⁵⁴, B. Pascual Dias ¹⁰⁸, L. Pascual Dominguez ¹⁵¹,
 E. Pasqualucci ^{75a}, S. Passaggio ^{57b}, F. Pastore ⁹⁵, P. Patel ⁸⁷, U.M. Patel ⁵¹, J.R. Pater ¹⁰¹,
 T. Pauly ³⁶, C.I. Pazos ¹⁵⁸, J. Pearkes ¹⁴³, M. Pedersen ¹²⁵, R. Pedro ^{130a}, S.V. Peleganchuk ³⁷,
 O. Penc ³⁶, E.A. Pender ⁵², G.D. Penn ¹⁷², K.E. Pensi ¹⁰⁹, M. Penzin ³⁷, B.S. Peralva ^{83d},
 A.P. Pereira Peixoto ⁶⁰, L. Pereira Sanchez ¹⁴³, D.V. Perepelitsa ^{29,aj}, E. Perez Codina ^{156a},
 M. Perganti ¹⁰, H. Pernegger ³⁶, O. Perrin ⁴⁰, K. Peters ⁴⁸, R.F.Y. Peters ¹⁰¹, B.A. Petersen ³⁶,
 T.C. Petersen ⁴², E. Petit ¹⁰², V. Petousis ¹³², C. Petridou ^{152,e}, T. Petru ¹³³, A. Petrukhin ¹⁴¹,
 M. Pettee ^{17a}, N.E. Pettersson ³⁶, A. Petukhov ³⁷, K. Petukhova ¹³³, R. Pezoa ^{137f},
 L. Pezzotti ³⁶, G. Pezzullo ¹⁷², T.M. Pham ¹⁷⁰, T. Pham ¹⁰⁵, P.W. Phillips ¹³⁴, G. Piacquadio ¹⁴⁵,
 E. Pianori ^{17a}, F. Piazza ¹²³, R. Piegai ³⁰, D. Pietreanu ^{27b}, A.D. Pilkington ¹⁰¹,
 M. Pinamonti ^{69a,69c}, J.L. Pinfeld ², B.C. Pinheiro Pereira ^{130a}, A.E. Pinto Pinoargote ^{100,135},
 L. Pintucci ^{69a,69c}, K.M. Piper ¹⁴⁶, A. Pirttikoski ⁵⁶, D.A. Pizzi ³⁴, L. Pizzimento ^{64b},
 A. Pizzini ¹¹⁴, M.-A. Pleier ²⁹, V. Plesanovs ⁵⁴, V. Pleskot ¹³³, E. Plotnikova ³⁸, G. Poddar ⁹⁴,
 R. Poettgen ⁹⁸, L. Poggioli ¹²⁷, I. Pokharel ⁵⁵, S. Polacek ¹³³, G. Polesello ^{73a}, A. Poley ^{142,156a},
 A. Polini ^{23b}, C.S. Pollard ¹⁶⁷, Z.B. Pollock ¹¹⁹, E. Pompa Pacchi ^{75a,75b}, D. Ponomarenko ¹¹³,
 L. Pontecorvo ³⁶, S. Popa ^{27a}, G.A. Popeneciu ^{27d}, A. Poreba ³⁶, D.M. Portillo Quintero ^{156a},
 S. Pospisil ¹³², M.A. Postill ¹³⁹, P. Postolache ^{27c}, K. Potamianos ¹⁶⁷, P.A. Potepa ^{86a},
 I.N. Potrap ³⁸, C.J. Potter ³², H. Potti ¹, T. Poulsen ⁴⁸, J. Poveda ¹⁶³, M.E. Pozo Astigarraga ³⁶,
 A. Prades Ibanez ¹⁶³, J. Pretel ⁵⁴, D. Price ¹⁰¹, M. Primavera ^{70a}, M.A. Principe Martin ⁹⁹,
 R. Privara ¹²², T. Procter ⁵⁹, M.L. Proffitt ¹³⁸, N. Proklova ¹²⁸, K. Prokofiev ^{64c}, G. Proto ¹¹⁰,
 J. Proudfoot ⁶, M. Przybycien ^{86a}, W.W. Przygoda ^{86b}, A. Psallidas ⁴⁶, J.E. Puddefoot ¹³⁹,

D. Pudzha [ID37](#), D. Pyatiizbyantseva [ID37](#), J. Qian [ID106](#), D. Qichen [ID101](#), Y. Qin [ID101](#), T. Qiu [ID52](#),
 A. Quadt [ID55](#), M. Queitsch-Maitland [ID101](#), G. Quetant [ID56](#), R.P. Quinn [ID164](#), G. Rabanal Bolanos [ID61](#),
 D. Rafanoharana [ID54](#), F. Ragusa [ID71a,71b](#), J.L. Rainbolt [ID39](#), J.A. Raine [ID56](#), S. Rajagopalan [ID29](#),
 E. Ramakoti [ID37](#), I.A. Ramirez-Berend [ID34](#), K. Ran [ID48,14e](#), N.P. Rapheeha [ID33g](#), H. Rasheed [ID27b](#),
 V. Raskina [ID127](#), D.F. Rassloff [ID63a](#), A. Rastogi [ID17a](#), S. Rave [ID100](#), B. Ravina [ID55](#), I. Ravinovich [ID169](#),
 M. Raymond [ID36](#), A.L. Read [ID125](#), N.P. Readioff [ID139](#), D.M. Rebuzzi [ID73a,73b](#), G. Redlinger [ID29](#),
 A.S. Reed [ID110](#), K. Reeves [ID26](#), J.A. Reidelsturz [ID171](#), D. Reikher [ID151](#), A. Rej [ID49](#), C. Rembser [ID36](#),
 M. Renda [ID27b](#), M.B. Rendel [ID110](#), F. Renner [ID48](#), A.G. Rennie [ID159](#), A.L. Rescia [ID48](#), S. Resconi [ID71a](#),
 M. Ressegotti [ID57b,57a](#), S. Rettie [ID36](#), J.G. Reyes Rivera [ID107](#), E. Reynolds [ID17a](#), O.L. Rezanova [ID37](#),
 P. Reznicek [ID133](#), H. Riani [ID35d](#), N. Ribaric [ID91](#), E. Ricci [ID78a,78b](#), R. Richter [ID110](#), S. Richter [ID47a,47b](#),
 E. Richter-Was [ID86b](#), M. Ridel [ID127](#), S. Ridouani [ID35d](#), P. Rieck [ID117](#), P. Riedler [ID36](#), E.M. Riefel [ID47a,47b](#),
 J.O. Rieger [ID114](#), M. Rijssenbeek [ID145](#), M. Rimoldi [ID36](#), L. Rinaldi [ID23b,23a](#), T.T. Rinn [ID29](#),
 M.P. Rinnagel [ID109](#), G. Ripellino [ID161](#), I. Riu [ID13](#), J.C. Rivera Vergara [ID165](#), F. Rizatdinova [ID121](#),
 E. Rizvi [ID94](#), B.R. Roberts [ID17a](#), S.H. Robertson [ID104,y](#), D. Robinson [ID32](#), C.M. Robles Gajardo [ID137f](#),
 M. Robles Manzano [ID100](#), A. Robson [ID59](#), A. Rocchi [ID76a,76b](#), C. Roda [ID74a,74b](#), S. Rodriguez Bosca [ID36](#),
 Y. Rodriguez Garcia [ID22a](#), A. Rodriguez Rodriguez [ID54](#), A.M. Rodríguez Vera [ID156b](#), S. Roe [ID36](#),
 J.T. Roemer [ID159](#), A.R. Roepe-Gier [ID136](#), J. Roggel [ID171](#), O. Røhne [ID125](#), R.A. Rojas [ID103](#),
 C.P.A. Roland [ID127](#), J. Roloff [ID29](#), A. Romaniouk [ID37](#), E. Romano [ID73a,73b](#), M. Romano [ID23b](#),
 A.C. Romero Hernandez [ID162](#), N. Rompotis [ID92](#), L. Roos [ID127](#), S. Rosati [ID75a](#), B.J. Rosser [ID39](#),
 E. Rossi [ID126](#), E. Rossi [ID72a,72b](#), L.P. Rossi [ID61](#), L. Rossini [ID54](#), R. Rosten [ID119](#), M. Rotaru [ID27b](#),
 B. Rottler [ID54](#), C. Rougier [ID102](#), D. Rousseau [ID66](#), D. Rousso [ID32](#), A. Roy [ID162](#), S. Roy-Garand [ID155](#),
 A. Rozanov [ID102](#), Z.M.A. Rozario [ID59](#), Y. Rozen [ID150](#), A. Rubio Jimenez [ID163](#), A.J. Ruby [ID92](#),
 V.H. Ruelas Rivera [ID18](#), T.A. Ruggeri [ID1](#), A. Ruggiero [ID126](#), A. Ruiz-Martinez [ID163](#), A. Rummler [ID36](#),
 Z. Rurikova [ID54](#), N.A. Rusakovich [ID38](#), H.L. Russell [ID165](#), G. Russo [ID75a,75b](#), J.P. Rutherford [ID7](#),
 S. Rutherford Colmenares [ID32](#), K. Rybacki [ID91](#), M. Rybar [ID133](#), E.B. Rye [ID125](#), A. Ryzhov [ID44](#),
 J.A. Sabater Iglesias [ID56](#), P. Sabatini [ID163](#), H.F.W. Sadrozinski [ID136](#), F. Safai Tehrani [ID75a](#),
 B. Safarzadeh Samani [ID134](#), M. Safdari [ID143](#), S. Saha [ID165](#), M. Sahinsoy [ID110](#), A. Saibel [ID163](#),
 M. Saimpert [ID135](#), M. Saito [ID153](#), T. Saito [ID153](#), D. Salamani [ID36](#), A. Salnikov [ID143](#), J. Salt [ID163](#),
 A. Salvador Salas [ID151](#), D. Salvatore [ID43b,43a](#), F. Salvatore [ID146](#), A. Salzburger [ID36](#), D. Sammel [ID54](#),
 D. Sampsonidis [ID152,e](#), D. Sampsonidou [ID123](#), J. Sánchez [ID163](#), V. Sanchez Sebastian [ID163](#),
 H. Sandaker [ID125](#), C.O. Sander [ID48](#), J.A. Sandesara [ID103](#), M. Sandhoff [ID171](#), C. Sandoval [ID22b](#),
 D.P.C. Sankey [ID134](#), T. Sano [ID88](#), A. Sansoni [ID53](#), L. Santi [ID75a,75b](#), C. Santoni [ID40](#), H. Santos [ID130a,130b](#),
 A. Santra [ID169](#), K.A. Saoucha [ID160](#), J.G. Saraiva [ID130a,130d](#), J. Sardain [ID7](#), O. Sasaki [ID84](#), K. Sato [ID157](#),
 C. Sauer [ID63b](#), F. Sauerburger [ID54](#), E. Sauvan [ID4](#), P. Savard [ID155,ah](#), R. Sawada [ID153](#), C. Sawyer [ID134](#),
 L. Sawyer [ID97](#), I. Sayago Galvan [ID163](#), C. Sbarra [ID23b](#), A. Sbrizzi [ID23b,23a](#), T. Scanlon [ID96](#),
 J. Schaarschmidt [ID138](#), U. Schäfer [ID100](#), A.C. Schaffer [ID66,44](#), D. Schaile [ID109](#), R.D. Schamberger [ID145](#),
 C. Scharf [ID18](#), M.M. Schefer [ID19](#), V.A. Schegelsky [ID37](#), D. Scheirich [ID133](#), F. Schenck [ID18](#),
 M. Schernau [ID159](#), C. Scheulen [ID55](#), C. Schiavi [ID57b,57a](#), M. Schioppa [ID43b,43a](#), B. Schlag [ID143,n](#),
 K.E. Schleicher [ID54](#), S. Schlenker [ID36](#), J. Schmeing [ID171](#), M.A. Schmidt [ID171](#), K. Schmieden [ID100](#),
 C. Schmitt [ID100](#), N. Schmitt [ID100](#), S. Schmitt [ID48](#), L. Schoeffel [ID135](#), A. Schoening [ID63b](#),
 P.G. Scholer [ID34](#), E. Schopf [ID126](#), M. Schott [ID100](#), J. Schovancova [ID36](#), S. Schramm [ID56](#), T. Schroer [ID56](#),
 H-C. Schultz-Coulon [ID63a](#), M. Schumacher [ID54](#), B.A. Schumm [ID136](#), Ph. Schune [ID135](#), A.J. Schuy [ID138](#),
 H.R. Schwartz [ID136](#), A. Schwartzman [ID143](#), T.A. Schwarz [ID106](#), Ph. Schwemling [ID135](#),
 R. Schwienhorst [ID107](#), A. Sciandra [ID136](#), G. Sciolla [ID26](#), F. Scuri [ID74a](#), C.D. Sebastiani [ID92](#),
 K. Sedlaczek [ID115](#), P. Seema [ID18](#), S.C. Seidel [ID112](#), A. Seiden [ID136](#), B.D. Seidlitz [ID41](#), C. Seitz [ID48](#),
 J.M. Seixas [ID83b](#), G. Sekhniaidze [ID72a](#), L. Selem [ID60](#), N. Semprini-Cesari [ID23b,23a](#), D. Sengupta [ID56](#),
 V. Senthilkumar [ID163](#), L. Serin [ID66](#), L. Serkin [ID69a,69b](#), M. Sessa [ID76a,76b](#), H. Severini [ID120](#),

F. Sforza ^{57b,57a}, A. Sfyrla ⁵⁶, Q. Sha ^{14a}, E. Shabalina ⁵⁵, R. Shaheen ¹⁴⁴, J.D. Shahinian ¹²⁸,
 D. Shaked Renous ¹⁶⁹, L.Y. Shan ^{14a}, M. Shapiro ^{17a}, A. Sharma ³⁶, A.S. Sharma ¹⁶⁴,
 P. Sharma ⁸⁰, P.B. Shatalov ³⁷, K. Shaw ¹⁴⁶, S.M. Shaw ¹⁰¹, A. Shcherbakova ³⁷, Q. Shen ^{62c,5},
 D.J. Sheppard ¹⁴², P. Sherwood ⁹⁶, L. Shi ⁹⁶, X. Shi ^{14a}, C.O. Shimmin ¹⁷², J.D. Shinner ⁹⁵,
 I.P.J. Shipsey ¹²⁶, S. Shirabe ⁸⁹, M. Shiyakova ^{38,w}, J. Shlomi ¹⁶⁹, M.J. Shochet ³⁹,
 J. Shojaii ¹⁰⁵, D.R. Shope ¹²⁵, B. Shrestha ¹²⁰, S. Shrestha ^{119,ak}, E.M. Shrif ^{33g}, M.J. Shroff ¹⁶⁵,
 P. Sicho ¹³¹, A.M. Sickles ¹⁶², E. Sideras Haddad ^{33g}, A. Sidoti ^{23b}, F. Siegert ⁵⁰, Dj. Sijacki ¹⁵,
 F. Sili ⁹⁰, J.M. Silva ⁵², M.V. Silva Oliveira ²⁹, S.B. Silverstein ^{47a}, S. Simion ⁶⁶, R. Simoniello ³⁶,
 E.L. Simpson ⁵⁹, H. Simpson ¹⁴⁶, L.R. Simpson ¹⁰⁶, N.D. Simpson ⁹⁸, S. Simsek ⁸², S. Sindhu ⁵⁵,
 P. Sinervo ¹⁵⁵, S. Singh ¹⁵⁵, S. Sinha ⁴⁸, S. Sinha ¹⁰¹, M. Sioli ^{23b,23a}, I. Siral ³⁶,
 E. Sitnikova ⁴⁸, J. Sjölin ^{47a,47b}, A. Skaf ⁵⁵, E. Skorda ²⁰, P. Skubic ¹²⁰, M. Slawinska ⁸⁷,
 V. Smakhtin ¹⁶⁹, B.H. Smart ¹³⁴, S.Yu. Smirnov ³⁷, Y. Smirnov ³⁷, L.N. Smirnova ^{37,a},
 O. Smirnova ⁹⁸, A.C. Smith ⁴¹, E.A. Smith ³⁹, H.A. Smith ¹²⁶, J.L. Smith ⁹², R. Smith ¹⁴³,
 M. Smizanska ⁹¹, K. Smolek ¹³², A.A. Snesarev ³⁷, S.R. Snider ¹⁵⁵, H.L. Snoek ¹¹⁴,
 S. Snyder ²⁹, R. Sobie ^{165,y}, A. Soffer ¹⁵¹, C.A. Solans Sanchez ³⁶, E.Yu. Soldatov ³⁷,
 U. Soldevila ¹⁶³, A.A. Solodkov ³⁷, S. Solomon ²⁶, A. Soloshenko ³⁸, K. Solovieva ⁵⁴,
 O.V. Solovyanov ⁴⁰, V. Solovyev ³⁷, P. Sommer ³⁶, A. Sonay ¹³, W.Y. Song ^{156b},
 A. Sopczak ¹³², A.L. Soppio ⁹⁶, F. Sopkova ^{28b}, J.D. Sorenson ¹¹², I.R. Sotarriva Alvarez ¹⁵⁴,
 V. Sothilingam ^{63a}, O.J. Soto Sandoval ^{137c,137b}, S. Sottocornola ⁶⁸, R. Soualah ¹⁶⁰, Z. Soumami ^{35e},
 D. South ⁴⁸, N. Soybelman ¹⁶⁹, S. Spagnolo ^{70a,70b}, M. Spalla ¹¹⁰, D. Sperlich ⁵⁴, G. Spigo ³⁶,
 S. Spinali ⁹¹, D.P. Spiteri ⁵⁹, M. Spousta ¹³³, E.J. Staats ³⁴, R. Stamen ^{63a}, A. Stampekis ²⁰,
 M. Standke ²⁴, E. Stanecka ⁸⁷, M.V. Stange ⁵⁰, B. Stanislaus ^{17a}, M.M. Stanitzki ⁴⁸, B. Stapf ⁴⁸,
 E.A. Starchenko ³⁷, G.H. Stark ¹³⁶, J. Stark ^{102,ac}, P. Staroba ¹³¹, P. Starovoitov ^{63a}, S. Stärz ¹⁰⁴,
 R. Staszewski ⁸⁷, G. Stavropoulos ⁴⁶, J. Steentoft ¹⁶¹, P. Steinberg ²⁹, B. Stelzer ^{142,156a},
 H.J. Stelzer ¹²⁹, O. Stelzer-Chilton ^{156a}, H. Stenzel ⁵⁸, T.J. Stevenson ¹⁴⁶, G.A. Stewart ³⁶,
 J.R. Stewart ¹²¹, M.C. Stockton ³⁶, G. Stoicea ^{27b}, M. Stolarski ^{130a}, S. Stonjek ¹¹⁰,
 A. Straessner ⁵⁰, J. Strandberg ¹⁴⁴, S. Strandberg ^{47a,47b}, M. Stratmann ¹⁷¹, M. Strauss ¹²⁰,
 T. Strebler ¹⁰², P. Strizenec ^{28b}, R. Ströhmer ¹⁶⁶, D.M. Strom ¹²³, R. Stroynowski ⁴⁴,
 A. Strubig ^{47a,47b}, S.A. Stucci ²⁹, B. Stugu ¹⁶, J. Stupak ¹²⁰, N.A. Styles ⁴⁸, D. Su ¹⁴³,
 S. Su ^{62a}, W. Su ^{62d}, X. Su ^{62a}, K. Sugizaki ¹⁵³, V.V. Sulin ³⁷, M.J. Sullivan ⁹²,
 D.M.S. Sultan ¹²⁶, L. Sultanaliyeva ³⁷, S. Sultansoy ^{3b}, T. Sumida ⁸⁸, S. Sun ¹⁰⁶, S. Sun ¹⁷⁰,
 O. Sunneborn Gudnadottir ¹⁶¹, N. Sur ¹⁰², M.R. Sutton ¹⁴⁶, H. Suzuki ¹⁵⁷, M. Svatos ¹³¹,
 M. Swiatlowski ^{156a}, T. Swirski ¹⁶⁶, I. Sykora ^{28a}, M. Sykora ¹³³, T. Sykora ¹³³, D. Ta ¹⁰⁰,
 K. Tackmann ^{48,v}, A. Taffard ¹⁵⁹, R. Tafirout ^{156a}, J.S. Tafoya Vargas ⁶⁶, Y. Takubo ⁸⁴,
 M. Talby ¹⁰², A.A. Talyshev ³⁷, K.C. Tam ^{64b}, N.M. Tamir ¹⁵¹, A. Tanaka ¹⁵³, J. Tanaka ¹⁵³,
 R. Tanaka ⁶⁶, M. Tanasini ^{57b,57a}, Z. Tao ¹⁶⁴, S. Tapia Araya ^{137f}, S. Tapprogge ¹⁰⁰,
 A. Tarek Abouelfadl Mohamed ¹⁰⁷, S. Tarem ¹⁵⁰, K. Tariq ^{14a}, G. Tarna ^{102,27b}, G.F. Tartarelli ^{71a},
 P. Tas ¹³³, M. Tasevsky ¹³¹, E. Tassi ^{43b,43a}, A.C. Tate ¹⁶², G. Tateno ¹⁵³, Y. Tayalati ^{35e,x},
 G.N. Taylor ¹⁰⁵, W. Taylor ^{156b}, A.S. Tee ¹⁷⁰, R. Teixeira De Lima ¹⁴³, P. Teixeira-Dias ⁹⁵,
 J.J. Teoh ¹⁵⁵, K. Terashi ¹⁵³, J. Terron ⁹⁹, S. Terzo ¹³, M. Testa ⁵³, R.J. Teuscher ^{155,y},
 A. Thaler ⁷⁹, O. Theiner ⁵⁶, N. Themistokleous ⁵², T. Thevenaux-Pelzer ¹⁰², O. Thielmann ¹⁷¹,
 D.W. Thomas ⁹⁵, J.P. Thomas ²⁰, E.A. Thompson ^{17a}, P.D. Thompson ²⁰, E. Thomson ¹²⁸,
 Y. Tian ⁵⁵, V. Tikhomirov ^{37,a}, Yu.A. Tikhonov ³⁷, S. Timoshenko ³⁷, D. Timoshyn ¹³³,
 E.X.L. Ting ¹, P. Tipton ¹⁷², S.H. Tlou ^{33g}, A. Tnourji ⁴⁰, K. Todome ¹⁵⁴, S. Todorova-Nova ¹³³,
 S. Todt ⁵⁰, M. Togawa ⁸⁴, J. Tojo ⁸⁹, S. Tokár ^{28a}, K. Tokushuku ⁸⁴, O. Toldaiev ⁶⁸, R. Tombs ³²,
 M. Tomoto ^{84,111}, L. Tompkins ^{143,n}, K.W. Topolnicki ^{86b}, E. Torrence ¹²³, H. Torres ^{102,ac},
 E. Torró Pastor ¹⁶³, M. Toscani ³⁰, C. Toscirri ³⁹, M. Tost ¹¹, D.R. Tovey ¹³⁹, A. Traeet ¹⁶,

I.S. Trandafir ^{id27b}, T. Trefzger ^{id166}, A. Tricoli ^{id29}, I.M. Trigger ^{id156a}, S. Trincaz-Duvoid ^{id127},
 D.A. Trischuk ^{id26}, B. Trocmé ^{id60}, L. Truong ^{id33c}, M. Trzebinski ^{id87}, A. Trzupek ^{id87}, F. Tsai ^{id145},
 M. Tsai ^{id106}, A. Tsiamis ^{id152,e}, P.V. Tsiareshka ³⁷, S. Tsigaridas ^{id156a}, A. Tsirigotis ^{id152,t},
 V. Tsiskaridze ^{id155}, E.G. Tskhadadze ^{id149a}, M. Tsopoulou ^{id152}, Y. Tsujikawa ^{id88}, I.I. Tsukerman ^{id37},
 V. Tsulaia ^{id17a}, S. Tsuno ^{id84}, K. Tsuru ^{id118}, D. Tsybychev ^{id145}, Y. Tu ^{id64b}, A. Tudorache ^{id27b},
 V. Tudorache ^{id27b}, A.N. Tuna ^{id61}, S. Turchikhin ^{id57b,57a}, I. Turk Cakir ^{id3a}, R. Turra ^{id71a},
 T. Turtuvshin ^{id38,z}, P.M. Tuts ^{id41}, S. Tzamarias ^{id152,e}, P. Tzani ^{id10}, E. Tzovara ^{id100}, F. Ukegawa ^{id157},
 P.A. Ulloa Poblete ^{id137c,137b}, E.N. Umaka ^{id29}, G. Unal ^{id36}, M. Unal ^{id11}, A. Undrus ^{id29}, G. Unel ^{id159},
 J. Urban ^{id28b}, P. Urquijo ^{id105}, P. Urrejola ^{id137a}, G. Usai ^{id8}, R. Ushioda ^{id154}, M. Usman ^{id108},
 Z. Uysal ^{id82}, V. Vacek ^{id132}, B. Vachon ^{id104}, K.O.H. Vadla ^{id125}, T. Vafeiadis ^{id36}, A. Vaitkus ^{id96},
 C. Valderanis ^{id109}, E. Valdes Santurio ^{id47a,47b}, M. Valente ^{id156a}, S. Valentinetti ^{id23b,23a}, A. Valero ^{id163},
 E. Valiente Moreno ^{id163}, A. Vallier ^{id102,ac}, J.A. Valls Ferrer ^{id163}, D.R. Van Arneman ^{id114},
 T.R. Van Daalen ^{id138}, A. Van Der Graaf ^{id49}, P. Van Gemmeren ^{id6}, M. Van Rijnbach ^{id125},
 S. Van Stroud ^{id96}, I. Van Vulpen ^{id114}, M. Vanadia ^{id76a,76b}, W. Vandelli ^{id36}, E.R. Vandewall ^{id121},
 D. Vannicola ^{id151}, L. Vannoli ^{id57b,57a}, R. Vari ^{id75a}, E.W. Varnes ^{id7}, C. Varni ^{id17b}, T. Varol ^{id148},
 D. Varouchas ^{id66}, L. Varriale ^{id163}, K.E. Varvell ^{id147}, M.E. Vasile ^{id27b}, L. Vaslin ⁸⁴, G.A. Vasquez ^{id165},
 A. Vasyukov ^{id38}, R. Vavricka ¹⁰⁰, F. Vazeille ^{id40}, T. Vazquez Schroeder ^{id36}, J. Veatch ^{id31},
 V. Vecchio ^{id101}, M.J. Veen ^{id103}, I. Veliscek ^{id126}, L.M. Veloce ^{id155}, F. Veloso ^{id130a,130c},
 S. Veneziano ^{id75a}, A. Ventura ^{id70a,70b}, S. Ventura Gonzalez ^{id135}, A. Verbytskyi ^{id110},
 M. Verducci ^{id74a,74b}, C. Vergis ^{id24}, M. Verissimo De Araujo ^{id83b}, W. Verkerke ^{id114},
 J.C. Vermeulen ^{id114}, C. Vernieri ^{id143}, M. Vessella ^{id103}, M.C. Vetterli ^{id142,ah}, A. Vgenopoulos ^{id152,e},
 N. Viaux Maira ^{id137f}, T. Vickey ^{id139}, O.E. Vickey Boeriu ^{id139}, G.H.A. Viehhauser ^{id126}, L. Vignani ^{id63b},
 M. Villa ^{id23b,23a}, M. Villaplana Perez ^{id163}, E.M. Villhauer ⁵², E. Vilucchi ^{id53}, M.G. Vincter ^{id34},
 G.S. Virdee ^{id20}, A. Vishwakarma ^{id52}, A. Visibile ¹¹⁴, C. Vittori ^{id36}, I. Vivarelli ^{id23b,23a},
 E. Voevodina ^{id110}, F. Vogel ^{id109}, J.C. Voigt ^{id50}, P. Vokac ^{id132}, Yu. Volkotrub ^{id86a}, J. Von Ahnen ^{id48},
 E. Von Toerne ^{id24}, B. Vormwald ^{id36}, V. Vorobel ^{id133}, K. Vorobev ^{id37}, M. Vos ^{id163}, K. Voss ^{id141},
 M. Vozak ^{id114}, L. Vozdecky ^{id120}, N. Vranjes ^{id15}, M. Vranjes Milosavljevic ^{id15}, M. Vreeswijk ^{id114},
 N.K. Vu ^{id62d,62c}, R. Vuillermet ^{id36}, O. Vujanovic ^{id100}, I. Vukotic ^{id39}, S. Wada ^{id157}, C. Wagner ¹⁰³,
 J.M. Wagner ^{id17a}, W. Wagner ^{id171}, S. Wahdan ^{id171}, H. Wahlberg ^{id90}, M. Wakida ^{id111}, J. Walder ^{id134},
 R. Walker ^{id109}, W. Walkowiak ^{id141}, A. Wall ^{id128}, E.J. Wallin ^{id98}, T. Wamorkar ^{id6}, A.Z. Wang ^{id136},
 C. Wang ^{id100}, C. Wang ^{id11}, H. Wang ^{id17a}, J. Wang ^{id64c}, R.-J. Wang ^{id100}, R. Wang ^{id61}, R. Wang ^{id6},
 S.M. Wang ^{id148}, S. Wang ^{id62b}, T. Wang ^{id62a}, W.T. Wang ^{id80}, W. Wang ^{id14a}, X. Wang ^{id14c},
 X. Wang ^{id162}, X. Wang ^{id62c}, Y. Wang ^{id62d}, Y. Wang ^{id14c}, Z. Wang ^{id106}, Z. Wang ^{id62d,51,62c},
 Z. Wang ^{id106}, A. Warburton ^{id104}, R.J. Ward ^{id20}, N. Warrack ^{id59}, S. Waterhouse ^{id95}, A.T. Watson ^{id20},
 H. Watson ^{id59}, M.F. Watson ^{id20}, E. Watton ^{id59,134}, G. Watts ^{id138}, B.M. Waugh ^{id96}, C. Weber ^{id29},
 H.A. Weber ^{id18}, M.S. Weber ^{id19}, S.M. Weber ^{id63a}, C. Wei ^{id62a}, Y. Wei ^{id126}, A.R. Weidberg ^{id126},
 E.J. Weik ^{id117}, J. Weingarten ^{id49}, M. Weirich ^{id100}, C. Weiser ^{id54}, C.J. Wells ^{id48}, T. Wenaus ^{id29},
 B. Wendland ^{id49}, T. Wengler ^{id36}, N.S. Wenke ¹¹⁰, N. Wermes ^{id24}, M. Wessels ^{id63a}, A.M. Wharton ^{id91},
 A.S. White ^{id61}, A. White ^{id8}, M.J. White ^{id1}, D. Whiteson ^{id159}, L. Wickremasinghe ^{id124},
 W. Wiedenmann ^{id170}, M. Wielers ^{id134}, C. Wiglesworth ^{id42}, D.J. Wilbern ¹²⁰, H.G. Wilkens ^{id36},
 D.M. Williams ^{id41}, H.H. Williams ¹²⁸, S. Williams ^{id32}, S. Willocq ^{id103}, B.J. Wilson ^{id101},
 P.J. Windischhofer ^{id39}, F.I. Winkel ^{id30}, F. Winklmeier ^{id123}, B.T. Winter ^{id54}, J.K. Winter ^{id101},
 M. Wittgen ¹⁴³, M. Wobisch ^{id97}, Z. Wolffs ^{id114}, J. Wollrath ¹⁵⁹, M.W. Wolter ^{id87}, H. Wolters ^{id130a,130c},
 E.L. Woodward ^{id41}, S.D. Worm ^{id48}, B.K. Wosiek ^{id87}, K.W. Woźniak ^{id87}, S. Wozniwski ^{id55},
 K. Wraight ^{id59}, C. Wu ^{id20}, M. Wu ^{id14d}, M. Wu ^{id113}, S.L. Wu ^{id170}, X. Wu ^{id56}, Y. Wu ^{id62a},
 Z. Wu ^{id135}, J. Wuerzinger ^{id110,af}, T.R. Wyatt ^{id101}, B.M. Wynne ^{id52}, S. Xella ^{id42}, L. Xia ^{id14c},
 M. Xia ^{id14b}, J. Xiang ^{id64c}, M. Xie ^{id62a}, X. Xie ^{id62a}, S. Xin ^{id14a,14c}, A. Xiong ^{id123}, J. Xiong ^{id17a},

D. Xu , H. Xu , L. Xu , R. Xu , T. Xu , Y. Xu , Z. Xu , Z. Xu ,
B. Yabsley , S. Yacoob , Y. Yamaguchi , E. Yamashita , H. Yamauchi ,
T. Yamazaki , Y. Yamazaki , J. Yan , S. Yan , Z. Yan , H.J. Yang ,
H.T. Yang , S. Yang , T. Yang , X. Yang , X. Yang , Y. Yang , Y. Yang ,
Z. Yang , W.-M. Yao , H. Ye , H. Ye , J. Ye , S. Ye , X. Ye , Y. Yeh ,
I. Yeletsikh , B. Yeo , M.R. Yexley , P. Yin , K. Yorita , S. Younas ,
C.J.S. Young , C. Young , C. Yu , Y. Yu , M. Yuan , R. Yuan , L. Yue ,
M. Zaazoua , B. Zabinski , E. Zaid , Z.K. Zak , T. Zakareishvili , N. Zakharchuk ,
S. Zambito , J.A. Zamora Saa , J. Zang , D. Zanzi , O. Zaplatilek ,
C. Zeitnitz , H. Zeng , J.C. Zeng , D.T. Zenger Jr , O. Zenin , T. Ženiš ,
S. Zenz , S. Zerradi , D. Zerwas , M. Zhai , D.F. Zhang , J. Zhang ,
J. Zhang , K. Zhang , L. Zhang , P. Zhang , R. Zhang , S. Zhang ,
S. Zhang , T. Zhang , X. Zhang , X. Zhang , Y. Zhang , Y. Zhang ,
Y. Zhang , Z. Zhang , Z. Zhang , H. Zhao , T. Zhao , Y. Zhao , Z. Zhao ,
A. Zhemchugov , J. Zheng , K. Zheng , X. Zheng , Z. Zheng , D. Zhong ,
B. Zhou , H. Zhou , N. Zhou , Y. Zhou , Y. Zhou , C.G. Zhu , J. Zhu ,
Y. Zhu , Y. Zhu , X. Zhuang , K. Zhukov , N.I. Zimine , J. Zinsser ,
M. Ziolkowski , L. Živković , A. Zoccoli , K. Zoch , T.G. Zorbas ,
O. Zormpa , W. Zou , L. Zwalinski .

¹Department of Physics, University of Adelaide, Adelaide; Australia.

²Department of Physics, University of Alberta, Edmonton AB; Canada.

³(^a)Department of Physics, Ankara University, Ankara; (^b)Division of Physics, TOBB University of Economics and Technology, Ankara; Türkiye.

⁴LAPP, Université Savoie Mont Blanc, CNRS/IN2P3, Annecy; France.

⁵APC, Université Paris Cité, CNRS/IN2P3, Paris; France.

⁶High Energy Physics Division, Argonne National Laboratory, Argonne IL; United States of America.

⁷Department of Physics, University of Arizona, Tucson AZ; United States of America.

⁸Department of Physics, University of Texas at Arlington, Arlington TX; United States of America.

⁹Physics Department, National and Kapodistrian University of Athens, Athens; Greece.

¹⁰Physics Department, National Technical University of Athens, Zografou; Greece.

¹¹Department of Physics, University of Texas at Austin, Austin TX; United States of America.

¹²Institute of Physics, Azerbaijan Academy of Sciences, Baku; Azerbaijan.

¹³Institut de Física d'Altes Energies (IFAE), Barcelona Institute of Science and Technology, Barcelona; Spain.

¹⁴(^a)Institute of High Energy Physics, Chinese Academy of Sciences, Beijing; (^b)Physics Department, Tsinghua University, Beijing; (^c)Department of Physics, Nanjing University, Nanjing; (^d)School of Science, Shenzhen Campus of Sun Yat-sen University; (^e)University of Chinese Academy of Science (UCAS), Beijing; China.

¹⁵Institute of Physics, University of Belgrade, Belgrade; Serbia.

¹⁶Department for Physics and Technology, University of Bergen, Bergen; Norway.

¹⁷(^a)Physics Division, Lawrence Berkeley National Laboratory, Berkeley CA; (^b)University of California, Berkeley CA; United States of America.

¹⁸Institut für Physik, Humboldt Universität zu Berlin, Berlin; Germany.

¹⁹Albert Einstein Center for Fundamental Physics and Laboratory for High Energy Physics, University of Bern, Bern; Switzerland.

²⁰School of Physics and Astronomy, University of Birmingham, Birmingham; United Kingdom.

- ²¹(*a*) Department of Physics, Bogazici University, Istanbul; (*b*) Department of Physics Engineering, Gaziantep University, Gaziantep; (*c*) Department of Physics, Istanbul University, Istanbul; Türkiye.
- ²²(*a*) Facultad de Ciencias y Centro de Investigaciones, Universidad Antonio Nariño, Bogotá; (*b*) Departamento de Física, Universidad Nacional de Colombia, Bogotá; Colombia.
- ²³(*a*) Dipartimento di Fisica e Astronomia A. Righi, Università di Bologna, Bologna; (*b*) INFN Sezione di Bologna; Italy.
- ²⁴Physikalisches Institut, Universität Bonn, Bonn; Germany.
- ²⁵Department of Physics, Boston University, Boston MA; United States of America.
- ²⁶Department of Physics, Brandeis University, Waltham MA; United States of America.
- ²⁷(*a*) Transilvania University of Brasov, Brasov; (*b*) Horia Hulubei National Institute of Physics and Nuclear Engineering, Bucharest; (*c*) Department of Physics, Alexandru Ioan Cuza University of Iasi, Iasi; (*d*) National Institute for Research and Development of Isotopic and Molecular Technologies, Physics Department, Cluj-Napoca; (*e*) National University of Science and Technology Politehnica, Bucharest; (*f*) West University in Timisoara, Timisoara; (*g*) Faculty of Physics, University of Bucharest, Bucharest; Romania.
- ²⁸(*a*) Faculty of Mathematics, Physics and Informatics, Comenius University, Bratislava; (*b*) Department of Subnuclear Physics, Institute of Experimental Physics of the Slovak Academy of Sciences, Kosice; Slovak Republic.
- ²⁹Physics Department, Brookhaven National Laboratory, Upton NY; United States of America.
- ³⁰Universidad de Buenos Aires, Facultad de Ciencias Exactas y Naturales, Departamento de Física, y CONICET, Instituto de Física de Buenos Aires (IFIBA), Buenos Aires; Argentina.
- ³¹California State University, CA; United States of America.
- ³²Cavendish Laboratory, University of Cambridge, Cambridge; United Kingdom.
- ³³(*a*) Department of Physics, University of Cape Town, Cape Town; (*b*) iThemba Labs, Western Cape; (*c*) Department of Mechanical Engineering Science, University of Johannesburg, Johannesburg; (*d*) National Institute of Physics, University of the Philippines Diliman (Philippines); (*e*) University of South Africa, Department of Physics, Pretoria; (*f*) University of Zululand, KwaDlangezwa; (*g*) School of Physics, University of the Witwatersrand, Johannesburg; South Africa.
- ³⁴Department of Physics, Carleton University, Ottawa ON; Canada.
- ³⁵(*a*) Faculté des Sciences Ain Chock, Université Hassan II de Casablanca; (*b*) Faculté des Sciences, Université Ibn-Tofail, Kénitra; (*c*) Faculté des Sciences Semlalia, Université Cadi Ayyad, LPHEA-Marrakech; (*d*) LPMR, Faculté des Sciences, Université Mohamed Premier, Oujda; (*e*) Faculté des sciences, Université Mohammed V, Rabat; (*f*) Institute of Applied Physics, Mohammed VI Polytechnic University, Ben Guerir; Morocco.
- ³⁶CERN, Geneva; Switzerland.
- ³⁷Affiliated with an institute covered by a cooperation agreement with CERN.
- ³⁸Affiliated with an international laboratory covered by a cooperation agreement with CERN.
- ³⁹Enrico Fermi Institute, University of Chicago, Chicago IL; United States of America.
- ⁴⁰LPC, Université Clermont Auvergne, CNRS/IN2P3, Clermont-Ferrand; France.
- ⁴¹Nevis Laboratory, Columbia University, Irvington NY; United States of America.
- ⁴²Niels Bohr Institute, University of Copenhagen, Copenhagen; Denmark.
- ⁴³(*a*) Dipartimento di Fisica, Università della Calabria, Rende; (*b*) INFN Gruppo Collegato di Cosenza, Laboratori Nazionali di Frascati; Italy.
- ⁴⁴Physics Department, Southern Methodist University, Dallas TX; United States of America.
- ⁴⁵Physics Department, University of Texas at Dallas, Richardson TX; United States of America.
- ⁴⁶National Centre for Scientific Research "Demokritos", Agia Paraskevi; Greece.
- ⁴⁷(*a*) Department of Physics, Stockholm University; (*b*) Oskar Klein Centre, Stockholm; Sweden.
- ⁴⁸Deutsches Elektronen-Synchrotron DESY, Hamburg and Zeuthen; Germany.

- ⁴⁹Fakultät Physik , Technische Universität Dortmund, Dortmund; Germany.
- ⁵⁰Institut für Kern- und Teilchenphysik, Technische Universität Dresden, Dresden; Germany.
- ⁵¹Department of Physics, Duke University, Durham NC; United States of America.
- ⁵²SUPA - School of Physics and Astronomy, University of Edinburgh, Edinburgh; United Kingdom.
- ⁵³INFN e Laboratori Nazionali di Frascati, Frascati; Italy.
- ⁵⁴Physikalisches Institut, Albert-Ludwigs-Universität Freiburg, Freiburg; Germany.
- ⁵⁵II. Physikalisches Institut, Georg-August-Universität Göttingen, Göttingen; Germany.
- ⁵⁶Département de Physique Nucléaire et Corpusculaire, Université de Genève, Genève; Switzerland.
- ⁵⁷(^a)Dipartimento di Fisica, Università di Genova, Genova;(^b) INFN Sezione di Genova; Italy.
- ⁵⁸II. Physikalisches Institut, Justus-Liebig-Universität Giessen, Giessen; Germany.
- ⁵⁹SUPA - School of Physics and Astronomy, University of Glasgow, Glasgow; United Kingdom.
- ⁶⁰LPSC, Université Grenoble Alpes, CNRS/IN2P3, Grenoble INP, Grenoble; France.
- ⁶¹Laboratory for Particle Physics and Cosmology, Harvard University, Cambridge MA; United States of America.
- ⁶²(^a) Department of Modern Physics and State Key Laboratory of Particle Detection and Electronics, University of Science and Technology of China, Hefei;(^b) Institute of Frontier and Interdisciplinary Science and Key Laboratory of Particle Physics and Particle Irradiation (MOE), Shandong University, Qingdao;(^c) School of Physics and Astronomy, Shanghai Jiao Tong University, Key Laboratory for Particle Astrophysics and Cosmology (MOE), SKLPPC, Shanghai;(^d) Tsung-Dao Lee Institute, Shanghai;(^e) School of Physics and Microelectronics, Zhengzhou University; China.
- ⁶³(^a) Kirchhoff-Institut für Physik, Ruprecht-Karls-Universität Heidelberg, Heidelberg;(^b) Physikalisches Institut, Ruprecht-Karls-Universität Heidelberg, Heidelberg; Germany.
- ⁶⁴(^a) Department of Physics, Chinese University of Hong Kong, Shatin, N.T., Hong Kong;(^b) Department of Physics, University of Hong Kong, Hong Kong;(^c) Department of Physics and Institute for Advanced Study, Hong Kong University of Science and Technology, Clear Water Bay, Kowloon, Hong Kong; China.
- ⁶⁵Department of Physics, National Tsing Hua University, Hsinchu; Taiwan.
- ⁶⁶IJCLab, Université Paris-Saclay, CNRS/IN2P3, 91405, Orsay; France.
- ⁶⁷Centro Nacional de Microelectrónica (IMB-CNM-CSIC), Barcelona; Spain.
- ⁶⁸Department of Physics, Indiana University, Bloomington IN; United States of America.
- ⁶⁹(^a) INFN Gruppo Collegato di Udine, Sezione di Trieste, Udine;(^b) ICTP, Trieste;(^c) Dipartimento Politecnico di Ingegneria e Architettura, Università di Udine, Udine; Italy.
- ⁷⁰(^a) INFN Sezione di Lecce;(^b) Dipartimento di Matematica e Fisica, Università del Salento, Lecce; Italy.
- ⁷¹(^a) INFN Sezione di Milano;(^b) Dipartimento di Fisica, Università di Milano, Milano; Italy.
- ⁷²(^a) INFN Sezione di Napoli;(^b) Dipartimento di Fisica, Università di Napoli, Napoli; Italy.
- ⁷³(^a) INFN Sezione di Pavia;(^b) Dipartimento di Fisica, Università di Pavia, Pavia; Italy.
- ⁷⁴(^a) INFN Sezione di Pisa;(^b) Dipartimento di Fisica E. Fermi, Università di Pisa, Pisa; Italy.
- ⁷⁵(^a) INFN Sezione di Roma;(^b) Dipartimento di Fisica, Sapienza Università di Roma, Roma; Italy.
- ⁷⁶(^a) INFN Sezione di Roma Tor Vergata;(^b) Dipartimento di Fisica, Università di Roma Tor Vergata, Roma; Italy.
- ⁷⁷(^a) INFN Sezione di Roma Tre;(^b) Dipartimento di Matematica e Fisica, Università Roma Tre, Roma; Italy.
- ⁷⁸(^a) INFN-TIFPA;(^b) Università degli Studi di Trento, Trento; Italy.
- ⁷⁹Universität Innsbruck, Department of Astro and Particle Physics, Innsbruck; Austria.
- ⁸⁰University of Iowa, Iowa City IA; United States of America.
- ⁸¹Department of Physics and Astronomy, Iowa State University, Ames IA; United States of America.
- ⁸²Istinye University, Sariyer, Istanbul; Türkiye.
- ⁸³(^a) Departamento de Engenharia Elétrica, Universidade Federal de Juiz de Fora (UFJF), Juiz de

- Fora;^(b)Universidade Federal do Rio De Janeiro COPPE/EE/IF, Rio de Janeiro;^(c)Instituto de Física, Universidade de São Paulo, São Paulo;^(d)Rio de Janeiro State University, Rio de Janeiro; Brazil.
- ⁸⁴KEK, High Energy Accelerator Research Organization, Tsukuba; Japan.
- ⁸⁵Graduate School of Science, Kobe University, Kobe; Japan.
- ⁸⁶^(a)AGH University of Krakow, Faculty of Physics and Applied Computer Science, Krakow;^(b)Marian Smoluchowski Institute of Physics, Jagiellonian University, Krakow; Poland.
- ⁸⁷Institute of Nuclear Physics Polish Academy of Sciences, Krakow; Poland.
- ⁸⁸Faculty of Science, Kyoto University, Kyoto; Japan.
- ⁸⁹Research Center for Advanced Particle Physics and Department of Physics, Kyushu University, Fukuoka ; Japan.
- ⁹⁰Instituto de Física La Plata, Universidad Nacional de La Plata and CONICET, La Plata; Argentina.
- ⁹¹Physics Department, Lancaster University, Lancaster; United Kingdom.
- ⁹²Oliver Lodge Laboratory, University of Liverpool, Liverpool; United Kingdom.
- ⁹³Department of Experimental Particle Physics, Jožef Stefan Institute and Department of Physics, University of Ljubljana, Ljubljana; Slovenia.
- ⁹⁴School of Physics and Astronomy, Queen Mary University of London, London; United Kingdom.
- ⁹⁵Department of Physics, Royal Holloway University of London, Egham; United Kingdom.
- ⁹⁶Department of Physics and Astronomy, University College London, London; United Kingdom.
- ⁹⁷Louisiana Tech University, Ruston LA; United States of America.
- ⁹⁸Fysiska institutionen, Lunds universitet, Lund; Sweden.
- ⁹⁹Departamento de Física Teórica C-15 and CIAFF, Universidad Autónoma de Madrid, Madrid; Spain.
- ¹⁰⁰Institut für Physik, Universität Mainz, Mainz; Germany.
- ¹⁰¹School of Physics and Astronomy, University of Manchester, Manchester; United Kingdom.
- ¹⁰²CPPM, Aix-Marseille Université, CNRS/IN2P3, Marseille; France.
- ¹⁰³Department of Physics, University of Massachusetts, Amherst MA; United States of America.
- ¹⁰⁴Department of Physics, McGill University, Montreal QC; Canada.
- ¹⁰⁵School of Physics, University of Melbourne, Victoria; Australia.
- ¹⁰⁶Department of Physics, University of Michigan, Ann Arbor MI; United States of America.
- ¹⁰⁷Department of Physics and Astronomy, Michigan State University, East Lansing MI; United States of America.
- ¹⁰⁸Group of Particle Physics, University of Montreal, Montreal QC; Canada.
- ¹⁰⁹Fakultät für Physik, Ludwig-Maximilians-Universität München, München; Germany.
- ¹¹⁰Max-Planck-Institut für Physik (Werner-Heisenberg-Institut), München; Germany.
- ¹¹¹Graduate School of Science and Kobayashi-Maskawa Institute, Nagoya University, Nagoya; Japan.
- ¹¹²Department of Physics and Astronomy, University of New Mexico, Albuquerque NM; United States of America.
- ¹¹³Institute for Mathematics, Astrophysics and Particle Physics, Radboud University/Nikhef, Nijmegen; Netherlands.
- ¹¹⁴Nikhef National Institute for Subatomic Physics and University of Amsterdam, Amsterdam; Netherlands.
- ¹¹⁵Department of Physics, Northern Illinois University, DeKalb IL; United States of America.
- ¹¹⁶^(a)New York University Abu Dhabi, Abu Dhabi;^(b)United Arab Emirates University, Al Ain; United Arab Emirates.
- ¹¹⁷Department of Physics, New York University, New York NY; United States of America.
- ¹¹⁸Ochanomizu University, Otsuka, Bunkyo-ku, Tokyo; Japan.
- ¹¹⁹Ohio State University, Columbus OH; United States of America.
- ¹²⁰Homer L. Dodge Department of Physics and Astronomy, University of Oklahoma, Norman OK; United

States of America.

¹²¹Department of Physics, Oklahoma State University, Stillwater OK; United States of America.

¹²²Palacký University, Joint Laboratory of Optics, Olomouc; Czech Republic.

¹²³Institute for Fundamental Science, University of Oregon, Eugene, OR; United States of America.

¹²⁴Graduate School of Science, Osaka University, Osaka; Japan.

¹²⁵Department of Physics, University of Oslo, Oslo; Norway.

¹²⁶Department of Physics, Oxford University, Oxford; United Kingdom.

¹²⁷LPNHE, Sorbonne Université, Université Paris Cité, CNRS/IN2P3, Paris; France.

¹²⁸Department of Physics, University of Pennsylvania, Philadelphia PA; United States of America.

¹²⁹Department of Physics and Astronomy, University of Pittsburgh, Pittsburgh PA; United States of America.

¹³⁰(^a)Laboratório de Instrumentação e Física Experimental de Partículas - LIP, Lisboa; (^b)Departamento de Física, Faculdade de Ciências, Universidade de Lisboa, Lisboa; (^c)Departamento de Física, Universidade de Coimbra, Coimbra; (^d)Centro de Física Nuclear da Universidade de Lisboa, Lisboa; (^e)Departamento de Física, Universidade do Minho, Braga; (^f)Departamento de Física Teórica y del Cosmos, Universidad de Granada, Granada (Spain); (^g)Departamento de Física, Instituto Superior Técnico, Universidade de Lisboa, Lisboa; Portugal.

¹³¹Institute of Physics of the Czech Academy of Sciences, Prague; Czech Republic.

¹³²Czech Technical University in Prague, Prague; Czech Republic.

¹³³Charles University, Faculty of Mathematics and Physics, Prague; Czech Republic.

¹³⁴Particle Physics Department, Rutherford Appleton Laboratory, Didcot; United Kingdom.

¹³⁵IRFU, CEA, Université Paris-Saclay, Gif-sur-Yvette; France.

¹³⁶Santa Cruz Institute for Particle Physics, University of California Santa Cruz, Santa Cruz CA; United States of America.

¹³⁷(^a)Departamento de Física, Pontificia Universidad Católica de Chile, Santiago; (^b)Millennium Institute for Subatomic physics at high energy frontier (SAPHIR), Santiago; (^c)Instituto de Investigación Multidisciplinario en Ciencia y Tecnología, y Departamento de Física, Universidad de La Serena; (^d)Universidad Andres Bello, Department of Physics, Santiago; (^e)Instituto de Alta Investigación, Universidad de Tarapacá, Arica; (^f)Departamento de Física, Universidad Técnica Federico Santa María, Valparaíso; Chile.

¹³⁸Department of Physics, University of Washington, Seattle WA; United States of America.

¹³⁹Department of Physics and Astronomy, University of Sheffield, Sheffield; United Kingdom.

¹⁴⁰Department of Physics, Shinshu University, Nagano; Japan.

¹⁴¹Department Physik, Universität Siegen, Siegen; Germany.

¹⁴²Department of Physics, Simon Fraser University, Burnaby BC; Canada.

¹⁴³SLAC National Accelerator Laboratory, Stanford CA; United States of America.

¹⁴⁴Department of Physics, Royal Institute of Technology, Stockholm; Sweden.

¹⁴⁵Departments of Physics and Astronomy, Stony Brook University, Stony Brook NY; United States of America.

¹⁴⁶Department of Physics and Astronomy, University of Sussex, Brighton; United Kingdom.

¹⁴⁷School of Physics, University of Sydney, Sydney; Australia.

¹⁴⁸Institute of Physics, Academia Sinica, Taipei; Taiwan.

¹⁴⁹(^a)E. Andronikashvili Institute of Physics, Iv. Javakhishvili Tbilisi State University, Tbilisi; (^b)High Energy Physics Institute, Tbilisi State University, Tbilisi; (^c)University of Georgia, Tbilisi; Georgia.

¹⁵⁰Department of Physics, Technion, Israel Institute of Technology, Haifa; Israel.

¹⁵¹Raymond and Beverly Sackler School of Physics and Astronomy, Tel Aviv University, Tel Aviv; Israel.

¹⁵²Department of Physics, Aristotle University of Thessaloniki, Thessaloniki; Greece.

- ¹⁵³International Center for Elementary Particle Physics and Department of Physics, University of Tokyo, Tokyo; Japan.
- ¹⁵⁴Department of Physics, Tokyo Institute of Technology, Tokyo; Japan.
- ¹⁵⁵Department of Physics, University of Toronto, Toronto ON; Canada.
- ¹⁵⁶(^a) TRIUMF, Vancouver BC; (^b) Department of Physics and Astronomy, York University, Toronto ON; Canada.
- ¹⁵⁷Division of Physics and Tomonaga Center for the History of the Universe, Faculty of Pure and Applied Sciences, University of Tsukuba, Tsukuba; Japan.
- ¹⁵⁸Department of Physics and Astronomy, Tufts University, Medford MA; United States of America.
- ¹⁵⁹Department of Physics and Astronomy, University of California Irvine, Irvine CA; United States of America.
- ¹⁶⁰University of Sharjah, Sharjah; United Arab Emirates.
- ¹⁶¹Department of Physics and Astronomy, University of Uppsala, Uppsala; Sweden.
- ¹⁶²Department of Physics, University of Illinois, Urbana IL; United States of America.
- ¹⁶³Instituto de Física Corpuscular (IFIC), Centro Mixto Universidad de Valencia - CSIC, Valencia; Spain.
- ¹⁶⁴Department of Physics, University of British Columbia, Vancouver BC; Canada.
- ¹⁶⁵Department of Physics and Astronomy, University of Victoria, Victoria BC; Canada.
- ¹⁶⁶Fakultät für Physik und Astronomie, Julius-Maximilians-Universität Würzburg, Würzburg; Germany.
- ¹⁶⁷Department of Physics, University of Warwick, Coventry; United Kingdom.
- ¹⁶⁸Waseda University, Tokyo; Japan.
- ¹⁶⁹Department of Particle Physics and Astrophysics, Weizmann Institute of Science, Rehovot; Israel.
- ¹⁷⁰Department of Physics, University of Wisconsin, Madison WI; United States of America.
- ¹⁷¹Fakultät für Mathematik und Naturwissenschaften, Fachgruppe Physik, Bergische Universität Wuppertal, Wuppertal; Germany.
- ¹⁷²Department of Physics, Yale University, New Haven CT; United States of America.
- ^a Also Affiliated with an institute covered by a cooperation agreement with CERN.
- ^b Also at An-Najah National University, Nablus; Palestine.
- ^c Also at Borough of Manhattan Community College, City University of New York, New York NY; United States of America.
- ^d Also at Center for High Energy Physics, Peking University; China.
- ^e Also at Center for Interdisciplinary Research and Innovation (CIRI-AUTH), Thessaloniki; Greece.
- ^f Also at Centro Studi e Ricerche Enrico Fermi, Italy.
- ^g Also at CERN, Geneva; Switzerland.
- ^h Also at Département de Physique Nucléaire et Corpusculaire, Université de Genève, Genève; Switzerland.
- ⁱ Also at Departament de Física de la Universitat Autònoma de Barcelona, Barcelona; Spain.
- ^j Also at Department of Financial and Management Engineering, University of the Aegean, Chios; Greece.
- ^k Also at Department of Physics, Ben Gurion University of the Negev, Beer Sheva; Israel.
- ^l Also at Department of Physics, California State University, Sacramento; United States of America.
- ^m Also at Department of Physics, King's College London, London; United Kingdom.
- ⁿ Also at Department of Physics, Stanford University, Stanford CA; United States of America.
- ^o Also at Department of Physics, Stellenbosch University; South Africa.
- ^p Also at Department of Physics, University of Fribourg, Fribourg; Switzerland.
- ^q Also at Department of Physics, University of Thessaly; Greece.
- ^r Also at Department of Physics, Westmont College, Santa Barbara; United States of America.
- ^s Also at Faculty of Physics, Sofia University, 'St. Kliment Ohridski', Sofia; Bulgaria.
- ^t Also at Hellenic Open University, Patras; Greece.

- ^u Also at Institutio Catalana de Recerca i Estudis Avancats, ICREA, Barcelona; Spain.
- ^v Also at Institut für Experimentalphysik, Universität Hamburg, Hamburg; Germany.
- ^w Also at Institute for Nuclear Research and Nuclear Energy (INRNE) of the Bulgarian Academy of Sciences, Sofia; Bulgaria.
- ^x Also at Institute of Applied Physics, Mohammed VI Polytechnic University, Ben Guerir; Morocco.
- ^y Also at Institute of Particle Physics (IPP); Canada.
- ^z Also at Institute of Physics and Technology, Mongolian Academy of Sciences, Ulaanbaatar; Mongolia.
- ^{aa} Also at Institute of Physics, Azerbaijan Academy of Sciences, Baku; Azerbaijan.
- ^{ab} Also at Institute of Theoretical Physics, Ilia State University, Tbilisi; Georgia.
- ^{ac} Also at L2IT, Université de Toulouse, CNRS/IN2P3, UPS, Toulouse; France.
- ^{ad} Also at Lawrence Livermore National Laboratory, Livermore; United States of America.
- ^{ae} Also at National Institute of Physics, University of the Philippines Diliman (Philippines); Philippines.
- ^{af} Also at Technical University of Munich, Munich; Germany.
- ^{ag} Also at The Collaborative Innovation Center of Quantum Matter (CICQM), Beijing; China.
- ^{ah} Also at TRIUMF, Vancouver BC; Canada.
- ^{ai} Also at Università di Napoli Parthenope, Napoli; Italy.
- ^{aj} Also at University of Colorado Boulder, Department of Physics, Colorado; United States of America.
- ^{ak} Also at Washington College, Chestertown, MD; United States of America.
- ^{al} Also at Yeditepe University, Physics Department, Istanbul; Türkiye.
- * Deceased